

**THE ROLE OF A CONSERVED ISOLEUCINE IN THE STRUCTURE,  
STABILITY AND FUNCTION OF HUMAN CLASS ALPHA  
GLUTATHIONE TRANSFERASE A1-1**

**Graeme Patrick Gordon**

**A dissertation submitted to the Faculty of Science, University of the Witwatersrand,  
Johannesburg, in fulfillment of the requirements for the degree of Master of Science.**

**Johannesburg, 11 June 2010**

## DECLARATION

I declare that this dissertation is my own, unaided work. It is being submitted for the degree of Master of Science in the University of the Witwatersrand, Johannesburg. It has not been submitted before for any degree or examination at any other University.

---

Graeme Patrick Gordon

11<sup>th</sup> day of June 2010

## DEDICATION

I dedicate this work to my family whom have supported me:

Tony, Lynette, Jennifer, Caroline and Veronica

*"One smallest new fact obtained in the laboratory, one brick built into the temple of science, far outweighs any second-hand exposition which passes an idle hour, but can leave no useful result behind it."*

Prof. George Edward Challenger  
The Lost World  
by Sir Arthur Conan Doyle

## ABSTRACT

Proteins have evolved to balance the structural requirements for stability with the need for specialised conformations imparting catalytic activity and ligand-binding capabilities. The glutathione transferases (GSTs) are a multi-gene family of ubiquitous proteins that are predominantly involved in the detoxification of reactive endo- and xenobiotic compounds through conjugation to the tripeptide glutathione. The family of cytosolic GSTs contain a canonical structure composed of a thioredoxin-like fold in domain 1 and an all- $\alpha$ -helical domain 2. Domain 1 of the cytosolic GSTs contains a highly conserved isoleucine residue in  $\alpha$ -helix 3, located below the active site at position 71 in human class Alpha glutathione transferase A1-1 (hGST A1-1), that is involved in maintaining the packing within the hydrophobic core of domain 1. The objective of this study was to provide insight into the role of the topologically conserved Ile-71 residue in the structure, stability, and the catalytic and non-substrate ligandin function of hGST A1-1. This was achieved by introducing a cavity-creating mutation into hGST A1-1 by replacing Ile-71 with Val and comparing the structural and functional properties of the mutant with those of the wild-type protein. The structural properties of the mutant were the same as those of the wild-type protein as shown by far- and near-UV circular dichroism and tryptophan fluorescence studies. The stability of the mutant, however, was lower than that of the wild-type protein as revealed by a thermal-induced unfolding study which indicated that the temperature transition midpoint ( $T_m$ ) value for the mutant ( $T_m = 54.71 \pm 0.06$  °C) was lower than that for the wild-type protein ( $T_m = 56.45 \pm 0.02$  °C). This finding is in agreement with that expected due to the loss of van der Waals contacts in the mutant protein. The catalytic properties of the mutant were found to be similar to those of the wild-type protein as indicated by a specific activity assay and a transition-state stabilisation study. Similarly, the non-substrate ligandin properties of the mutant were comparable to those of the wild-type protein as confirmed by 8-anilino-1-naphthalene sulfonate (ANS)-binding studies using active site ligands. This non-substrate ligand, ANS, is known to bind the H-site of the enzyme's active site. This study reveals that although the Ile-71 residue does not play a significant role in the structure and function of the protein, it makes a significant contribution to the stability of the protein by forming van der Waals contacts within the hydrophobic core of domain 1.

## **ACKNOWLEDGEMENTS**

I extend my gratitude and thanks to the following people:

Prof. Heini Dirr, for his patience, guidance and motivation. Thank-you for teaching the scientific method in your inspiring manner and for imparting some of your wealth of knowledge.

Dr Sayed, Dr Burke, Dr Mosebi, Dr Fannuchi and Dr Gildenhuis for their assistance.

The members of the Protein Structure-Function Research Unit, University of the Witwatersrand for their encouragement and assistance.

The University of the Witwatersrand for the opportunity and resources to conduct my study and the National Research Foundation for financial support.

# TABLE OF CONTENTS

<b>DECLARATION</b> .....	ii
<b>DEDICATION</b> .....	iii
<b>ABSTRACT</b> .....	iv
<b>ACKNOWLEDGEMENTS</b> .....	v
<b>LIST OF ABBREVIATIONS</b> .....	ix
<b>LIST OF FIGURES</b> .....	xii
<b>LIST OF TABLES</b> .....	xiv

## CHAPTER 1

### INTRODUCTION

1.1 The stability of proteins.....	1
1.2 The canonical cytosolic family of GSTs.....	3
1.3 The structure of cytosolic GSTs.....	4
1.4 Catalytic and ligandin functions of cytosolic GSTs.....	10
1.5 Objectives.....	13

## CHAPTER 2

### EXPERIMENTAL PROCEDURES

2.1 Materials.....	15
2.2 Preparation of the mutant and wild-type pKHA1 plasmids.....	15
2.2.1 Purification of pKHA1 plasmids.....	15
2.2.2 Sequencing of the mutant and wild-type pKHA1 plasmids.....	17
2.3 Preparation of I71V and wild-type hGST A1-1 proteins.....	18
2.3.1 Protein over-expression and purification.....	18
2.3.2 Determination of protein concentration.....	21

2.4 Spectroscopic structural studies of the I71V and wild-type hGST A1-1 proteins.....	22
2.4.1 Circular dichroism spectroscopy.....	23
2.4.1.1 Far-UV circular dichroism spectroscopy.....	23
2.4.1.2 Near-UV circular dichroism spectroscopy.....	23
2.4.2 Intrinsic fluorescence spectroscopy – Tryptophan fluorescence.....	24
2.5 Functional assays of the I71V and wild-type hGST A1-1 proteins.....	24
2.5.1 Non-substrate ligand-binding assays – ANS fluorescence.....	24
2.5.1.1 ANS binding assay.....	25
2.5.1.2 ANS displacement assays using EA and GSO <sub>3</sub> <sup>-</sup> ligands.....	25
2.5.2 Standard GSH-CDNB conjugation assay.....	26
2.5.3 Formation of the $\sigma$ -complex between GSH and TNB.....	27
2.5.3.1 Spectroscopic characterisation of the $\sigma$ -complex.....	27
2.5.3.2 Spectrophotometric determination of the formation constant of the $\sigma$ - complex.....	28
2.6 Thermal-induced unfolding study of the I71V and wild-type hGST A1-1 proteins.....	29

## CHAPTER 3

### RESULTS AND DISCUSSION

3.1 Purity and sequencing of the mutant and wild-type cDNA.....	30
3.2 Purity of the I71V and wild-type hGST A1-1 proteins.....	31
3.3 Structural properties of the I71V and wild-type hGST A1-1 proteins.....	35
3.3.1 Secondary structure.....	35
3.3.2 Tertiary structure.....	37
3.3.1 Intrinsic fluorescence properties.....	37
3.3.2 Near-UV circular dichroism properties.....	40
3.3.3 Structures of the I71V and wild-type hGST A1-1 proteins.....	42
3.4 Non-substrate ligand-binding properties of the G- and H-sites.....	45
3.4.1 Fluorescence properties of ANS bound to the H-site.....	45
3.4.2 Displacement of ANS by G- and H-site ligands.....	48
3.5 Catalytic properties of the I71V and wild-type enzymes.....	54

3.5.1 Specific activity.....	54
3.5.2 Formation of the $\sigma$ -complex within the active sites.....	58
3.6 Thermal stability of the I71V and wild-type proteins.....	66
<b>CHAPTER 4</b>	
<b>CONCLUSIONS.....</b>	<b>70</b>
<b>CHAPTER 5</b>	
<b>REFERENCES.....</b>	<b>71</b>

## LIST OF ABBREVIATIONS

$A_{\lambda}$	Absorbance at a wavelength of $\lambda$ nm
$A_{260}/A_{230}$	Ratio of the absorbance at 260 nm to the absorbance at 230 nm
$A_{260}/A_{280}$	Ratio of the absorbance at 260 nm to the absorbance at 280 nm
$A_{\max}$	Absorbance maximum
Amp	Ampicillin
Å	Angstrom ( $10^{-10}$ m)
ANS	8-anilino-1-naphthalene sulfonic acid
°C	Degrees Celsius
CD	Circular Dichroism
cDNA	Complementary DNA
CDNB	1-chloro-2,4-dinitrobenzene
Clic1	Chloride intracellular channel protein-1
deg	Degrees of rotation of light
DNA	Deoxyribonucleic Acid
EA	Ethacrynic acid
EDTA	Ethylenediaminetetraacetic acid
EF1 $\gamma$	The gamma subunit of eukaryotic translation elongation factor 1
ExPASy	Expert Protein Analysis System
$\times g$	Multiplied by the gravitational force of the earth
Grx2	Glutaredoxin-2
G-site	Glutathione-binding site
GSH	Reduced glutathione
GS $^{-}$	Oxidised glutathione
GSO $_3^{-}$	Glutathione sulfonate
GST	Glutathione S-Transferase
h	Hour
H-site	Hydrophobic electrophile binding site
hGST A1-1	Human class Alpha Glutathione S-Transferase with two type one

	subunits
$IC_{50}$	Inhibitor concentration at which 50 percent of ANS is displaced
I71V	Replacement of wild-type isoleucine (I) with valine (V) at position 71
IPTG	Isopropyl $\beta$ -D-1-thiogalactopyranoside
kDa	kilo Daltons
$K_d$	Dissociation constant
$K_F$	Formation constant
$k_{cat}/K_M$	Catalytic efficiency
L	Litre
LB	Luria-Bertani
m	meter
M	Molar
$[\Theta]$	Mean residue ellipticity
n	Non-bonding molecular orbital
$\epsilon$	Molar absorption coefficient
$\epsilon_\lambda$	Molar absorption coefficient at wavelength $\lambda$ nm
$\pi$	Pi bonding orbital
$\pi^*$	Pi anti-bonding orbital
pdb	Protein data bank
$pK_a$	Acid ionisation constant
ORF	Open reading frame
$R$	Universal gas constant = 8.3145 J/mol.K
rpm	Revolutions per minute
SDS	Sodium Dodecyl Sulphate
SDS-PAGE	Sodium Dodecyl Sulphate-Polyacrylamide Gel Electrophoresis
$S_NAr$	Nucleophilic Aromatic Substitution Reaction
TEMED	$N,N,N',N'$ -tetramethylethylenediamine
$T$	Temperature in Kelvin
$T_m$	Temperature-induced transition midpoint
TE	Tris-EDTA

TNB	1,3,5-trinitrobenzene
UV	Ultra-violet
Ure2p	Yeast prion protein
v/v	Volume of solute per volume solvent
2YT	2× Yeast-Tryptone

The one- and three-letter symbolism for amino acids (IUPAC-IUB, 1984), and the one-letter symbolism for deoxyribonucleic acids (IUPAC-IUB, 1974) have been used in accordance with the IUPAC-IUBMB system of nomenclature.

## LIST OF FIGURES

	<b>Page</b>
Figure 1. Ribbon representation of the crystal structure of human class Alpha glutathione transferase A1-1 in complex with <i>S</i> -benzylglutathione.	5
Figure 2. Structure-based sequence alignments of a sample of canonical cytosolic GSTs and members of the GST-like proteins.	7
Figure 3. Spacefilling representation of the hydrophobic environment of Ile-71 in the thioredoxin fold of wild-type hGST A1-1.	9
Figure 4. Diagrammatic representation of the nucleophilic aromatic substitution ( $S_NAr$ ) reaction catalysed by glutathione transferases involving the conjugation of (A) 1-chloro-2,4-dinitrobenzene and (B) 1,3,5-trinitrobenzene to GSH.	12
Figure 5. A portion of the nucleotide sequencing chromatograms for the hGST A1-1 cDNA ORFs emphasising the desired codon mutation responsible for the corresponding I71V hGST A1-1 protein sequence.	32
Figure 6. Elution profile of the wild-type hGST A1-1 protein eluted from the fast-flow CM-Sepharose cation-exchange column.	33
Figure 7. SDS-PAGE analysis of the purity and size of the I71V and wild-type hGST A1 subunits.	34
Figure 8. Far-UV CD spectra of I71V (○▽) and wild-type (●▼) hGST A1-1.	36
Figure 9. Fluorescence emission spectra of native and unfolded I71V and wild-type hGST A1-1.	39
Figure 10. Near-UV CD spectra for native wild-type (●) and I71V (○) hGST A1-1.	41
Figure 11. Wire-frame ribbon diagram depicting the secondary structures of the superimposed crystal structures of subunit A of the I71V and wild-type hGST A1-1 proteins.	43
Figure 12. Spacefilling representation of the cavity created within a hydrophobic core of domain 1 in the I71V hGST A1-1 protein and the loss of van der	44

	Waals contacts.	
Figure 13.	Ball-and-stick representation of the tertiary environment around Trp-21 in subunit A of the crystal structures of the I71V and wild-type hGST A1-1 proteins.	46
Figure 14.	Fluorescence emission spectra of free, unbound ANS and ANS bound to native and denatured I71V and wild-type hGST A1-1.	47
Figure 15.	Displacement of ANS bound to I71V (○) and wild-type (●) hGST A1-1 by ethacrynic acid (EA).	49
Figure 16.	Displacement of ANS bound to I71V (○) and wild-type (●) hGST A1-1 by glutathione sulfonate (GSO <sub>3</sub> <sup>-</sup> ).	50
Figure 17.	Ball-and-stick representation of the active-site residues involved in van der Waals interactions with the non-substrate ligand ANS.	53
Figure 18.	Progress curve of the conjugation reaction between reduced glutathione and 1-chloro-2,4-dinitrobenzene as catalysed by I71V hGST A1-1.	56
Figure 19.	Specific activity of (A) wild-type and (B) I71V hGST A1-1 using the standard CDNB conjugation assay.	57
Figure 20.	Absorbance spectra of the $\sigma$ -complex formed between TNB and GSH in the active sites of I71V (---) and wild-type (—) hGST A1-1.	59
Figure 21.	Saturation curve for the formation of the $\sigma$ -complex at the active sites of I71V (○) and wild-type (●) hGST A1-1.	60
Figure 22.	Ball-and-stick representation of the active-site residues involved in van der Waals interactions with the $\sigma$ -complex bound to hGST A1-1.	65
Figure 23.	Thermal-induced transitions of I71V mutant and wild-type hGST A1-1.	67

## LIST OF TABLES

	<b>Page</b>
Table 1. $IC_{50}$ values for the displacement of ANS bound to I71V and wild-type hGST A1-1 by the inhibitors ethacrynic acid and glutathione sulfonate.	52
Table 2. Equilibrium formation parameters for the formation of the 1-( <i>S</i> -glutathionyl)-1,3,5-trinitrocyclohexadienate $\sigma$ -complex in the active sites of I71V and wild-type hGST A1-1.	61

# CHAPTER 1

## INTRODUCTION

### 1.1 The stability of proteins

Structurally-similar proteins contain a number of common structural patterns despite the existence of a low degree of sequence identity between them. There appear to be at least four general patterns throughout all globular proteins, as reviewed in Shortle *et al.* (1990): (i) most of the charged side chains are found at the surface of the protein where they interact with water (Chothia, 1976), (ii) most hydrophobic side chains are found buried within the interior of the protein (Chothia, 1976), (iii) the backbone and side-chain residues pack in compressed conformations that are comparable in density to crystallised amino acids (Richards, 1977; reviewed in Shortle *et al.* (1990)), and (iv) extensive networks of intramolecular hydrogen bonds appear to traverse the protein interior (Baker and Hubbard, 1984). Analysis of these patterns reveals that non-covalent forces, namely hydrophobic interactions, van der Waals interactions, electrostatic forces and hydrogen bonds, play dominant roles in controlling the native structure of proteins (Shortle *et al.*, 1990).

Nature has overcome the thermodynamic and kinetic restraints that accompany the folding of a denatured protein into its singular, native ‘wild-type’ conformation. Small globular proteins fold by a reversible means to achieve the thermodynamically most stable state, i.e. the global minima of their free energies is reached under thermodynamic control that is independent of a particular pathway (Anfinsen *et al.*, 1961; Anfinsen *et al.*, 1973). There are, however, an inconceivably high number of possible conformations to search in order for a denatured protein to reach the desired native structure and as such an unbiased search would take longer than the age of the universe (Levinthal, 1968; reviewed in Dill and Chan (1997)). There is, thus, sufficient evidence to support the existence of distinct ‘folding pathways’ that provide the kinetically controlled means of rapidly advancing to the native conformation. The current view on protein folding synthesises two theses. The first concept involves the presence of multiple folding pathways that are taken simultaneously by different members populating the

denatured protein state to produce a folding funnel of thermodynamic states and structural conformations. The second concept incorporates the ideas of nucleation-condensation that involve the rapid formation and loss of particular secondary and tertiary structural interactions at different times of the folding process that seed the folding of the protein into its native state. Nature, therefore, conserves particular residues that aid in the formation of these particular interactions. As such, the attainment of particular structural conformations and the impending stability of the transient conformations in the folding pathways as well as that of the final native conformation depend on the conservation of particular residues.

As reviewed in Di Nardo *et al.* (2003), there is general consensus that the burial of hydrophobic residues in the interior of globular protein accounts for the major stabilizing force in proteins (Dill, 1990). Randomisation experiments conducted on barnase and lamda repressor proteins have revealed that a protein core of certain protein structures can tolerate drastic changes in its composition while still maintaining a stable, enzymatically active conformation (Axe *et al.*, 1996; Lim and Sauer, 1989; reviewed in Di Nardo *et al.* (2003)). Studies conducted on the stability of the ubiquitin structure has, however, revealed that its stability is strongly dependant on the specific packing arrangements within the protein core (Finucane and Woolfson, 1999). The substitution of core residues most often introduces cavities into the structure that reduce the stability of the protein by a factor proportional to the loss in van der Waals contacts (Vlassi, *et al.*, 1999; Ratnaparkhi and Varadarajan, 2000). The resultant cavity is either minimised by the introduction of strain to the local environment (Xu *et al.*, 1998) or the cavity persists with the resultant energy cost to the core stability. Mutational studies at the interface between an  $\alpha$ -helix and  $\beta$ -sheet in the small ribonuclease from *Bacillus amyloliquefaciens* (barnase) have revealed that the substitution of isoleucine for valine destabilizes a protein structure by 1.1 kcal mol<sup>-1</sup> due to the loss of the single, terminal  $\delta$ -methyl group that decreases the number of stabilising van der Waals contacts (Kellis Jr., 1988).

## 1.2 The canonical cytosolic family of GSTs

It appears widely accepted that the evolution of autotrophic species led to the perpetual conversion of the reducing atmosphere of the Oparin-Haldane primordial world to that of the oxidising atmosphere characteristic of the modern, oxygen-rich environment (Miller *et al.*, 1997). It is reasonable that this transformation forced organisms to develop defence mechanisms that protected themselves against endogenously produced oxygen and xenobiotic compounds that degraded their deoxyribonucleic acid (DNA) and ribonucleic acid (RNA), inactivated their enzymes and structural proteins, and lysed their cells through the attack and disintegration of membranes (Hayes and Pulford, 1995; Hayes and McLellan, 1999; reviewed in Sheehan *et al.* (2001)). Aerobic microorganisms, plants and animals have thus created and evolved a family of multi-functional enzymes called the glutathione *S*-transferases (GSTs) (Wilce and Parker, 1994).

The glutathione *S*-transferases (GSTs) (EC 2.5.1.18) are a multi-gene family of enzymes that primarily catalyse the nucleophilic addition of the sulfhydryl group of the reduced tripeptide L-glutathione (GSH) to a variety of nonpolar molecules containing electrophilic functional groups (Armstrong, 1991; Rushmore and Pickett, 1993). In addition to their catalytic properties, GSTs possess extensive non-substrate ligand-binding properties (Ketley *et al.*, 1975).

As reviewed in Hayes *et al.* (2005), the family of cytosolic GSTs are predominantly involved in biotransformation of toxic endobiotics and xenobiotics. The cytosolic superfamily is composed of at least sixteen classes of dimeric enzymes with subunit lengths of 199-244 amino acids (Sheehan *et al.*, 2001; Hayes *et al.*, 2005). Of the 16 known classes, at least seven are mammalian, namely Alpha (A), Mu (M), Omega (O), Pi (P), Sigma (S), Theta (T), and Zeta (Z) (Sheehan *et al.*, 2001; Hayes *et al.*, 2005) and at least seven are non-mammalian: Beta (B), Delta(D), Epsilon, Lambda, Phi, Rho, Tau and "U" (Hayes *et al.*, 2005). In humans and rodents, cytosolic GSTs share >40% identity for isoenzymes within a class, and <25% identity for isoenzymes between classes (Sheehan *et al.*, 2001; Hayes *et al.*, 2005).

The numerous detoxification processes that occur in the liver require the localisation of high concentrations of detoxification enzymes. The GSTs constitute an average of 3.7% of the total mass of cytosolic proteins in human hepatic tissue. Human hepatic class Alpha glutathione transferase constitutes the predominant class of GSTs accounting for 84% of the total mass of hepatic cytosolic GSTs (van Ommen *et al.*, 1990). The specific class Alpha GST isoenzyme, human class Alpha glutathione transferase composed of two type 1 monomers (hGST A1-1), is the most abundant of all isoenzymes in the liver comprising 1.9% of the total mass of hepatic proteins (van Ommen *et al.*, 1990). The hGST A1-1 protein, therefore, plays a significant role in the function of the liver and warrants further scrutiny.

### 1.3 The structure of cytosolic GSTs

The canonical cytosolic GSTs are dimeric proteins,  $M_r \approx 50$  kilo Dalton (kDa), with globular three-dimensional structures of average dimensions  $62 \text{ \AA} \times 51 \text{ \AA} \times 46 \text{ \AA}$  (Dirr *et al.*, 1994). They are homodimeric or heterodimeric proteins that are assembled from identical or non-identical subunits from the same gene class, respectively (Dirr *et al.*, 1994). The cytosolic GSTs adopt a canonical structure that may be illustrated by the structure of hGST A1-1 (Figure 1). The homodimer is formed by a two-fold axis of symmetry that creates a solvent inaccessible channel down the subunit interface (Sinning *et al.*, 1993). Each monomer contains a single active site at each end of the dimer interface,  $14 \text{ \AA}$  apart from each other (Sinning *et al.*, 1993), that are composed of a glutathione-binding site (G-site) and an adjacent hydrophobic-binding site (H-site) that binds the ubiquitous tri-peptide glutathione, and hydrophobic, electrophilic molecules, respectively (Mannervik *et al.*, 1978; reviewed in Sinning *et al.* (1993)).

Each monomer has a total secondary structural content of 59%  $\alpha$ -helices and 10%  $\beta$ -strands which is apportioned into two distinct domains: a thioredoxin-like *N*-terminal domain (domain 1) and an all- $\alpha$ -helical *C*-terminal domain (domain 2) connected by the amino acid residues in positions 82 and 192 (Sinning *et al.*, 1993). A tryptophan residue, corresponding to position 21 in hGST A1-1 (Figure 1), is located at the domain interface where its indole-ring side chain protrudes from  $\alpha$ -helix 1 in domain 1 into the hydrophobic environment of

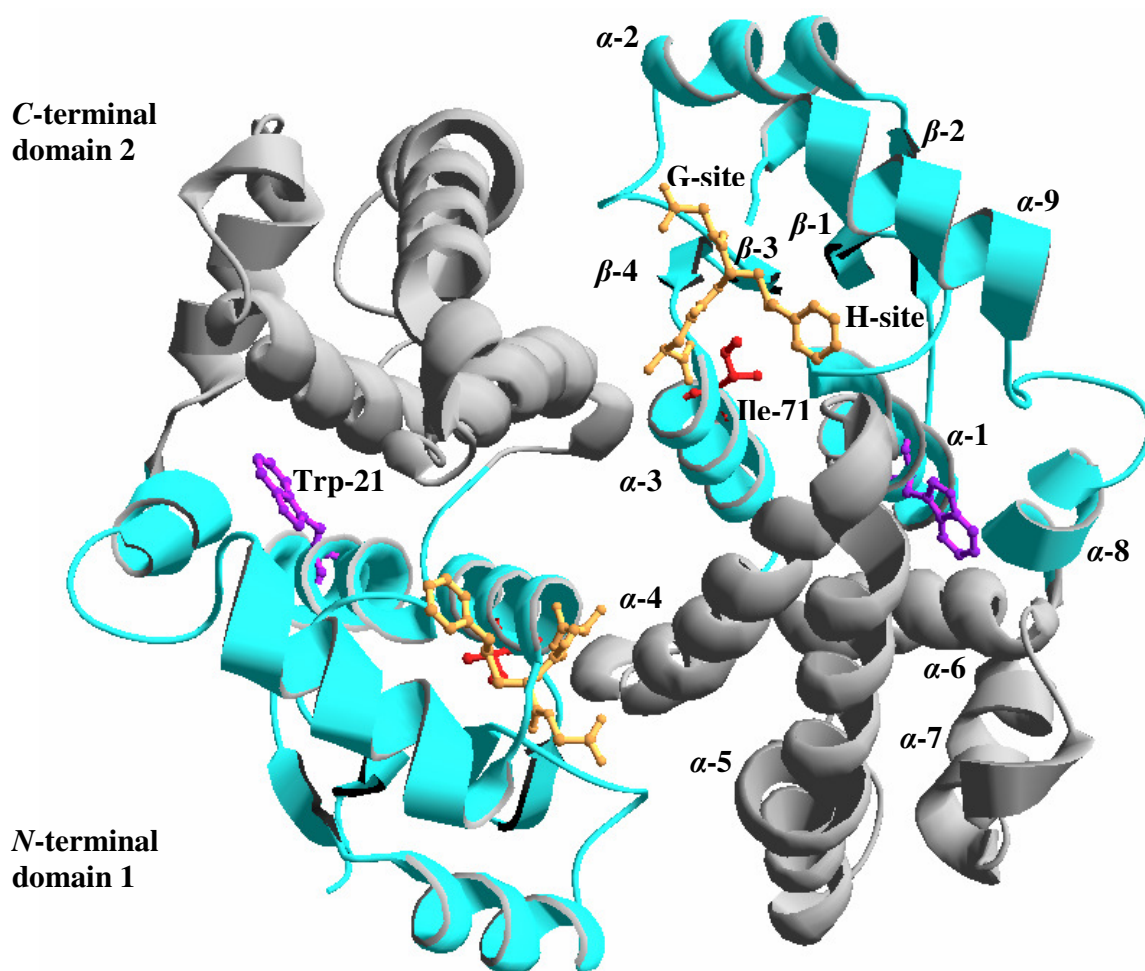


**Figure 1. Ribbon representation of the crystal structure of human class Alpha glutathione transferase A1-1 in complex with *S*-benzylglutathione.**

The interface between the *N*-terminal domain (turquoise blue), composed of alternating  $\alpha$ -helices and  $\beta$ -strands, and *C*-terminal domain (grey), all  $\alpha$ -helical, contains the intrinsic fluorescence residue Trp-21 (purple). The topologically conserved Ile-71 residue (red) is positioned below the active site, which is occupied by the ligand *S*-benzylglutathione (orange). The linear glutathione moiety of *S*-benzylglutathione is seen occupying the glutathione binding site (G-site) and the benzyl ring moiety the hydrophobic, electrophilic ligand binding site (H-site). This figure was generated from pdb file 1GUH (Sinning *et al.*, 1993) using Swiss-PdbViewer version 4.0.1 (Guex and Peitsch, 1997).

domain 2.

This indole-ring side chain is inaccessible to solvent, with a solvent accessible surface area (SASA) of 4 Å<sup>2</sup> (Wallace *et al.*, 1998a), which has allowed its use in structural and functional studies to probe changes in the inter-domain region (Wallace *et al.*, 1998a) including the dissociation of the two domains (Atkins *et al.*, 1997). Domain 1 is an  $\alpha/\beta$ -structure composed of a  $\beta\alpha\beta$ -motif connected to a  $\beta\beta\alpha$ -motif by an  $\alpha$ -helix ( $\alpha$ -helix 2) that spans the face of a  $\beta$ -sheet that is assembled from the four  $\beta$ -strands (Sinning *et al.*, 1993). This topology is known as the thioredoxin fold and is found in the GST-like proteins of *Escherichia coli* thioredoxin (Holmgren *et al.*, 1975), bacteriophage T4 glutaredoxin (Eklund *et al.*, 1992) and glutathione peroxidase (Epp *et al.*, 1983). A hydrophobic core is found just below the G-site in domain 1 that contains a buried, topologically-conserved isoleucine residue, corresponding to position 71 in the hGST A1-1 protein, near the *N*-terminus of  $\alpha$ -helix 3 (Figure 1). The final structural components of domain 1 are  $\alpha$ -helices 8 and 9 of which the latter forms a dynamic flap over the active site that contributes to the hydrophobicity of the H-site (Sinning *et al.*, 1993). Domain 2 is larger in structure and composed of 5 amphiphilic  $\alpha$ -helices in which  $\alpha$ -helices 4–7 associate their hydrophobic residues to form a stable hydrophobic core (Sinning *et al.*, 1993).

The preservation of the canonical GST fold throughout the cytosolic GSTs and GST-like proteins highlights the need for conserved residues. Figure 2 depicts a structure-based sequence alignment of a portion of the sequences for the thioredoxin-like domain 1 of 15 of the mammalian and non-mammalian canonical cytosolic GSTs (Figure 2 A) and 4 of the canonical GST-like proteins including chloride intracellular channel protein-1 (Clic1), the gamma subunit of eukaryotic translation elongation factor 1 (EF1 $\gamma$ ) (Koonin *et al.*, 1994), glutaredoxin-2 (Grx2) and yeast prion protein (Ure2p) (Figure 2 B). The alignments show that the sequences share a low sequence identity with the prevalence of extensive amino acid substitutions between the gene classes. There are, however, a number of fully and semi-conserved residues at invariant locations in the protein secondary structure that play functional and structural roles in the proteins.



An isoleucine residue, corresponding to position 71 in  $\alpha$ -helix 3 in the hGST A1-1 protein, is topologically conserved throughout the canonical cytosolic GSTs and GST-like proteins, with the exceptions of the replacement of isoleucine for leucine in class Lamda GST and threonine in class Omega GST O. An analysis of the side chains of leucine and isoleucine reveals that they are isosteric variants of each other and are both hydrophobic in nature. Although the side chain of threonine is polarised, containing a  $\gamma$ -hydroxyl group, and one methyl group shorter than isoleucine, both residues are of similar size and bulk. These substitutions are therefore conservative replacements and may be tolerated in the hydrophobic core of domain 1.

An analysis of the crystal structure of wild-type hGST A1-1 (pdb accession code: 1K3L; Le Trong *et al.*, 2002) reveals that the hydrophobic core within domain 1 is composed of the amino-acid side chains of  $\beta$ -strand 1 and  $\alpha$ -helix 1 of the  $\beta\alpha\beta$ -motif, and  $\beta$ -strands 3 and 4 and  $\alpha$ -helix 3 of the  $\beta\beta\alpha$ -motif of the thioredoxin fold. Figure 3 depicts the hydrophobic environment of the topologically conserved Ile-71 residue located in the hydrophobic core of the thioredoxin fold. The Ile-71 side-chain is buried in a hydrophobic cleft formed from the side chains of a number of surrounding hydrophobic residues. The residues forming van der Waals contacts with the side chain of Ile-71 include Thr-19 ( $\alpha$ -helix 1), Pro-56, Val-58 ( $\beta$ -strand 3), Leu-65 ( $\beta$ -strand 4) and Ile-75 ( $\alpha$ -helix 3). The hydrophobic effect formed by the unfavourable solvation of these hydrophobic core residues in the denatured protein drives the folding process. The formation of favourable van der Waals interactions between these hydrophobic residues directs the folding process to the formation of hydrophobic cores around which the surrounding secondary structures assemble to form the native hGST A1-1 protein structure. These van der Waals interactions are also important in maintaining the stability of the hydrophobic cores that stabilise the native hGST A1-1 structure. It is hypothesised that the extended length, steric bulk and nonpolar nature of the Ile-71 side chain has been conserved to fill the hydrophobic cleft of the hydrophobic core in domain 1 and to maximise the number of van der Waals contacts with the surrounding hydrophobic residues. It is, thus, inferred that the Ile-71 residue has been topologically conserved to play a role in forming the correct structure of the thioredoxin fold in the native hGST A1-1 protein and to contribute to the stability of the hydrophobic core in domain 1.

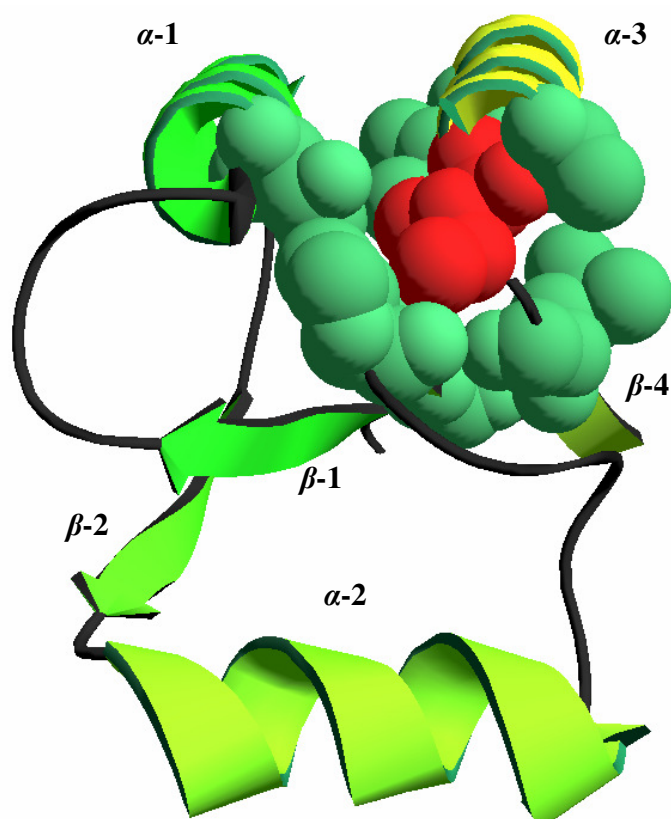
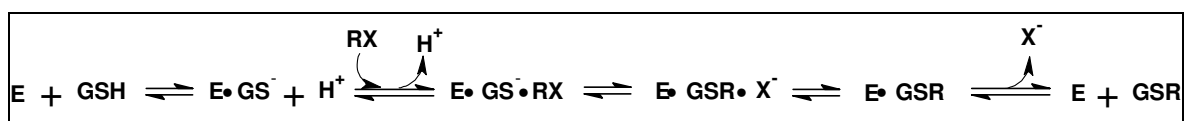


**Figure 3. Spacefilling representation of the hydrophobic environment of Ile-71 in the thioredoxin fold of wild-type hGST A1-1.**

Isoleucine is shown in red and the amino-acids forming side-chain hydrophobic interactions are coloured green. The thioredoxin fold is shown as a ribbon representation labelled and coloured according to the succession of the secondary structural components. The portion of  $\alpha$ -helix 3 ribbon masking the Ile-71 residue has been omitted for clarity. This figure was generated from pdb file 1K3L (Le Trong *et al.*, 2002) using Swiss-PdbViewer version 4.0.1 (Guex and Peitsch, 1997).

#### 1.4 Catalytic and ligandin functions of cytosolic GSTs

Cytosolic GSTs are primarily involved in Phase-2 detoxification of endogenous and xenobiotic alkylating agents in the mercapturic pathway (Sheehan *et al.*, 2001). Cytosolic GSTs are, paradoxically, also involved in the activation of certain xenobiotics (Hayes *et al.*, 2005). The metabolism of endogenous compounds includes the degradation of products from oxidative stress and aromatic amino acids metabolism, and the synthesis of steroid hormones (Sheehan *et al.*, 2001). Cytosolic GSTs are capable of catalysing epoxide ring-opening reactions, Michael additions to  $\alpha,\beta$ -unsaturated aldehydes and ketones, and nucleophilic aromatic substitution ( $S_NAr$ ) reactions on alkyl and aryl halides which all produce glutathione conjugates (Armstrong, 1991; Sheehan *et al.*, 2001). In addition to this, cytosolic GSTs catalyse the reduction of hydroperoxides to produce oxidized glutathione (GSSG) (Sheehan *et al.*, 2001). The following scheme depicts the general reaction between reduced glutathione (GSH) and an electrophilic substrate (R) catalysed by the GST enzyme (E) (Armstrong, 1991):



The GST enzyme binds GSH at the G-site and abstracts the GSH sulfhydryl group proton to yield an enzyme-bound glutathionoate anion ( $\text{GS}^-$ ). The proton is released and the electrophilic substrate, containing a good leaving group ( $\text{X}$ ), binds to the H-site. The next sequential reaction is characterised by the nucleophilic addition of the thiolate to the electrophilic substrate (in the ternary complex of enzyme,  $\text{GS}^-$  and electrophile) followed by the elimination of the leaving group (Armstrong, 1991). The final stage involves the release of the GSR conjugate. This scheme was generated using ACD/ChemSketch (Freeware) version 12.01 (Advanced Chemistry Development Inc., 2009; <http://www.acdlabs.com>).

The reaction is catalysed due to the contributions made by a number of residues in the active site that interact with the GSH and electrophilic substrates. In the hGST A1-1 protein, the side-chain hydroxyl group of topologically conserved Tyr-9 forms hydrogen-bond interactions, in its undissociated neutral form, with the sulfhydryl group of GSH thereby

lowering the  $pK_a$  of the GSH sulfhydryl group from a  $pK_a$  value of 9.0 to between 6.2 and 7.1 (Björnstedt *et al.*, 1995) and activating the sulfhydryl group for deprotonation (Stenberg *et al.*, 1991). The Arg-15 side chain is involved in excluding solvent molecules from the H-site whereas its main-chain backbone amide group forms hydrogen-bond interactions with the hydroxyl group of Tyr-9 thereby aiding in the stabilisation of the  $GS^-$  thiolate anion (Björnstedt *et al.*, 1995). The pyrrolidine ring of topologically conserved Pro-56 packs against Tyr-9 and Met-16 thereby ensuring the correct conformation of the G-site for formation of the hydrogen-bond interactions between GSH, Tyr-9 and Arg-15 (Nathaniel *et al.*, 2003).

The conjugation reactions between a number of arene substrates and GSH follow a nucleophilic aromatic substitution ( $S_NAr$ ) reaction. The  $S_NAr$  reaction involves sequential addition and elimination reactions (Armstrong, 1997) between which a short-lived  $\sigma$ -complex intermediate or Meisenheimer complex is formed (Miller, 1968; Bernasconi, 1980; reviewed in Graminski *et al.* (1989)). Figure 4 is a diagrammatic representation of the conjugation of the electrophilic substrates 1-chloro-2,4-dinitrobenzene (CDNB) and 1,3,5-trinitrobenzene (TNB) to GSH with the inclusion of the TNB  $\sigma$ -complex, 1-(*S*-glutathionyl)-2,4,6-trinitrocyclohexadienate anion, an analogue of the  $\sigma$ -complex intermediate formed in the CDNB reaction (Clark and Sinclair, 1988; Graminski *et al.*, 1989).

Kinetic studies on rat liver class GST M4-4 have suggested that the formation of the  $\sigma$ -complex from GSH and electron-deficient arenes is the rate limiting step in the  $S_NAr$  reaction and that the  $\sigma$ -complex is stabilised by hydrogen-bonding interactions with tyrosine residues and water molecules in the active site (Chen *et al.*, 1988; Ji *et al.*, 1993). Kinetic studies conducted on the rat liver class GST M3-3, have revealed that enzymes that have a greater efficiency for catalysing nucleophilic aromatic substitution reactions are capable of stabilising the  $\sigma$ -complex intermediate because of its ability to stabilise the transition state leading up to the formation of the  $\sigma$ -complex intermediate (Graminski *et al.*, 1989). The hGST A1-1 enzyme is capable of dramatically increasing the concentration of the 1-(*S*-glutathionyl)-2,4,6-trinitrocyclohexadienate  $\sigma$ -complex in the enzyme's active site, at pH 6.5, as compared to the concentration formed between  $GS^-$  and TNB in aqueous solution at

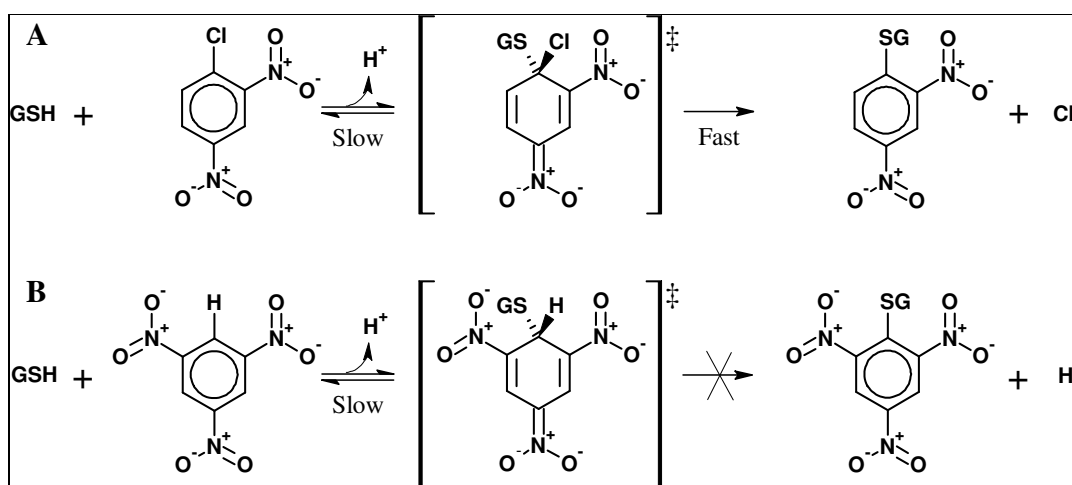


**Figure 4. Diagrammatic representation of the nucleophilic aromatic substitution ( $S_NAr$ ) reaction catalysed by glutathione transferases involving the conjugation of (A) 1-chloro-2,4-dinitrobenzene and (B) 1,3,5-trinitrobenzene to GSH.**

(A) The initial slow step involves (i) the GST-catalysed abstraction of the enzyme-bound glutathione thiol proton producing an enzymatically-stabilised thiolate anion, followed by (ii) the nucleophilic addition of the thiolate to the electrophilic aromatic carbon as directed by the mesomeric effects of the *ortho*- and *para*-nitro aryl substituents and the inductive effect of the electronegative chloride group. The resultant 1-(*S*-glutathionyl)-2,4-dinitrocyclohexadienate anionic  $\sigma$ -complex is believed to resemble the transition state of the reaction and is characterised by a strained  $Sp^3$ -hybridised ring carbon and a net anionic charge that is stabilised by the resonance between the delocalised-ring  $\pi$  electrons and the nitro-substituent  $\pi$  electrons. The final fast step involves the rapid elimination of the better leaving chloride group to form the 1-(*S*-glutathionyl)-2,4-dinitrobenzene product and chloride. (B) The initial step of the reaction proceeds as per reaction A except that the thiolate group adds to any of the three equivalent methyne carbons on the deactivated aromatic ring to form the anionic 1-(*S*-glutathionyl)-2,4,6-trinitrocyclohexadienate  $\sigma$ -complex. The  $\sigma$ -complex decomposes to the reactants because the hydride group is a weaker leaving group compared to the glutathionyl group thereby providing a high kinetic barrier for the formation of a 1-(*S*-glutathionyl)-2,4,6-trinitrobenzene product. This figure was adapted from Armstrong (1997) and Graminski *et al.* (1989) and generated using ACD/ChemSketch (Freeware) version 12.01 (Advanced Chemistry Development Inc., 2009).

pH 9.0 (Gan, 1977). The structural reason for this catalytic ability is unknown due to the lack of a crystal structure of the  $\sigma$ -complex bound to the enzyme's active site. Kinetic studies on hGST A1-1 suggest that the enzyme's ability to stabilise the  $\sigma$ -complex is not the only major factor contributing to the enzyme's high catalytic rate for aromatic substrates (Widersten *et al.*, 1996).

In light of the above knowledge, it is argued that the residues involved in the catalytic process, including those required to stabilise the  $\sigma$ -complex, are required to be in the correct conformation to ensure the optimal catalytic activity of the protein. The proximity of the Ile-71 residue to the active site suggests that the presence of a stable hydrophobic core at the base of the active site is required to maintain the correct conformations of the catalytic residues.

## 1.5 Objectives

An analysis of the structural data for the canonical cytosolic GSTs indicates the presence of a topologically conserved isoleucine residue in the hydrophobic core of domain 1. The objective of this study is to determine the role of the conserved Ile-71 residue in the structure, stability, and the catalytic and non-substrate ligandin function of hGST A1-1. Specifically, the contribution of the extended hydrophobic bulk of the Ile-71 side chain shall be evaluated. A comparative study shall be conducted between an Ile-71  $\rightarrow$  Val hGST A1-1 mutant protein and wild-type hGST A1-1 protein to assess the impact of the loss in steric bulk and hydrophobic van der Waals contacts made by the truncated Ile-71 side chain. This mutation raises the questions of what role the extended structure of Ile-71 side chain plays in: the structure of the protein and catalytic G- and H-sites; the stability of the protein; and the catalytic and non-substrate ligandin function. The choice of the mutant is based on the destabilising effect that the removal of one methyl group from an aliphatic amino acid side chain in the hydrophobic core of other proteins has on their structure (Kellis *et al.*, 1988; Kellis *et al.*, 1989). It is, therefore, predicted that the Ile-71  $\rightarrow$  Val mutation destabilises the hGST A1-1 protein by  $\sim 4.6 \text{ kJ.mol}^{-1}$  in direct proportion to the loss in steric bulk and van der Waals contacts associated with the removal of a single methyl group. Similarly, it is

predicted that a change in the structure of the catalytic site shall decrease the catalytic ability of the enzyme and reduce the affinity for non-substrate ligands. It is thus hypothesised that Ile-71 is conserved to maintain the structure, stability, and enzymatic and ligandin function of the protein.

## CHAPTER 2

### EXPERIMENTAL PROCEDURES

#### 2.1 Materials

The wild-type pKHA1 expression vector encoding recombinant wild-type human class Alpha glutathione transferase A1-1 (hGST A1-1) protein was a generous gift from Prof. B. Mannervik (Department of Biochemistry, Uppsala University, Uppsala, Sweden; Stenberg *et al.*, 1992). The mutant pKHA1 expression vector encoding recombinant mutant I71V hGST A1-1 protein was a generous gift from Dr J. Burke (Protein Structure-Function Research Unit, University of the Witwatersrand, Johannesburg, South Africa). The *Escherichia coli* BL21 (DE3) and BL21 (DE3) pLysS competent cells were obtained from Stratagene (USA). The GeneJET™ Plasmid Miniprep Kit was obtained from Inqaba Biotech, Pretoria, South Africa. The compounds 8-anilino-1-naphthalenesulfonic acid (ANS), ethacrynic acid (EA), glutathione sulfonic acid, reduced L-glutathione (GSH), and 1,3,5-trinitrobenzene (TNB) were of ultrapure grade and were purchased from Sigma-Aldrich Co. (St. Louis, MO, USA). 1-Chloro-2,4-dinitrobenzene (CDNB) was of ultrapure grade and was purchased from Merck KGaA (Darmstadt, Germany). Sodium dodecyl sulfate polyacrylamide gel electrophoresis (SDS-PAGE) protein molecular weight markers (SM0431) were obtained from Fermentas. All other reagents were of analytical grade. All solutions and media were prepared using distilled water and filtered through a 0.45  $\mu\text{m}$  filter.

#### 2.2 Preparation of the mutant and wild-type pKHA1 plasmids

##### 2.2.1 Purification of the pKHA1 plasmids

The mutant and wild-type pKHA1 plasmids were purified in accordance with the same procedure given below, unless where otherwise stipulated. All inoculation and growth periods discussed below were conducted under sterile conditions using pre-sterilised media, containers and measuring equipment.

The snap-frozen glycerol stock of *Escherichia coli* BL21 (DE3) cells, transformed with the wild-type pKHA1 plasmid that confers ampicillin (AMP) resistance, was used to inoculate 200 mL 2× Yeast-Tryptone (2YT) medium (1% (w/v) yeast extract, 1.6% (w/v) tryptone and 0.5% (w/v) sodium chloride containing 100 µg/mL Amp). Similarly, the snap-frozen glycerol stock of *Escherichia coli* BL21 (DE3) pLysS cells, transformed with the mutant pKHA1 plasmid and the pLysS plasmid (that confers Amp and chloramphenicol resistance, respectively), was used to inoculate 200 mL 2YT medium containing 100 µg/mL Amp and 35 µg/mL chloramphenicol. The cells were cultured overnight in a shaker-incubator under aerobic conditions at 37 °C for 14–16 h at 250 rpm agitation. A 1.5 mL sample of turbid overnight culture was centrifuged at 13 400 rpm for 3 min on a benchtop rotor and an aliquot of both supernatant and resuspended pellet used to streak 25 mL plates of Luria-Bertani (LB) agar medium (0.5% (w/v) yeast extract, 1% (w/v) tryptone, 1% (w/v) sodium chloride and 1.5% (w/v) agar) containing 100 µg/mL Amp, for both wild-type and mutant pKHA1 transformants, and 35 µg/mL chloramphenicol, exclusively for mutant pKHA1 transformants. The streaked cells were incubated at 37 °C for 16–18 h. A single, medium-sized, dark colony of each of the mutant and wild-type cells was isolated from an LB-agar plate for further propagation. The selected colony was used to inoculate 100 mL 2YT medium supplemented with 100 µg/mL Amp and incubated at 37 °C for 14–16 h at 250 rpm agitation. The turbid overnight culture was used for the small scale DNA purification procedure.

The pKHA1 plasmids were extracted and purified from the respective turbid overnight culture using the GeneJET™ Plasmid Miniprep Kit (Inqaba Biotech, Pretoria, South Africa) in accordance with the protocol detailed in the manufacturer's instruction manual. The Miniprep Kit procedure is adapted from the standard alkaline-sodium dodecyl sulfate (SDS) lysis procedure (Ish-Horowicz and Burke, 1981; based on Birnboim and Doly, 1979) used to extract the DNA from the bacterial cells, and purify it from bacterial chromosomal DNA, RNA and proteins. The only deviation used was employing a 4.5 mL sample of overnight culture in place of the required 1.5 mL.

The purified mutant pKHA1 plasmid stock was used to transform the high-copy number ECloni supercompetant cells, in accordance with the Ecloni transformation protocol, in order to improve the yield of plasmid for further transformations and sequencing. A single colony was isolated from an LB-agar plate, originally streaked using an overnight culture of transformed ECloni competent cells, used to inoculate a fresh 100 mL solution of 2YT medium supplemented with 100  $\mu\text{g}/\text{mL}$  Amp. The freshly inoculated media was incubated under the aforementioned conditions. The turbid overnight culture was subsequently used to extract and purify the mutant pKHA1 plasmid.

The concentration of purified pKHA1 in each sample was determined using a NanoDrop<sup>TM</sup> ND-1000 spectrophotometer (ThermoScientific, USA) by measuring the absorbance spectrum (220–350 nm) of a 2  $\mu\text{L}$  sample of pKHA1 plasmid, in accordance with NanoDrop protocol. The absorbance contribution from the buffer was accounted for by using the TE buffer as a blank solution. The ratio of the absorbance at 260 nm to the absorbance at 280 nm ( $A_{260}/A_{280}$ ) was determined by the NanoDrop software program and used as an indicator of the level of protein contamination within the sample. Similarly, the  $A_{260}/A_{320}$  value was determined as an indicator of the level of carbohydrate contamination.

### **2.2.2 Sequencing of the mutant and wild-type pKHA1 plasmids**

A sample (10  $\mu\text{L}$ ) of each of the purified mutant and wild-type pKHA1 plasmids was submitted to Inqaba Biotec (Pretoria, South Africa) for sequencing. The mutant pKHA1 cDNA open reading frame (ORF), encoding the I71V hGST A1-1 protein, was sequenced to confirm the presence of the desired ATT  $\rightarrow$  GTC mutation and to confirm the absence of any other miscellaneous mutations. Similarly, the wild-type pKHA1 cDNA open reading frame, encoding the wild-type hGST A1-1 protein, was sequenced to confirm the absence of incorporated mutations. The nucleotide sequences were sequenced using modern techniques in accordance with the DNA sequencing technique suggested by Sanger *et al.* (1977). Primers previously designed for the pKHA1 plasmid by Samantha Gildenhuys (Protein Structure-Function Research Unit, University of the Witwatersrand) were used:

**Forward:**

5' CGGCTCGTATAATGTGTGG 3'

**Reverse:**

5' CAGACCGCTTCTGCGTTC 3'

The determined nucleotide sequences were aligned with the known mRNA nucleotide sequence encoding *Homo sapiens* glutathione S-transferase A1 (GENE ID: 2938 GSTA1) using the alignment tool, BLASTN, in the NCBI BLAST suite of tools (Altschul *et al.*, 1990). The nucleotide sequence was translated using the Translate Tool on the ExPASy server and the I71V hGST A1 peptide sequence aligned with the known wild-type hGST A1 peptide sequence using the peptide alignment tool, LALIGN on the ExPASy server, to confirm the presence of the I71V mutation.

## **2.3 Preparation of I71V and wild-type hGST A1-1 proteins**

### **2.3.1 Protein over-expression and purification**

The heterologous over-expression of both I71V and wild-type hGST A1-1 protein was performed in accordance with in-house protocols, based on the method devised by Wallace *et al.* (1999), that incorporate the optimal growth conditions for the optimal expression of each protein. The *Escherichia coli* BL21 (DE3) cells transformed with wild-type pKHA1 plasmid were selectively cultured in the presence of the antibiotic Amp due to the conferred resistance encoded by the pKHA1 plasmid. *Escherichia coli* BL21 (DE3) pLysS cells transformed with the mutant pKHA1 plasmid were selectively cultured in the presence of both Amp and chloramphenicol due to the additional resistance conferred by the pLysS plasmid. All over-expression steps were conducted under sterile conditions. Cultures were propagated in sealed Erlenmeyer flasks that were five times greater in volume than that of the culture to ensure that the agitation supplied sufficient aeration during growth. The protocol for the heterologous over-expression of wild-type protein was the same as that for the mutant protein and is given below with included deviations where necessary.

A thawed glycerol stock of *Escherichia coli* BL21 (DE3) cells transformed with wild-type pKHA1 plasmid was used to inoculate 100 mL 2YT media supplemented with 100  $\mu\text{g}/\text{mL}$  Amp. Similarly, *Escherichia coli* BL21 (DE3) pLysS cells transformed with mutant pKHA1 plasmid were used for media supplemented with both 100  $\mu\text{g}/\text{mL}$  Amp and 34  $\mu\text{g}/\text{mL}$  chloramphenicol. The fresh cultures of *Escherichia coli* BL21 cells were incubated overnight (~16 h) at 37 °C under 250 rpm agitation. A 1:100 dilution of the overnight culture was used to inoculate ten 100 mL solutions of fresh 2YT media that contained the equivalent concentrations of appropriate antibiotic. The cells were incubated at 37 °C under 250 rpm agitation until mid-log phase ( $OD_{600} = 0.4\text{--}0.6$ ) (~4 h for wild-type and ~4.5 h for mutant) whereupon the over-expression of protein was induced by the addition of 1.0 mM IPTG and 0.2 mM IPTG for wild-type and mutant protein, respectively. The culture was incubated overnight under the aforementioned conditions.

The cultures were held on ice during brief transportation after which the cells were harvested by centrifugation at 5000 rpm for 20 min at 4 °C in a Sorvall SLA-3000 rotor. The supernatant was decanted and discarded. The pelleted cells were resuspended in minimal equilibration start buffer (10 mM sodium phosphate buffer, pH 7.45, containing 1 mM ethylenediaminetetraacetic acid (EDTA) and 0.02% sodium azide) using vigorous agitation on a benchtop vortex, and stored overnight at -20 °C to promote cell lysis. After thawing the frozen pellet at 4 °C under gentle rotation, the resuspended cells were lysed by incubation with 0.3 mg/mL lysozyme for 0.5–1 h at 4 °C, followed by pulse sonication on ice for six cycles of 30 s of medium intensity pulses using 0.5 s pulse intervals. The gelatinous lysate was diluted to 50 mL using equilibrium start buffer and the soluble cytosolic protein harvested by centrifugation at ~8000  $\times g$  for 30 min at 4 °C (15000 rpm in a Sorvall SS-34 rotor). The supernatant was decanted, diluted to 100 mL using equilibration buffer and filtered through a 0.2  $\mu\text{m}$  syringe filter. The final dilution and filtration steps were included to promote efficient binding of the proteins to the chromatographic column (see below) and to prevent clogging the chromatographic resin with residual cells or large aggregates of cleaved membranes.

The mutant and wild-type hGST A1-1 proteins were purified from the respective mutant and wild-type protein filtrates using CM-Sepharose cation-exchange chromatography in accordance with an in-house protocol adapted from the method proposed by Wallace *et al.* (1999). The pH of the filtrate was adjusted to pH 7.45 when necessary and loaded onto a CM-Sepharose column (58 mL resin-bed volume) pre-equilibrated with 8 column volumes (600 mL) equilibration buffer (see above for composition). The column was washed with ten column volumes (600 mL) equilibration buffer until the absorbance of column eluent at 280 nm was zero to ensure that all weakly interacting, unbound protein had been eluted. The bound hGST A1-1 protein was eluted from the column using a 0–0.3 M linear salt gradient (200 mL final volume) produced from the sequential mixing of equilibration buffer and elution buffer (10 mM sodium phosphate buffer, pH 7.45, containing 300 mM sodium chloride, 1 mM EDTA and 0.02% sodium azide). The eluent was collected as 2.5 mL fractions.

The presence of eluted protein was detected by measuring the absorbance at 280 nm ( $A_{280}$ ) of the eluent, in real-time, using the onboard spectrophotometer on the AKTA automated chromatographic system or by measuring the  $A_{280}$  values of each fraction using a Jasco V-550 UV/Vis spectrophotometer. Fractions containing pure hGST A1-1 protein with an  $A_{280} \geq 0.1$  were pooled and, only when necessary, concentrated on ice by ultrafiltration through an Amicon PM-10 membrane with a molecular weight cut-off of 10 kDa. The pooled hGST A1-1 solution was exhaustively dialysed into 1,3,5-trinitrobenzene (TNB) assay buffer (100 mM sodium phosphate, pH 6.5, containing 1 mM EDTA and 0.02% sodium azide) and filtered through a 0.2  $\mu\text{m}$  syringe.

A 10  $\mu\text{L}$  sample from each fraction was withdrawn for the assessment of protein size and homogeneity by discontinuous sodium dodecyl sulphate polyacrylamide gel electrophoresis (SDS-PAGE) using a 4% stacking gel, 15% separating gel as per the method established by Laemmli (1970). Samples of the filtered solution of pooled hGST A1-1 fractions were assessed by SDS-PAGE to determine the purity and size of the protein subunits. The filtered hGST A1-1 solution was aliquoted into cryogenic tubes and snap-frozen in liquid nitrogen. The hGST A1-1 aliquots were stored at -70 °C until use upon which they were thawed and

extensively redialysed into fresh TNB assay buffer. All experiments used the TNB assay buffer unless otherwise stated. It should be noted that whole cell extract samples were withdrawn from uninduced and induced transformed *Escherichia coli* BL21 (DE3) cells and analysed by SDS-PAGE for confirmation of induction. Similarly, samples were withdrawn from the supernatant and pellet of the lysed cells to ensure the success of the lyses steps, and from eluent at various stages of the loading and washing steps of the columning procedure to ensure the efficient binding of hGST A1-1 and removal of nonspecifically bound bacterial proteins.

### 2.3.2 Determination of protein concentration

The molar concentration of wild-type or mutant protein ( $c$ ) was determined spectrophotometrically using the Beer-Lambert law:

$$A = \epsilon_{\lambda}cl$$

where,  $A$  is the absorbance at 280 nm,  $\epsilon_{\lambda}$  is the molar absorption coefficient ( $M^{-1} cm^{-1}$ ) at the given wavelength  $\lambda$ , and  $l$  is the pathlength (cm) through which the light passes. The molar absorption coefficient ( $\epsilon$ ) for the wild-type and mutant protein was calculated using the equation (Perkins, 1986):

$$\epsilon = 5550 \Sigma Trp + 1340 \Sigma Tyr + 150 \Sigma Cys$$

where,  $\Sigma Trp$  is the sum of tryptophan residues,  $\Sigma Tyr$  is the sum of tyrosine residues and  $\Sigma Cys$  is the sum of cysteine residues within the protein; and the constants indicate the molar absorption coefficients for the respective residues. The sequencing results confirmed the presence of 1 Trp, 10 Tyr and 1 Cys residues per subunit. The molar absorption coefficient at 280 nm for dimeric wild-type and mutant hGST A1-1 was, therefore, calculated at  $38200 M^{-1} cm^{-1}$ .

The absorbance values at 280 nm were measured for a serially-diluted solution of hGST A1-1 and corrected for the effects of light scattering in accordance with the method proposed by Winder and Gent (1971). This correction method briefly involves the use of linear-regression analysis on plots of absorbance versus wavelength in the range 320–370 nm to determine the expected interference at 280 nm contributed from light scattering effects. This determined interference at 280 nm was subtracted from the measured absorbance at 280 nm to yield the corrected absorbance at 280 nm. Substitution of the corrected absorbance, the 38200 M<sup>-1</sup> cm<sup>-1</sup> absorption coefficient, and the 1 cm pathlength into the Beer-Lambert law (see above) yielded the corrected concentration (M) of soluble, dimeric hGST A1-1 protein.

#### **2.4 Spectroscopic structural studies of the I71V and wild-type hGST A1-1 proteins**

Structural characterisation studies were conducted on native and unfolded I71V and wild-type hGST A1-1 protein samples using the spectroscopic techniques far- and near-ultraviolet circular dichroism (far- and near-UV CD) and fluorescence spectroscopy. All samples of unfolded protein were prepared by the addition of concentrated urea stock solution (10.0 M) into protein solution and incubating the resultant 8.0 M-urea protein sample for a minimum of 1 h at 20 °C before collecting spectra. Urea stock solutions (10.2 M) were prepared by gravimetric analysis using ultra-pure urea in 2 mM sodium phosphate buffer, pH 6.5, containing 0.1 mM EDTA and 0.002% sodium azide. Fresh stock solutions of urea were prepared every 14 days and stored at -20 °C to prevent thermal decomposition. The concentrations of the urea stock solutions were confirmed through the analysis of the refractive index of the solution using equation (Pace, 1986):

$$[\text{Urea}] = 117.66(\Delta N) + 29.753(\Delta N)^2 + 18.56(\Delta N)^3$$

where, [Urea] is the concentration of urea (M) and  $\Delta N$  is the difference in refractive index between the buffered urea solution and the buffer solvent at the sodium D line.

## 2.4.1 Circular dichroism spectroscopy

### 2.4.1.1 Far-UV circular dichroism spectroscopy

Triplicate sample solutions (500  $\mu\text{L}$ ) of native and unfolded 2  $\mu\text{M}$  I71V and wild-type hGST A1-1 protein were prepared in 2 mM sodium phosphate buffer, pH 6.5, containing 0.1 mM EDTA and 0.002% sodium azide, in the absence and presence of 8.0 M urea, respectively. The unfolded samples were prepared using the aforementioned method of incubation in the presence of urea. Samples, at 20 °C, were irradiated with circular polarised light in the wavelength range 180–250 nm in a Jasco J-810 CD spectropolarimeter (Jasco, Japan) using a scan speed of 100 nm/min, 5 nm bandwidth filter and a 0.2 cm pathlength. The far-UV CD spectra between 180 and 250 nm were concurrently collected using a detector sensitivity of 100 mdeg, a response time of 0.5 s and a data pitch of 0.1 nm. The averaged spectrum for each sample was determined from the accumulation of spectra from five scans per sample. All contributions to the far-UV CD spectra from the buffer solution were accounted for by subtracting the spectrum collected for the blank buffer solution in the absence of protein.

The mean residue ellipticity,  $[\Theta]$  ( $\text{deg cm}^2 \text{ dmol}^{-1}$ ), was calculated at each wavelength using the equation (Woody, 1995):

$$[\Theta] = \frac{100 \times \Theta}{Cnl}$$

where,  $\Theta$  (mdeg) is the measured ellipticity signal at the respective wavelength,  $C$  is the protein concentration (mM),  $n$  is the total number of residues, and  $l$  is the pathlength (cm).

### 2.4.1.2 Near-UV circular dichroism spectroscopy

Triplicate sample solutions (500  $\mu\text{L}$ ) of native 40  $\mu\text{M}$  I71V and wild-type hGST A1-1 protein were prepared in 20 mM sodium phosphate buffer, pH 6.5, containing 1 mM EDTA and 0.02% sodium azide. Samples, at 4 °C, were irradiated with circular polarised light in the wavelength range 240–350 nm in a Jasco J-810 CD spectropolarimeter (Jasco, Japan) using a scan speed of 50 nm/min, 0.5 nm bandwidth filter and a 1 cm pathlength. The near-UV CD

spectra between 240 and 350 nm were concurrently recorded using a high detector sensitivity of 5 mdeg, a response time of 2.0 s and a data pitch of 0.2 nm. The averaged spectrum for each sample was determined from the accumulation of spectra from five scans per sample. All contributions to the near-UV CD spectra from the buffer solution were accounted for by subtracting the spectrum collected for the blank buffer solution in the absence of protein. The  $[\Theta]$  value at each wavelength was calculated using the equation given in section 2.4.1.1.

#### **2.4.2 Intrinsic fluorescence spectroscopy – Tryptophan fluorescence**

Triplicate sample solutions (500  $\mu$ L) of native and unfolded 2  $\mu$ M I71V and wild-type hGST A1-1 protein were prepared in 2 mM sodium phosphate buffer, pH 6.5, containing 0.1 mM EDTA and 0.002% sodium azide, in the absence and presence of 8.0 M urea, respectively. The unfolded samples were prepared using the aforementioned method of incubation in the presence of urea. Samples, at 20 °C, were irradiated with planar polarised light at the wavelengths 280 and 295 in a Perkin Elmer LS-50B Luminescence Spectrophotometer (Perkin Elmer, South Africa) using both excitation and emission bandwidth filters of 4 nm and a 1 cm pathlength. The intrinsic fluorescence emission spectra between 280 and 500 nm, for 280 nm excitation, and between 295 and 500 nm, for 295 nm excitation, were concurrently recorded using a scan speed of 100 nm/min. The averaged spectrum for each sample was determined from the accumulation of spectra from three scans per sample. All contributions to the fluorescence spectra from the buffer solution were accounted for by subtracting the spectrum collected for the blank buffer solution in the absence of protein.

### **2.5 Functional assays of the I71V and wild-type hGST A1-1 proteins**

#### **2.5.1 Non-substrate ligand-binding assays – ANS fluorescence**

The non-substrate, ligand-binding function of the I71V and wild-type hGST A1-1 proteins was investigated using the electrophilic, non-substrate ligands 8-anilino-1-naphthalene sulfonate (ANS), ethacrynic acid (EA) and glutathione sulfonate ( $\text{GSO}_3^-$ ). Stock solutions of the fluorescent ligand ANS (~2 mM) were prepared in accordance with the general procedure for spectrophotometrically determining the concentration of ANS at 350 nm ( $\epsilon_{350} = 4950 \text{ M}^{-1}$

cm<sup>-1</sup>) (Weber and Young, 1964). All stock solutions of ANS were prepared in 20 mM sodium phosphate buffer, pH 6.5, containing 1 mM EDTA and 0.02% sodium azide, and stored at 4 °C in a dedicated, foil-wrapped, dark glass bottle to circumvent photodecomposition and were used within 14 days of preparation. All samples were prepared by the addition of a concentrated stock solution of ANS to the buffer solution and the resultant 200 μM ANS sample solution incubated for a minimum of 1 h at 20 °C in the dark to promote the complete binding of ANS to the protein.

#### **2.5.1.1 ANS binding assay**

The binding of the anionic ligand ANS to the I71V and wild-type hGST A1-1 proteins was monitored by fluorescence enhancement in accordance with the method of Sluis-Cremer *et al.* (1996). Triplicate sample solutions (500 μL) of native and unfolded 2 μM I71V and wild-type hGST A1-1 protein were prepared in the presence of 200 μM ANS in 20 mM sodium phosphate buffer, pH 6.5, containing 1 mM EDTA and 0.02% sodium azide, and in the absence and presence of 8.0 M urea, respectively. The unfolded samples were prepared using the aforementioned method of incubation in the presence of urea. Samples, at 20 °C, were irradiated with planar polarised light at an excitation wavelength of 390 nm in a Jasco V-630 Luminescence Spectrophotometer (Jasco, Japan) using both excitation and emission bandwidth filters of 5 nm and a 1 cm pathlength. Primary inner filter effects were, thus, minimised by using a fluorescence excitation wavelength “on the red edge of the longest wavelength absorption band” (Birdsall *et al.*, 1983), i.e., at 390 nm. The ANS fluorescence emission spectra between 390 and 600 nm were concurrently recorded using a fast response scan speed of 200 nm/min, a 0.5 nm data pitch and a detector sensitivity of 420 V PMT voltage. The averaged spectrum for each sample was determined from the accumulation of spectra from three scans per sample. All spectra were subsequently adjusted for the fluorescence contribution from the free, unbound ANS.

#### **2.5.1.2 ANS displacement assays using EA and GSO<sub>3</sub><sup>-</sup> ligands**

The displacement of the anionic ligand ANS, bound to the H-site of the I71V and wild-type hGST A1-1 proteins, by the non-substrate ligands ethacrynic acid (EA) and glutathione

sulfonate ( $\text{GSO}_3^-$ ) was monitored by fluorescence quenching in accordance with the method of Dirr *et al.* (2005). The primary and secondary inner filter effects on the excitation and fluorescence of ANS were initially determined for the ligands EA and  $\text{GSO}_3^-$ . The absorbance of 200  $\mu\text{M}$  ANS in 20 mM sodium phosphate buffer, pH 6.5, containing 1 mM EDTA and 0.02% sodium azide, was measured at 390 and 480 nm in the presence of either 0–1000  $\mu\text{M}$  EA or 0–2000  $\mu\text{M}$   $\text{GSO}_3^-$ . All values were subsequently corrected for the contribution from the buffer component. All inhibitor concentrations with corresponding optical density increases below 0.2 absorbance units for each wavelength were used for subsequent displacement assays.

Triplicate sample solutions of 2  $\mu\text{M}$  I71V and wild-type hGST A1-1 protein were prepared in the presence of 200  $\mu\text{M}$  ANS in 20 mM sodium phosphate buffer, pH 6.5, containing 1 mM EDTA and 0.02% sodium azide. The displacement assay was initiated by supplementing an assay solution with either 0–1000  $\mu\text{M}$  EA or 0–2000  $\mu\text{M}$   $\text{GSO}_3^-$  to create a final assay volume of 500  $\mu\text{L}$ . Samples, at 20 °C, were irradiated with planar polarised light at an excitation wavelength of 390 nm in a Jasco V–630 Luminescence Spectrophotometer (Jasco, Japan) using both excitation and emission bandwidth filters of 5 nm and a 1 cm pathlength. The ANS fluorescence emitted at 480 nm was concurrently monitored using a fast response scan speed of 100 nm/min, a 0.5 nm data pitch and a detector sensitivity of 420 V PMT voltage. The averaged spectrum for each sample was determined from the accumulation of spectra from three scans per sample. All spectra were subsequently adjusted for the fluorescence contribution from free, unbound ANS.

### **2.5.2 Standard GSH-CDNB conjugation assay**

The specific activities of the I71V and wild-type hGST A1-1 proteins were determined using the standard GSH-CDNB conjugation assay proposed by Habig *et al.* (1974). The enzyme-catalysed conjugation of 1-chloro-2,4-dinitrobenzene (CDNB) to GSH at 20 °C was monitored spectrophotometrically by measuring the absorbance at 340 nm upon formation of the chromophoric product 1-(*S*-glutathionyl)-2,4-dinitrobenzene. Triplicate sample solutions of 1–10  $\mu\text{M}$  mutant and wild-type hGST A1-1 protein were prepared in 0.1 M sodium

phosphate buffer, pH 6.5, containing 1 mM EDTA and 0.02% sodium azide, in the presence of 1 mM GSH. The conjugation reaction was initiated by the addition of 90  $\mu\text{L}$  of a 33.3 mM stock solution of CDNB (solubilised in ethanol) to create a final assay CDNB concentration of 1 mM and a final assay volume of 3.0 mL. The reaction was followed as linear progress curves by measuring the absorbance at 340 nm for 1 min at 20 °C using a Jasco V-630 UV/Vis spectrophotometer interfaced with a computer. The ethanol concentration was held constant at 3% (v/v).

The change in concentration of the 1-(*S*-glutathionyl)-2,4-dinitrobenzene complex formed at the active sites was calculated using the extinction coefficient of the chromophore at 340 nm ( $\epsilon_{340} = 9600 \text{ M}^{-1} \text{ cm}^{-1}$ ) (Habig *et al.*, 1974) after correcting for the absorbance contribution from the 1-(*S*-glutathionyl)-2,4-dinitrobenzene complex formed in the absence of enzyme. The specific activity ( $\mu\text{mol min}^{-1} \text{ mg}^{-1}$ ) was determined by linear regression as the slope of a plot between the initial velocity of complex formation ( $\mu\text{mol min}^{-1}$ ) versus the mass of protein (mg).

### **2.5.3 Formation of the $\sigma$ -complex between GSH and TNB**

#### **2.5.3.1 Spectroscopic characterisation of the $\sigma$ -complex**

The formation of the 1-(*S*-glutathionyl)-2,4,6-trinitrocyclohexadienate  $\sigma$ -complex between GSH and 1,3,5-trinitrobenzene (TNB) at the active sites of the I71V and wild-type hGST A1-1 proteins at 20 °C was monitored by spectrophotometry in accordance with the general method of Graminski *et al.* (1989) but employing the adaptations proposed by Widersten *et al.* (1996). Triplicate sample solutions of 20  $\mu\text{M}$  I71V and wild-type hGST A1-1 protein were prepared in 0.1 M sodium phosphate buffer, pH 6.5, containing 1 mM EDTA and 0.02% sodium azide, in the presence of 5 mM GSH. The formation of the  $\sigma$ -complex was initiated by the titration of concentrated stock solutions (2.5–60 mM) of TNB, dissolved in acetonitrile, into the sample solutions to create a final TNB concentration of between 0 and 1200  $\mu\text{M}$  and a final assay volume of 1 mL. The concentration of acetonitrile was held constant at 2% (v/v). Absorbance spectra between 270 and 650 nm were recorded on a Jasco V-630 spectrophotometer using a standard 1.5 nm bandwidth. The averaged spectrum for

each sample was determined from the accumulation of spectra from three scans per sample using a scan speed of 400 nm/min. All spectra were subsequently adjusted for the absorbance contribution from the formation of the  $\sigma$ -complex in the absence of protein.

### 2.5.3.2 Spectrophotometric determination of the formation constant of the $\sigma$ -complex

The formation constant ( $K_F$ ) of the 1-(*S*-glutathionyl)-2,4,6-trinitrocyclohexadienate  $\sigma$ -complex formed at the active sites of I71V and wild-type hGST A1-1 protein at 20 °C was determined from spectrophotometric titrations in accordance with a method adapted from that of Widersten *et al.* (1996). The spectrophotometric titration employed conditions in which TNB was in excess of the concentration of the  $\sigma$ -complex, a condition obtained using a concentration of TNB in far excess of the concentration of the GST·GSH complex, i.e., [TNB]  $\gg$  [E·GSH] (Widersten *et al.*, 1996).

Triplicate sample solutions of 17  $\mu$ M I71V and 15  $\mu$ M wild-type hGST A1-1 protein were prepared in 0.1 M sodium phosphate buffer, pH 6.5, containing 1 mM EDTA and 0.02% sodium azide, in the presence of 5 mM GSH. The formation of the  $\sigma$ -complex was initiated by the titration of concentrated stock solutions (25 mM, 50 mM and 100 mM) of TNB, dissolved in acetonitrile, into the sample solutions to create a final TNB concentration of between 0 and 1050  $\mu$ M and a final assay volume of 1 mL. The concentration of acetonitrile was held constant at 2% (v/v). The formation of the  $\sigma$ -complex was monitored by measuring the absorbance at 450 nm on a Jasco V-630 spectrophotometer using a standard 1.5 nm bandwidth. The recorded absorbance values were adjusted for the absorbance contribution from the formation of the  $\sigma$ -complex in the absence of protein.

The value of  $K_F$  was determined by non-linear regression analysis of a plot of absorbance at 450 nm versus the concentration of TNB using the equation (Widersten *et al.*, 1996):

$$A_{450} = \frac{(A_{\max}/[E]_0)([TNB])}{1/K_F + [TNB]}$$

where,  $A_{450}$  is the measured absorbance at 450 nm,  $A_{\max}$  is the absorbance at 450 nm under saturating conditions of GSH and TNB,  $[E]_0$  is the concentration of hGST A1 subunit,  $[TNB]$  is the final concentration of TNB, and  $K_F$  is the formation constant of the  $\sigma$ -complex derived from the inverse of  $K_d$  value that is directly determined by the regression analysis (hence the  $1/K_F$  expression).

## 2.6 Thermal-induced unfolding study of the I71V and wild-type hGST A1-1 proteins

The thermal-induced equilibrium unfolding of the I71V and wild-type hGST A1-1 proteins was assessed by probing the extent of  $\alpha$ -helix denaturation in response to changes in temperature. Triplicate samples of 2  $\mu$ M I71V and wild-type hGST A1-1 protein were prepared in 20 mM sodium phosphate buffer, pH 6.5, containing 1 mM EDTA and 0.02% sodium azide. Samples were subjected to the elevation and subsequent depression of temperature between 4 and 80  $^{\circ}$ C using a continuous temperature gradient of 1  $^{\circ}$ C/min, controlled by a Jasco PTC-423S Peltier-Type thermostat control system attached to a water-cooling bath. Samples were concurrently irradiated with 222 nm circular polarised light using a Jasco J-810 CD spectropolarimeter (Jasco, Japan) employing a 5 nm bandwidth filter and a 0.2 cm pathlength. The far-UV CD measurements of ellipticity  $\Theta$  (mdeg) at 222 nm was monitored using a 0.5 s response time, standard (100 mdeg) sensitivity and a 0.1  $^{\circ}$ C data pitch. The recorded ellipticity values were corrected for solvent contributions, converted to mean residue ellipticity (see section 2.4.1.1 for method) and plotted against the corresponding temperature values.

## CHAPTER 3

### RESULTS AND DISCUSSION

#### 3.1 Purity and sequencing of the mutant and wild-type cDNA

The miniprep plasmid purification procedures produced 5.0  $\mu\text{g}$  (50  $\mu\text{L}$  of 100  $\text{ng}/\mu\text{L}$ ) mutant pKHA1 plasmid complementary deoxyribonucleic acid (cDNA) and 9.0  $\mu\text{g}$  (50  $\mu\text{L}$  of 180  $\text{ng}/\mu\text{L}$ ) wild-type pKHA1 plasmid cDNA. The ratio of the absorbance at 260 nm ( $A_{260}$ ), contributed from the cDNA, to the absorbance at 280 nm ( $A_{280}$ ), contributed from protein impurities, (i.e.,  $A_{260}/A_{280}$ ) for the purified stock solution of mutant pKHA1 plasmid was equal to 2.0 whereas the ratio for the purified stock solution of wild-type pKHA1 plasmid was equal to 1.9. These  $A_{260}/A_{280}$  values exceeded the minimum requirement of  $1.8 \leq A_{260}/A_{280} \leq 1.95$  (Maniatis *et al.*, 1982). Similarly, the ratio of the  $A_{260}$  to the absorbance at 230 nm ( $A_{230}$ ), contributed from bacterial carbohydrate impurities, (i.e.,  $A_{260}/A_{230}$ ) for the purified stock solution of mutant pKHA1 plasmid was equal to 2.1 whereas the ratio for the purified stock solution of wild-type pKHA1 plasmid was equal to 2.2. The stock solutions of mutant and wild-type pKHA1 plasmid were, therefore, of sufficient concentration and purity for the sequence analysis and competent-cell transformation procedures.

The sequencing results indicate that the nucleotide sequence of the wild-type hGST A1-1 cDNA ORF corresponds exactly to the sequence identified by Stenberg *et al.* (1992). The only discrepancy between the Stenberg *et al.* (1992) nucleotide sequence and the expected 'wild-type hGST A1-1' nucleotide sequence is the inclusion of a thymine nucleotide in place of the expected cytosine nucleotide at the position 426. The presence of this single, silent, point mutation does not alter the translated amino acid sequence of the wild-type hGST A1-1 protein due to the degeneracy of the mis-incorporated GTC and 'wild-type' GCC codons that both encode a serine residue (Stenberg *et al.*, 1992) at amino acid position 142.

Figure 5 shows a portion of the nucleotide sequencing chromatograms with the corresponding DNA base sequences and deduced amino acid sequences of the wild-type (Figure 5 A) and mutant (Figure 5 B) hGST A1-1 ORFs that verify the incorporation of the desired mutation. Six base mutations were observed in the ORF encoding the I71V hGST A1-1 protein. Only one of the six in-frame mutations (ATT → GTC) was translationally active, thus, incorporating the GTC codon that encodes a valine residue (Figure 5 B) in place of the ATT codon that encodes the isoleucine residue (Figure 5 A) at amino acid position 71.

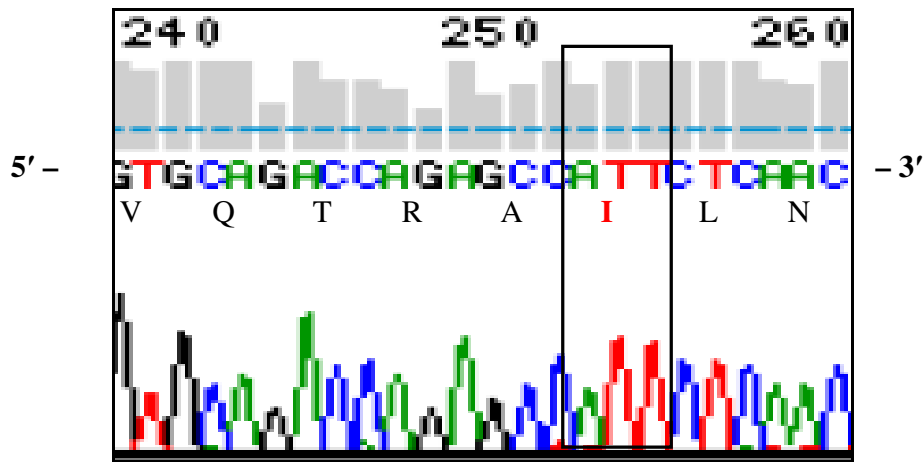
### **3.2 Purity of the I71V and wild-type hGST A1-1 proteins**

The purification of the I71V and wild-type hGST A1-1 proteins produced a single, symmetrical peak at ~160 mM sodium chloride in the elution profiles for each protein. Figure 6 depicts a representative elution profile for the wild-type hGST A1-1 protein. The presence of the single peak suggested that a homogeneous population of proteins were found in the eluent.

The SDS-PAGE analysis of the eluted proteins verified the purity and size of the I71V and wild-type hGST A1-1 proteins (Figure 7). A single, broad band above the 25.0 kDa marker was observed for each of the electrophoresed mutant and wild-type proteins (Figure 7 A). The distance migrated by each of the aforementioned bands corresponded to a subunit molecular mass of ~27 kDa (Figure 7 B). These values compared well with the calculated molecular mass of 25.631 kDa for the wild-type hGST A1-1 subunit and 25.617 kDa for the I71V hGST A1-1 subunit, determined using the software program ProtParam (Gasteiger *et al.*, 2005). The presence of a single discrete band for each protein comparable in size to the Alpha GST subunit verified that the purifications yielded electrophoretically homogeneous batches of the I71V and wild-type hGST A1-1 proteins.

One litre of culture of the mutant and wild-type *Escherichia coli* transformants was found to yield ~270 mg of purified I71V hGST A1-1 and ~200 mg of purified wild-type hGST A1-1 protein, respectively.

A



B

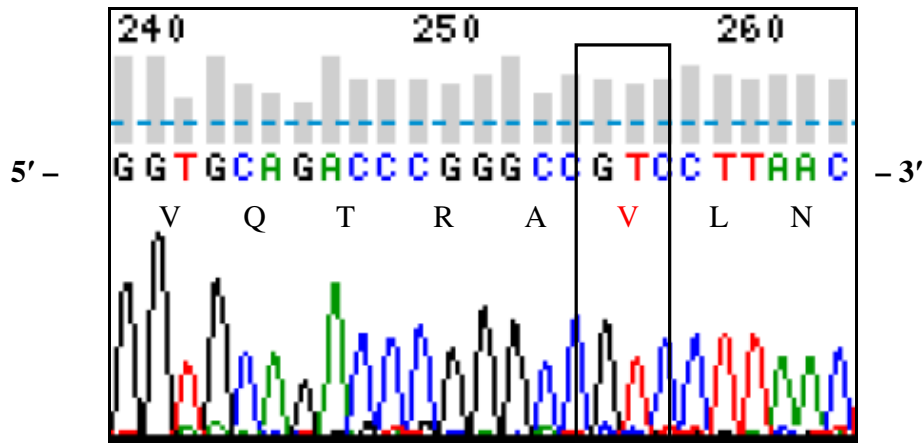


**Figure 5. A portion of the nucleotide sequencing chromatograms for the hGST A1-1 cDNA ORF emphasising the desired codon mutation responsible for the corresponding I71V hGST A1-1 protein sequence.**

(A) A segment of the sequenced wild-type, and (B) I71V hGST A1-1 cDNA ORFs aligned with the corresponding translated amino acid sequences that respectively correlate with the I71V and wild-type hGST A1-1 protein sequences between amino acids 66–73 (Stenberg *et al.*, 1992). The black rectangles indicate the translationally active ATT → GTC mutation responsible for the Ile-71 → Val mutation in the amino acid sequence. The grey blocks indicate the percentage signal intensity of the respective base above the 20% signal value (—) delineating the lower limit for reliable, significant sequencing results.

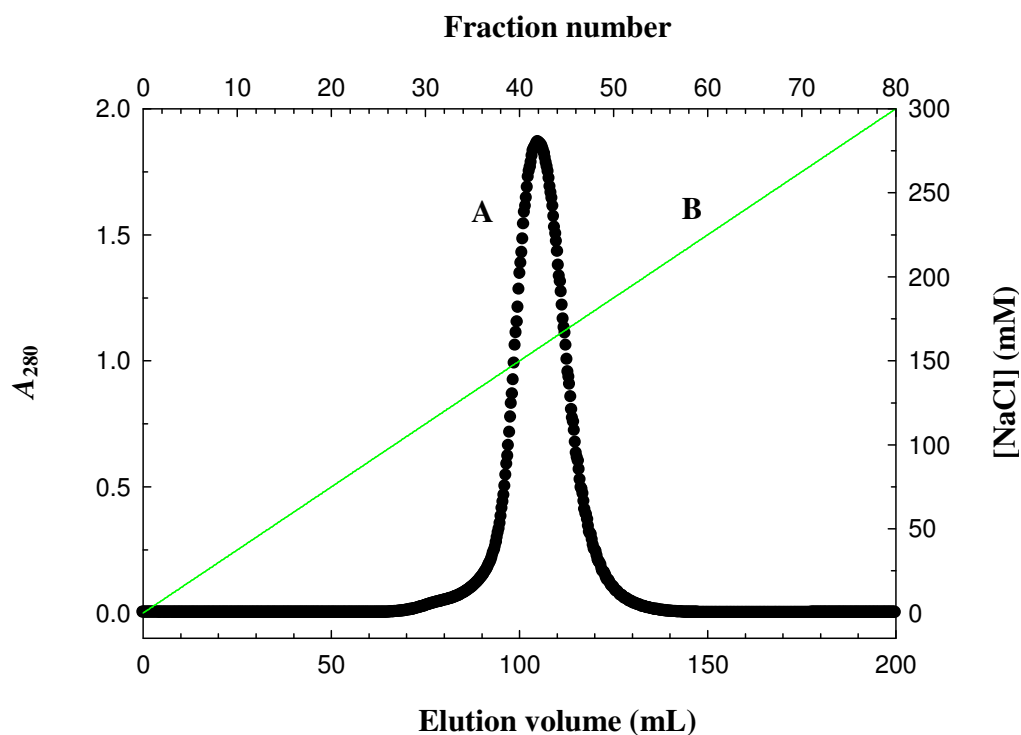


**Figure 6. Elution profile of the wild-type hGST A1-1 protein eluted from the fast-flow CM-Sephacrose cation-exchange column.**

Plots are of (A) the absorbance at 280 nm ( $A_{280}$ ) of eluted protein (●) corrected for the absorbance contribution of solvent, and (B) the linear, 200 mL 0 – 0.3 M sodium chloride gradient (∕) used to elute the protein. The protein was eluted in 10 mM sodium phosphate buffer, pH 7.45, containing 1 mM EDTA and 0.02% sodium azide and collected in 2.5 mL fractions.

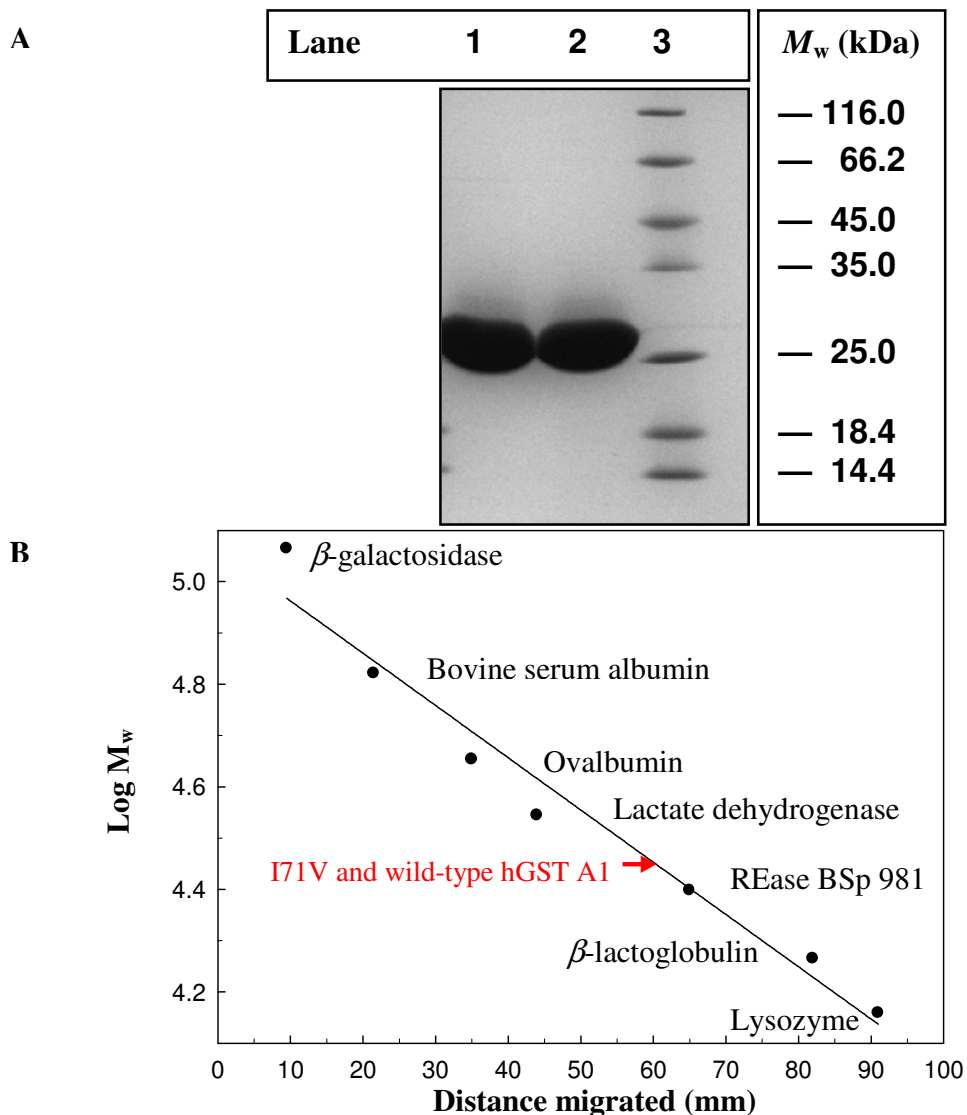


**Figure 7. SDS-PAGE analysis of the purity and size of the I71V and wild-type hGST A1 subunits.**

(A) SDS-PAGE gel (15%) depicting the hGST A1 subunits of the I71V and wild-type proteins. Lanes 1 and 2 contain 10  $\mu$ g samples of I71V and wild-type hGST A1-1 protein, respectively. Lane 3 contains Fermentas molecular mass markers:  $\beta$ -galactosidase (116.0 kDa), bovine serum albumin (66.2 kDa), ovalbumin (45.0 kDa), lactate dehydrogenase (35.0 kDa), REase BSp 981 (25.0 kDa),  $\beta$ -lactoglobulin (18.4 kDa) and lysozyme (14.4 kDa). (B) Calibration curve constructed from the mobilities of SDS-PAGE molecular mass standards depicting the logarithm of molecular mass ( $M_w$ ) versus the respective distances migrated. The molecular mass of the I71V and wild-type hGST A1 subunits ( $\rightarrow$ ) is determined by interpolating their mobilities on the straight line, using linear regression analysis ( $R^2 = 0.97$ ).

### 3.3 Structural properties of the I71V and wild-type hGST A1-1 proteins

#### 3.3.1 Secondary structure

The far-UV CD spectral properties of the folded and chemically unfolded secondary structures of the I71V and wild-type hGST A1-1 proteins are illustrated in Figure 8. The spectra of both the native I71V and wild-type hGST A1-1 proteins (Figure 8 A) were characterised by an intense positive band of mean residue ellipticity at 190 nm and two weaker-intensity negative bands at 208 and 220 nm. These spectral features are characteristic of native proteins composed of predominantly  $\alpha$ -helical peptides (Woody, 1995).

The 190 and 208 nm bands are a result of the absorption of circular polarised electromagnetic waves by the electrons in the carbonyl  $\pi$ -bonding orbital of the peptide-backbone amide bonds. The electrons are consequently excited resulting in their low-energy electronic transition to the next available higher energy orbital, the empty anti-bonding pi-bond orbital, i.e.  $\pi \rightarrow \pi^*$  (Woody, 1995). Similarly, the negative band observed at 220 nm is associated with the transition of an electron from the amide non-bonding orbital to the anti-bonding pi orbital, i.e.  $n \rightarrow \pi^*$ , normally present at 222 nm (Woody, 1995). High concentrations of anti-parallel  $\beta$ -sheet amide bonds typically result in a comparably weaker-intensity spectrum composed of a positive band between 195 nm and 198 nm due to the  $\pi \rightarrow \pi^*$  transition and a negative band between 215 nm and 217 nm from the  $n \rightarrow \pi^*$  transition (Woody, 1996). Both bands are invisible in the far-UV CD spectra, which corroborates the deduction that the native protein is composed of predominantly  $\alpha$ -helical peptides.

The aforementioned bands disappeared upon the exposure of the mutant and wild-type proteins to the unfolding conditions of an 8 M concentration of the chemical denaturant urea (Figure 8 B). The featureless CD spectra at a mean residue ellipticity  $[\Theta]$  equal to  $\sim 0 \text{ deg cm}^2 \text{ dmol}^{-1}$  is characteristic of a denatured, unfolded protein that has undergone the urea-induced disruption of all its secondary structural components, i.e., the absence of  $\alpha$ -helices and  $\beta$ -strands with the resultant predominance of random coils. The spectral properties of the native and unfolded wild-type protein are similar to those illustrated for the wild-type hGST A1-1 protein by Wallace *et al.* (1999), thus, confirming the precision and accuracy of the results

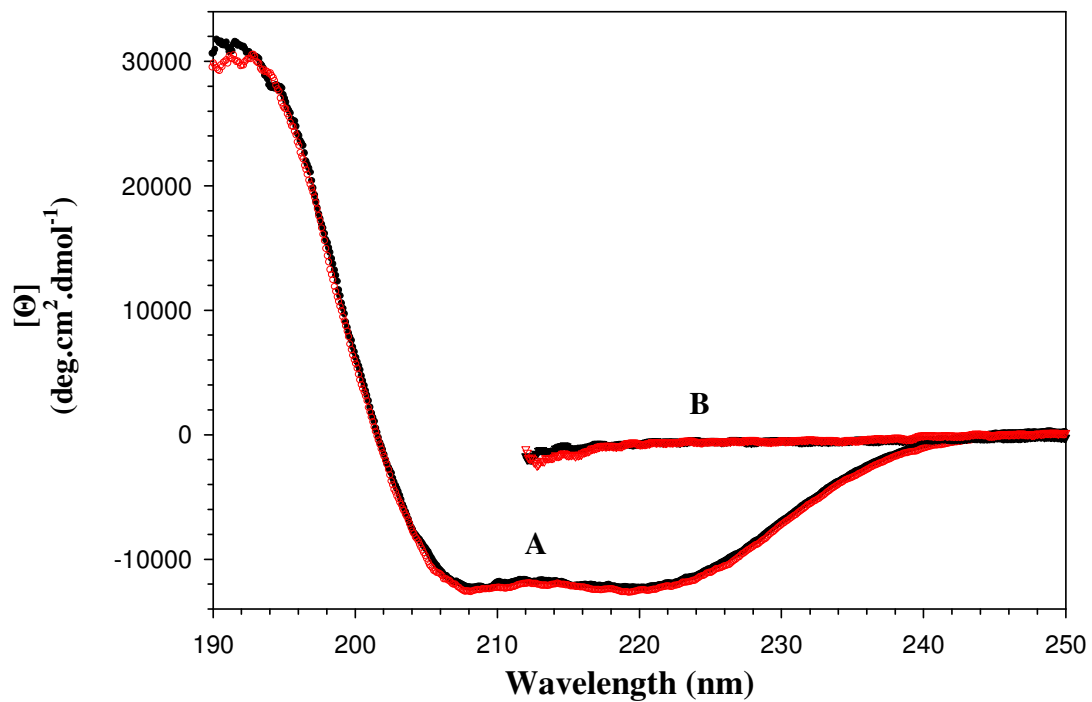


**Figure 8. Far-UV CD spectra of I71V (○▽) and wild-type (●▼) hGST A1-1.**

Spectra are recorded from (A) native wild-type (●) and I71V (○) hGST A1-1 in the absence of urea, and (B) denatured wild-type (▼) and I71V (▽) hGST A1-1 in the presence of 8 M urea. The protein concentration was 2  $\mu$ M in 2 mM sodium phosphate buffer, pH 6.5, containing 0.1 mM EDTA and 0.002% sodium azide. Each spectrum represents the average spectrum obtained from three or four different protein samples at 20 °C.

within the current study. The spectral properties of the native and unfolded mutant protein are similar to those of the wild-type protein, suggesting that there is no significant difference in the secondary structural content of the protein upon the introduction of the I71V mutation.

This resolution limit of the far-UV CD technique is, however, duly acknowledged by the fact that the CD technique characterises the average global protein structure.  $\alpha$ -Helices are known to produce the most pronounced far-UV CD spectral bands for polypeptides (Holzwarth and Doty, 1965). In addition to this, far-UV CD produces the most accurate determinations of  $\alpha$ -helix content compared to other secondary structure components (Woody, 1995). These technical advantages are, however, overshadowed by the fact that  $\alpha$ -helix 3, the site of the Ile-71  $\rightarrow$  Val mutation, constitutes only a small portion of the global secondary structural content of hGST A1-1 making an equivalently small contribution to the far-UV CD spectrum. Should a structural change have occurred in  $\alpha$ -helix 3, the intrinsically poor resolution of the technique could render such changes undetectable.

### **3.3.2 Tertiary structure**

#### **3.3.2.1 Intrinsic fluorescence properties**

The electrons in the indole-ring side chain of tryptophan undergo fluorescence relaxation when irradiated with an excitation wavelength of 295 nm (Lakowicz, 1983). The fluorescence properties of the indole ring are influenced by the polarity of its environment and, thus, provide a sensitive indicator of changes in the local environment of tryptophan. The presence of one tryptophan residue in each subunit of the I71V and wild-type proteins allows one to probe for changes in the tertiary conformation of these proteins. The phenyl ring of tyrosine exhibits weaker fluorescence properties to those of tryptophan when irradiated at its excitation wavelength maxima at 280 nm. The use of 280 nm excitation does, however, result in the transfer of fluorescence resonance energy (FRET) from excited tyrosine to tryptophan that culminates in a more intense fluorescence emission spectrum (Lakowicz, 1983). The 10 tyrosine residues within each subunit of the mutant and wild-type proteins therefore provide a more sensitive detection system of changes to the tertiary structure of a protein through the FRET system. A difference in fluorescence intensity

between the emission spectra of the native I71V and wild-type proteins would indicate a difference in the tertiary environment's ability to quench the fluorescence energy emitted by the excited tryptophan residue. A blue or red shift in the maximum emission wavelength between the emission spectra of the native I71V and wild-type proteins would indicate a respective decrease or increase in the polarity of the tertiary environment around the tryptophan residues.

The selective excitation of the tryptophan and tyrosine residues within each subunit, by irradiation at 280 nm, yielded a fluorescence emission maximum at 331 nm for both the native I71V and wild-type hGST A1-1 proteins (Figure 9 A (N)). The fluorescence emission maximum for both the mutant and wild-type protein shifted to 357 nm upon the denaturation of the proteins (Figure 9 A (U)). An additional weaker intensity secondary peak was observed at 310 nm in the denatured protein emission spectra which corresponds to the emission wavelength of denatured tyrosine residues submerged in solvent. Figure 9 B depicts the emission spectra for the I71V and wild-type proteins in native (Figure 9 B (N)) and denaturing (Figure 9 B (U)) conditions using an excitation wavelength of 295 nm. The spectra for the native mutant and wild-type proteins exhibited a fluorescence emission maximum at 331 nm and 332 nm, respectively, which both shifted to 357 nm upon denaturation of the proteins. The 7% decrease in fluorescence intensity, at both 280 and 295 nm excitation, between the spectra of native mutant and wild-type proteins is mirrored by the 8% decrease in fluorescence intensity between the corresponding spectra of the denatured proteins, a characteristic that is assigned to small discrepancy in the concentration of the proteins rather than to small changes between the tertiary conformations of the mutant and wild-type proteins. The lack of a significant difference in fluorescent intensity or difference in maximum emission wavelength between the emission spectra of the mutant and wild-type proteins suggests the absence of a significant change to the local and global tertiary conformation upon the introduction of the Ile-71 → Val mutation.

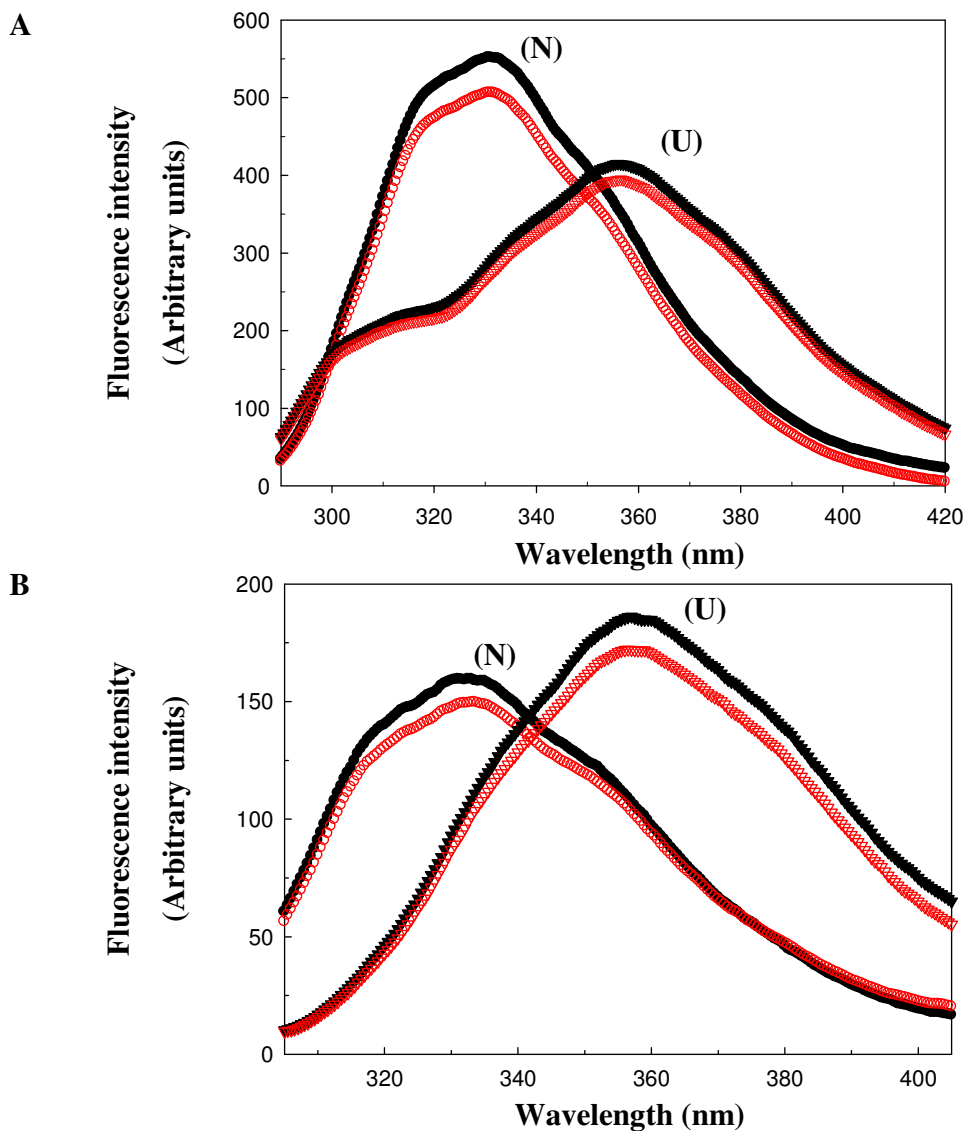


**Figure 9. Fluorescence emission spectra of native and unfolded I71V and wild-type hGST A1-1.**

The proteins were excited at (A) 280 nm and (B) 295 nm and the emission spectra recorded using an excitation and emission bandwidth filter of 5 nm. (N) Represents the emission maxima at 331 nm for the native I71V (○) and wild-type (●) proteins in the absence of urea. (U) Represents the emission maxima at 357 nm for the denatured I71V (▽) and wild-type (▼) proteins in the presence of 8.0 M urea. The spectra from the 280 nm excitation of denatured protein exhibited an additional peak at 310 nm. The protein concentration was 2  $\mu$ M in 2 mM sodium phosphate buffer, pH 6.5, containing 0.1 mM EDTA and 0.002% sodium azide.

### 3.3.2.2 Near-UV circular dichroism properties

Near-ultraviolet circular dichroism was employed to probe the tertiary structure of the I71V and wild-type protein by characterising the CD anisotropy present in the overlapping absorbance bands of the amino acid side chains. The near-UV CD spectrum (Figure 10) recorded from the wild-type protein does not overlay with that from the mutant but appears to contain the same number of minima and maxima bands at the same wavelengths distinguished only by a translation along the  $[\Theta]$  ordinate axis. The wild-type spectrum reveals a negative band between 250 nm and 275 nm and between 292 nm and 300 nm, and a positive band between 275 and 292 nm. This spectrum is in agreement with the near-UV CD spectrum reported for wild-type hGST A1-1 by Dirr and Wallace (1999). The mutant protein spectrum reveals a comparable near-UV CD spectrum between the same ranges of wavelengths except for the initial negative band extending to 280 nm resulting in the positive band extending only from 280–292 nm. Negative bands are observed in both spectra at 260 nm, 266 nm and 295 nm. Positive bands are observed in the wild type spectrum in the order of increasing intensity at 273 nm, 283 nm and 288 nm, respectively. The I71V spectrum reveals the same pattern of intensity and location of maxima as that found in the wild-type but differs in the fact that the 273 nm band is a negative band. The enhancement of the 266 nm negative band suggests that the environment around the phenylalanine residues have become more asymmetrical. The near-UV spectra do, however, suggest that the environment surrounding the tyrosine residues are more asymmetrical in I71V hGST A1-1 as compared to wild-type hGST A1-1.

The near-UV CD spectra and intrinsic fluorescence spectra indicate that the global tertiary structure of I71V hGST A1-1 protein is largely indistinguishable from that of wild-type hGST A1-1 protein.

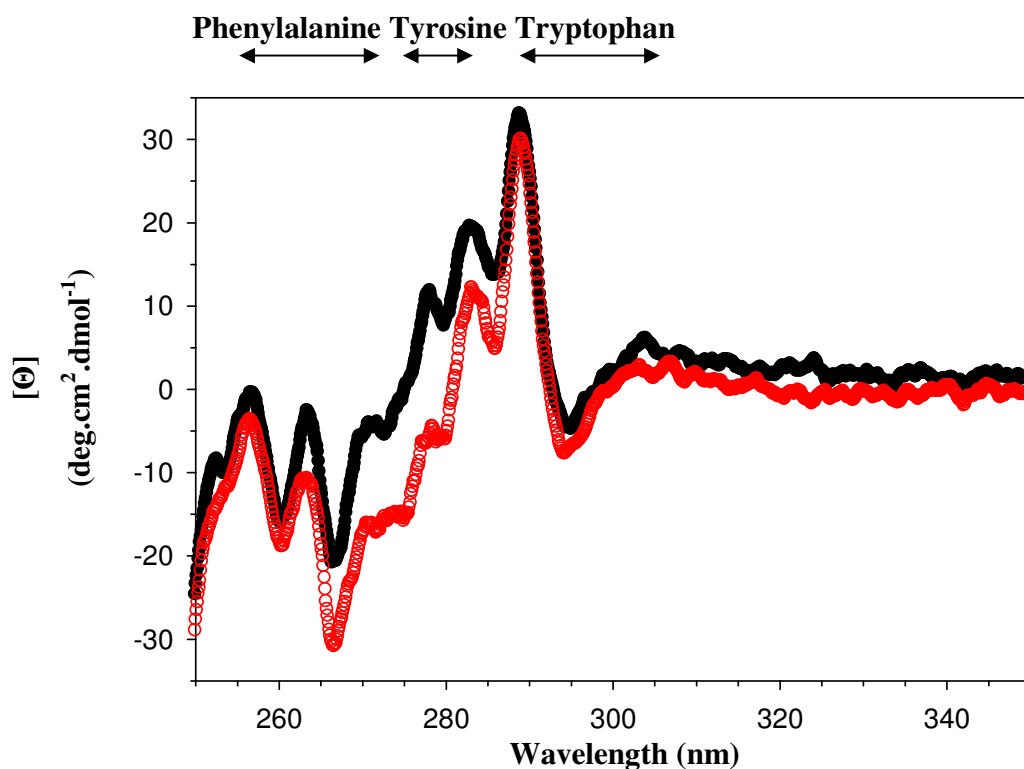


**Figure 10. Near-UV CD spectra for native I71V (○) and wild-type (●) hGST A1-1.**

The wavelength ranges for typical vibronic transitions for phenylalanine, tyrosine and tryptophan are indicated (Kelly *et al.*, 2005). The protein concentration was 40  $\mu$ M in 20 mM sodium phosphate buffer, pH 6.5, containing 1 mM EDTA and 0.02% sodium azide. Four replicate samples per protein were each scanned three times at 4 °C to produce the average spectra above.

### 3.3.3 Structures of the I71V and wild-type hGST A1-1 proteins

The crystal structure of the mutant protein I71V hGST A1-1 (2R6K, Dirr *et al.*, to be published) became available during the course of this study. A structural analysis of the crystal structures of mutant and wild-type hGST A1-1 (1K3L, Le Trong *et al.*, 2002) has, therefore, been conducted to contextualise the experimental results. The conclusions drawn from the far-UV CD spectra of predominantly  $\alpha$ -helical native mutant and wild-type hGST A1-1 protein structures is consistent with the 59%  $\alpha$ -helical crystal structures of the mutant and wild-type hGST A1-1 proteins. The findings of a similar far-UV CD spectral properties of the mutant and wild-type proteins are supported by the analysis of the superimposed fits of the mutant and wild-type proteins that illustrate the similar super-secondary structures of the protein (Figure 11).

The fluorescence and near-UV CD results indicated that there was no significant difference between the tertiary conformations of the I71V and wild-type proteins. An analysis of the superimposed crystal structures of the I71V hGST A1-1 (2R6K, Dirr *et al.*, to be published) and wild-type hGST A1-1 (1K3L, Le Trong *et al.*, 2002) proteins reveals that the removal of the  $\delta$ -methyl group of Ile-71 upon replacement of Ile-71 with valine in the mutant protein results in the formation of a cavity in a hydrophobic core of domain 1 (Figure 12). Figure 12 A depicts the superimposed crystal structures of the environment of the Ile-71 (wild-type protein) and Val-71 residues (mutant protein) in subunit B highlighting the 27 Å<sup>3</sup> cavity found in the mutant protein structure. The cavity has a surface area of 48 Å<sup>2</sup> which is defined by its contacts with residues Thr-19 and Met-16 ( $\alpha$ -helix 1), Pro-56, Val-58 ( $\beta$ -strand 3), and Thr-68 and Val-71 ( $\alpha$ -helix 3). In addition to this, the cavity is within a short distance of the backbone of Val-66 ( $\alpha$ -helix 3) and the side chains of Gln-67 and Leu-72 ( $\alpha$ -helix 3). The truncation of the Ile-71  $\delta$ -residue upon replacement of Ile-71 with valine in the mutant protein results in the loss of a van der Waals contact with Pro-56 (Figure 12 B). This loss in hydrophobic-hydrophobic interaction does not appear to affect the conformation of the side chains surrounding the Ile-71 residue but it does indicate that the stability of the hydrophobic core in domain 1 is likely to be compromised.

The similarity of the tertiary conformation of the I71V and wild-type proteins is illustrated by

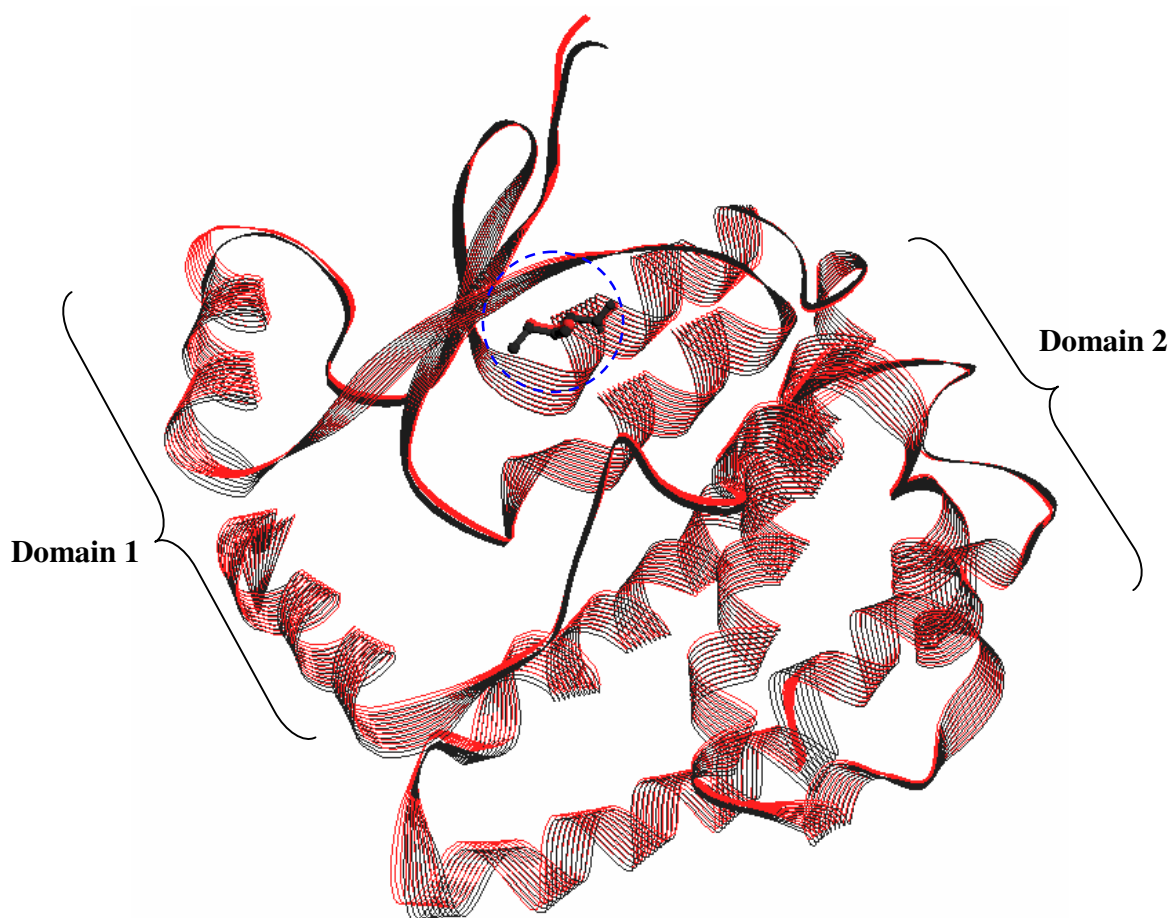


**Figure 11. Wire-frame ribbon diagram depicting the secondary structures of the superimposed crystal structures of subunit A of the I71V and wild-type hGST A1-1 proteins.**

The superimposed crystal structures of the mutant (red) and wild-type (black) proteins reveal the similarity between the secondary structures of protein subunit A. The Val-71 (mutant protein) and Ile-71 (wild-type protein) residues within domain 1 of each protein are enclosed within the dashed blue circle. The superimposed fits were generated from the coordinates of the backbone  $\alpha$ -carbons and the root mean square deviation between the two structures was calculated as 0.51 Å. This figure was generated from pdb files 2R6K (Dirr *et al.*, to be published) (I71V hGST A1-1) and 1K3L (Le Trong *et al.*, 2002) (wild-type hGST A1-1) using Swiss-PdbViewer version 4.0.1 (Guex and Peitsch, 1997).

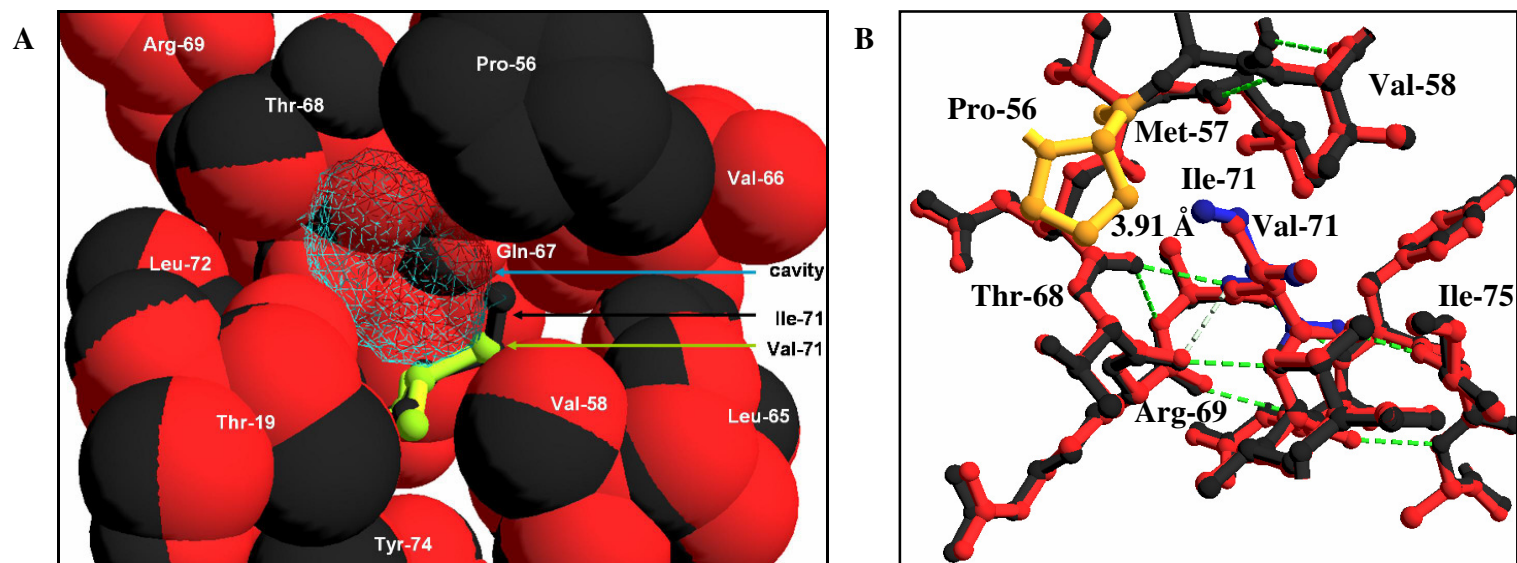


**Figure 12. Spacefilling representation of the cavity created within a hydrophobic core of domain 1 in the I71V hGST A1-1 protein and the loss of van der Waals contacts.**

(A) The aligned crystal structures of the mutant (red) and wild-type (black) proteins reveal the presence of a cavity (blue mesh) in domain 1 of the mutant protein. The amino acid residues neighbouring the cavity are labelled and depicted in spacefilling mode; the surrounding Ile-71 (wild-type protein) and Val-71 (mutant protein) residues are shown in ball and stick mode for clarity. The cavity has a volume of  $27 \text{ \AA}^3$  and a surface area of  $48 \text{ \AA}^2$ . (B) The loss of the van der Waals contact between the side chain of the residue at position 71 in hGST A1-1 upon introduction of the Ile-71  $\rightarrow$  Val mutation. The Ile-71 residue is shown in blue. The distance between the Ile-71 residue and Pro-56 is shown in angstroms. This figure was generated from the pdb files 2R6K (Dirr *et al.*, to be published) (I71V hGST A1-1) and 1K3L (Le Trong *et al.*, 2002) (wild-type hGST A1-1) using Swiss-PdbViewer version 4.0.1 (Guex and Peitsch, 1997).

the analysis of the tertiary environment of the Trp-21 residue in the superimposed fits of the crystal structures of the mutant (2R6K, Dirr *et al.*, to be published) and wild-type (1K3L, Le Trong *et al.*, 2002) proteins (Figure 13). The single Trp-21 residue in each subunit is located 11 Å from the site of the Ile-71 → Val mutation at the interface between domain 1 and domain 2. The indole-ring side chain protrudes from  $\alpha$ -helix 1 into the space between  $\alpha$ -helices 6 and 8 (Wallace *et al.* 1998a) and is found to be within van der Waals contact distance (4.5 Å) of the  $\alpha$ -helix 1 residue Glu-17, the  $\alpha$ -helix 6 residues Val-161, Glu-162, Tyr-165 and Tyr-166, and the  $\alpha$ -helix 8 residues Val-194, Phe-197, Leu-198 and Arg-204 within both the mutant and wild-type proteins. The two polar residues Glu-17 and Glu-162, that are capable of quenching the fluorescence of Trp-21 during the fluorescence studies mentioned in section 3.3.2.1, appear to remain as distant from Trp-21 in the mutant protein as in the wild-type protein. The similarity of the side-chain conformations and low RMSD value between the mutant and wild-type residue side chains (RMSD = 0.26 Å) reveal that the cavity formed by the introduction of the Ile-71 → Val mutation does not significantly impact the environment of the Trp-21 indole ring.

### **3.4 Non-substrate ligand-binding properties of the G- and H-sites**

#### **3.4.1 Fluorescence properties of ANS bound to the H-site**

The amphipathic ligand 8-anilino-1-naphthalene sulfonate (ANS) binds the H-site of hGST A1-1 with the hydrophobic anilino and naphthyl rings occupying the H-site and the polar sulfonate moiety located at the interface of the G- and H-sites (Dirr *et al.*, 2005). The fluorescence properties of ANS are characterised by the polarity of its environment in which a shift in the polarity of the environment is accompanied by the concomitant bathochromic (red) shift in wavelength and hypochromic shift (decrease) in intensity of the fluorescence emission spectrum (Slavik, 1982). The ANS fluorescence properties were therefore used to probe for changes to the conformation of the H-site upon introduction of the Ile-71 → Val mutation. I71V and wild-type hGST A1-1 protein were titrated with ANS and the fluorescence emission spectrum recorded after selectively exciting the ANS at a wavelength of 390 nm (Figure 14). In the absence of protein, the fluorescence emission spectrum of free

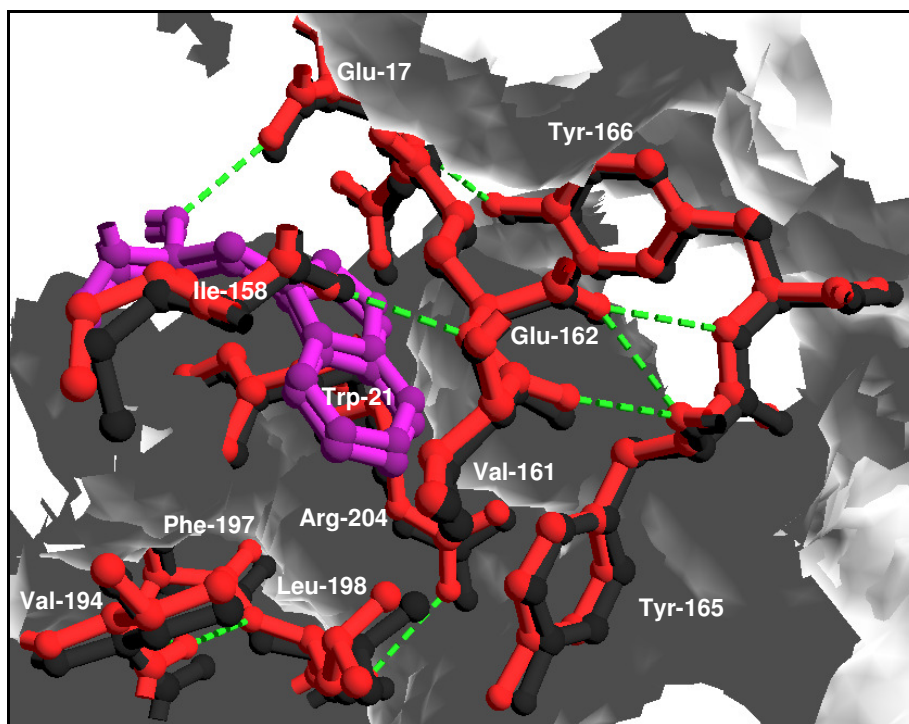


**Figure 13. Ball-and-stick representation of the tertiary environment around Trp-21 in subunit A of the crystal structures of the I71V and wild-type hGST A1-1 proteins.**

The superimposed crystal structures of the mutant (red) and wild-type (black) proteins reveal the residues within van der Waals radii ( $4.5 \text{ \AA}$ ) of the indole-ring side chain of Trp-21. The hydrogen bonds between interacting residues are indicated by green dashed lines. The superimposed fits were generated from the coordinates of the backbone  $\alpha$ -carbons and the RMSD calculated between the atoms of the respective mutant and wild-type residue side chains (RMSD =  $0.26 \text{ \AA}$ ) This figure was generated from pdb files 2R6K (Dirr *et al.*, to be published) and 1K3L (Le Trong *et al.*, 2002) using Swiss-PdbViewer version 4.0.1 (Guex and Peitsch, 1997).

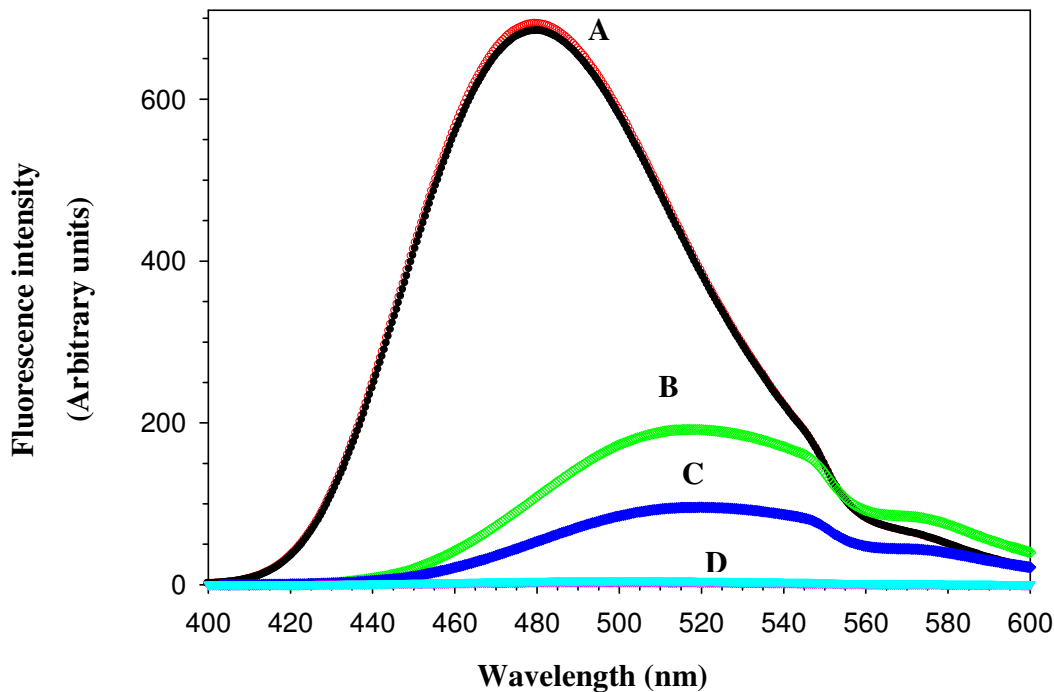


**Figure 14. Fluorescence emission spectra of free, unbound ANS and ANS bound to native and denatured I71V and wild-type hGST A1-1.**

Spectra of ANS bound to (A) native wild-type (●) and I71V (○) hGST A1-1; (B) free, unbound ANS in denaturing buffer; (C) free, unbound ANS in native buffer; and (D) ANS in the presence of denatured I71V mutant (▽) and wild-type hGST A1-1 (▼). ANS was selectively excited at 390 nm and the fluorescence emission spectra recorded between 390 nm and 600 nm using an excitation and emission bandwidth of 5 nm. Each spectrum represents the average spectrum of three replicate samples in 20 mM sodium phosphate buffer, pH 6.5, containing 1 mM EDTA and 0.02% sodium azide in the presence of 200  $\mu$ M ANS). I71V and wild-type hGST A1-1 dimer concentration was 2  $\mu$ M (subunit concentration of 4  $\mu$ M). Native samples were in the absence of urea; denatured samples were in the presence of 8 M urea. All spectra from ANS bound to protein were corrected for the fluorescence contribution from free, unbound ANS in the respective buffer solution.

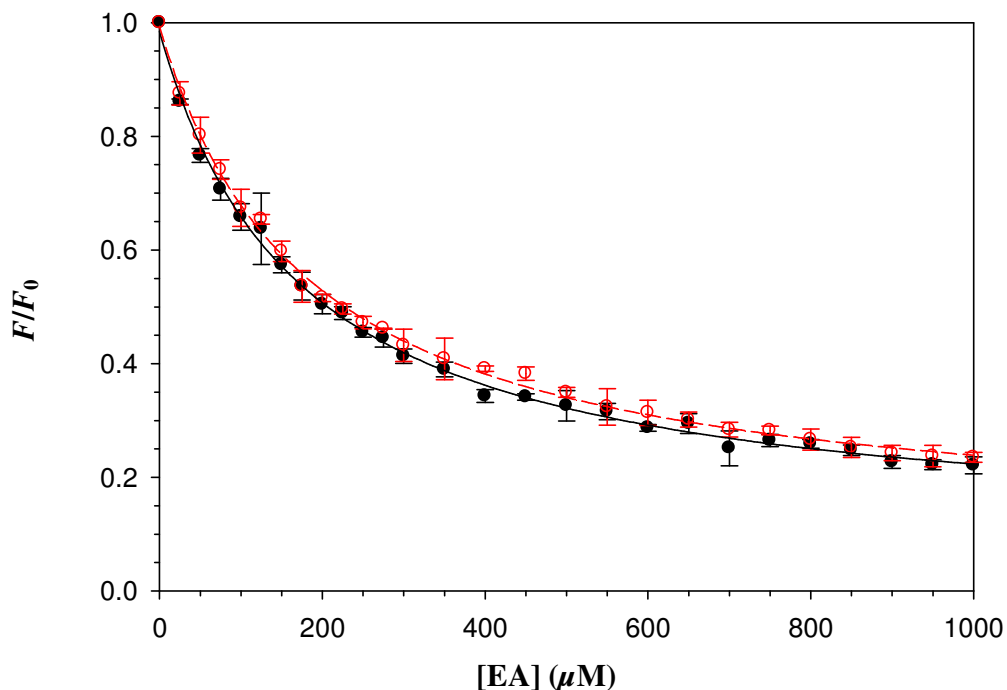
ANS exhibited a weak, broad band with a maximum at 520 nm in 0 M urea buffer (Figure 14 C) and at 519 nm, of twice the fluorescence intensity, in 8 M urea buffer (Figure 14 B). The emission spectrum of protein-bound ANS displayed a 36 nm, hypsochromic (blue) shift in wavelength to an emission maximum at 484 nm and was accompanied by a seven-fold increase in fluorescence intensity for both native I71V mutant and wild-type hGST A1-1 (Figure 14 A). In the presence of denatured protein, ANS exhibited a featureless baseline spectrum for denatured I71V mutant and wild-type hGST A1-1 (Figure 14 D).

The emission maximum of ANS bound to native wild-type hGST A1-1 was in agreement with the 480 nm wavelength maxima reported in the literature (Sluis-Cremer *et al.*, 1996; Dirr and Wallace, 1999; Sayed *et al.*, 2000). This emission maxima is consistent with the burial of the ANS residue in the highly hydrophobic environment of the H-site. Upon denaturation of the proteins, the bound ANS becomes exposed to the polar environment of the solvent and is accompanied by the shift in the wavelength maxima to lower energy wavelengths. The lack of difference between the emission spectrum of ANS bound to native I71V hGST A1-1 and wild-type hGST A1-1 suggests that the cavity formed by the mutation in domain 1 does not significantly impact the hydrophobicity of the H-site.

### **3.4.2 Displacement of ANS by G- and H-site ligands**

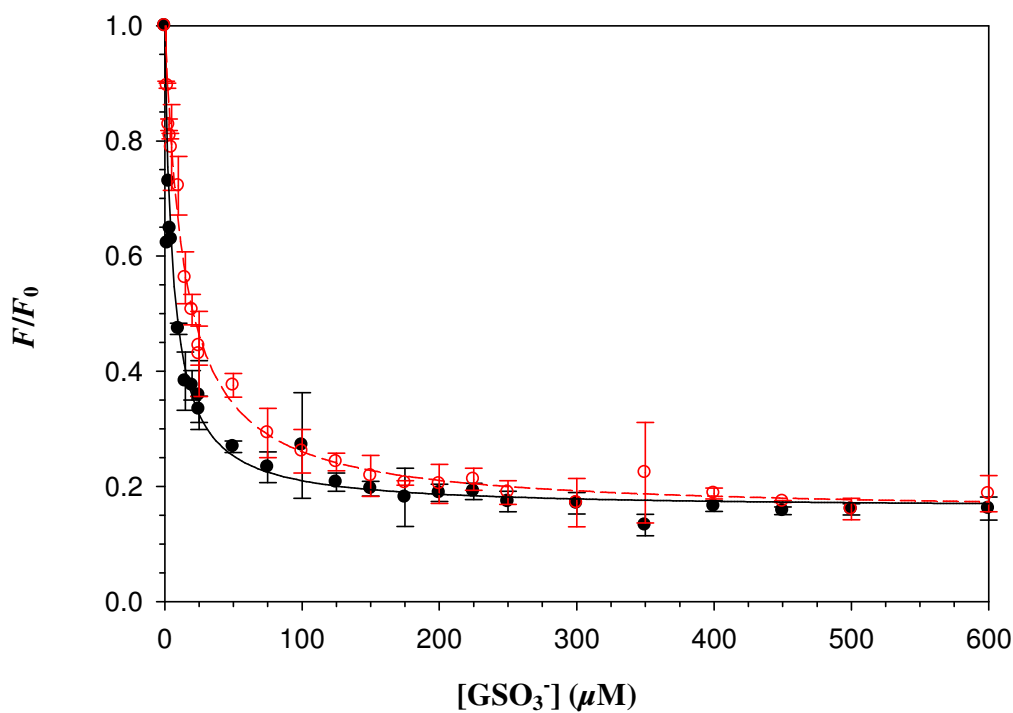
The polar ligand glutathione sulfonate ( $\text{GSO}_3^-$ ) binds the G- and H-sites of hGST A1-1 whereas the hydrophobic ligand ethacrynic acid (EA) binds exclusively to the H-site. Competitive displacement studies were conducted on the I71V and wild-type proteins that had their H-sites occupied by ANS in order to investigate whether the non-substrate ligandin properties of the G- and H-site had been affected by the Ile-71  $\rightarrow$  Val mutation.

Figure 15 depicts the decrease in fluorescence intensity accompanying the displacement of ANS from the H-site of I71V and wild-type hGST A1-1 by EA. The fraction of initial ANS fluorescence intensity ( $F/F_0$ ) underwent a hyperbolic decrease to 20% of its original value. The displacement curve for mutant protein was similar to that for wild-type protein. Figure 16 depicts the decrease in fluorescence intensity accompanying the displacement of ANS



**Figure 15. Displacement of ANS bound to I71V (○) and wild-type (●) hGST A1-1 by ethacrynic acid (EA).**

The ratio  $F/F_0$  is the quotient of fluorescence intensity at the current concentration of EA ( $F$ ) and the initial fluorescence intensity in the absence of EA ( $F_0$ ). The concentration of I71V and wild-type hGST A1-1 protein was  $2 \mu\text{M}$  in  $20 \text{ mM}$  sodium phosphate buffer, pH 6.5, containing  $1 \text{ mM}$  EDTA and  $0.02\%$  sodium azide in the presence of  $200 \mu\text{M}$  ANS. Solutions were titrated with  $0\text{--}1000 \mu\text{M}$  ethacrynic acid and the fluorescence of ANS bound to protein monitored at  $480 \text{ nm}$  using an excitation wavelength of  $390 \text{ nm}$ . The  $IC_{50}$  value was determined using non-linear regression analysis of the data: I71V hGST A1-1 (---) ( $R^2 = 0.992$ ), and wild-type hGST A1-1 (—) ( $R^2 = 0.992$ ). Circles denote the data mean from three replicate samples ( $n = 3$ ) and the error bars represent the standard deviation.



**Figure 16. Displacement of ANS bound to I71V (○) and wild-type (●) hGST A1-1 by glutathione sulfonate (GSO<sub>3</sub><sup>-</sup>).**

The ratio  $F/F_0$  is the quotient of fluorescence intensity at the current concentration of GSO<sub>3</sub><sup>-</sup> ( $F$ ) and the initial fluorescence intensity in the absence of GSO<sub>3</sub><sup>-</sup> ( $F_0$ ). The concentration of I71V and wild-type hGST A1-1 protein was 2 μM in 20 mM sodium phosphate buffer, pH 6.5, containing 1 mM EDTA and 0.02% sodium azide and in the presence of 200 μM ANS. Solutions were titrated with 0–2000 μM glutathione sulfonate and the fluorescence of ANS bound to protein monitored at 480 nm using an excitation wavelength of 390 nm. The  $IC_{50}$  value was determined using non-linear regression analysis of the data: I71V hGST A1-1 (---) ( $R^2 = 0.980$ ), and wild-type hGST A1-1 (—) ( $R^2 = 0.968$ ). Circles denote the data mean from three replicate samples ( $n = 3$ ) and the error bars represent the standard deviation.

from the H-site of I71V and wild-type hGST A1-1 by  $\text{GSO}_3^-$ . The  $F/F_0$  value underwent a steep hyperbolic decrease to 20% of its original value for increasing concentrations of  $\text{GSO}_3^-$ . The inhibitor concentration at which 50% of ANS bound to the H-site is displaced ( $IC_{50}$ ) by EA from the mutant protein was 0.1-fold greater than the corresponding value for the wild-type protein (Table 1). The lack of a significant increase in the  $IC_{50}$  values suggests that the H-sites of the mutant protein have a similar affinity for EA as that of the wild-type proteins. The  $IC_{50}$  value for the mutant protein was 2.4-fold greater than the corresponding value for the wild-type protein from displacement by  $\text{GSO}_3^-$  (Table 1). The difference in shape in the displacement curves and increase in  $IC_{50}$  value suggests that the mutant protein H-site has a weaker affinity for  $\text{GSO}_3^-$  compared to that of the wild-type protein.

The 2.4-fold increase in the  $IC_{50}$  value for glutathione sulfonate compared to the lack of change in the  $IC_{50}$  value for ethacrynic acid for I71V hGST A1-1 reveals that the Ile-71  $\rightarrow$  Val has a greater impact on the G-site compared to the H-site. The observed changes in the  $IC_{50}$  values are, however, not significant based on the “rule-of-thumb” that a significant difference is characterised by a 10-fold change in the  $IC_{50}$  value. These results are consistent with the lack of significant change in the ANS binding spectra detailed in section 3.4.1. The Ile-71 residue appears to not play a significant role in the binding of non-ligand substrates.

A molecular docking study performed with ANS and wild-type hGST A1-1 has revealed that the aniline and naphthyl rings of ANS are located within van der Waals distance of Leu-107, Leu-108, Val-111, Met-308, Leu-213, Ala-216, Phe-220 and Phe-222 (Dirr *et al.*, 2005). The sulfonate moiety of ANS is located within van der Waals distance of Tyr-9, Phe-10, Arg-15 and Val-55 (Dirr *et al.*, 2005). A comparison of the superimposed crystal structures of the mutant and wild-type proteins highlighting the conformation of the aforementioned amino acids is shown in Figure 17.

Small differences are detected between the respective conformations of H-site residues Val-111, Leu-107, and Leu-108 in the mutant and wild-type proteins (Figure 17). Since the aniline and naphthyl rings of ANS are found to interact with these H-site residues, one would expect a change in the binding affinity of the ANS molecule, which binds the H-site (Dirr

**Table 1.  $IC_{50}$  values for the displacement of ANS bound to I71V and wild-type hGST A1-1 by the inhibitors ethacrynic acid and glutathione sulfonate.**

<b>Inhibitor</b>	<b><math>IC_{50}</math> (<math>\mu</math>M)*</b>	
	<b>I71V</b>	<b>Wild-type</b>
Ethacrynic acid	227.5 $\pm$ 15.3	210.6 $\pm$ 11.3
Glutathione sulfonate	22.1 $\pm$ 2.4	9.4 $\pm$ 1.4

\* The  $IC_{50}$  value is the inhibitor concentration at which 50% of ANS bound to the H-site is displaced. The  $IC_{50}$  values were determined by nonlinear regression analysis of the displacement curves in Figures 15 and 16.

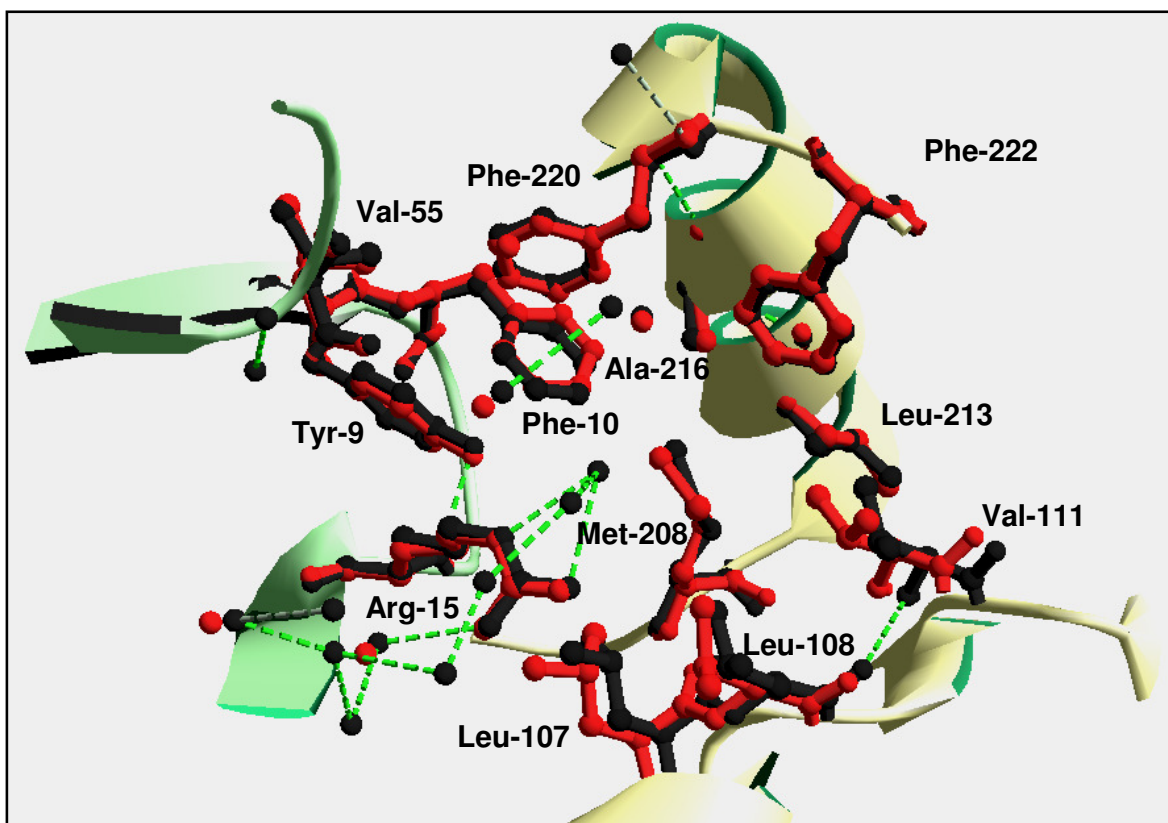


**Figure 17. Ball-and-stick representation of the active-site residues involved in van der Waals interactions with the non-substrate ligand ANS.**

The superimposed crystal structures of the active site in subunit B of the mutant (red) and wild-type (black) proteins. This structural representation is used to model the conformation of the residues in the G- and H-site that have been found to form van der Waals interactions with the non-substrate ligand ANS. Residues attached to the yellow secondary structural elements form van der Waals contacts with the aniline and naphthyl rings of ANS. Residues attached to the green secondary structural elements form van der Waals contacts with the sulfonate moiety of ANS. Water molecules within 4.5 Å of the active site are depicted as balls coloured red and black according to its proximity to the mutant and wild-type proteins, respectively. The hydrogen-bonds interactions are indicated by green dashed lines. An RMSD of 0.44 Å was calculated for the side chains between mutant and wild-type protein. This figure was generated from pdb files 2R6K (Dirr *et al.*, to be published) and 1K3L (Le Trong *et al.*, 2002) using Swiss-PdbViewer version 4.0.1 (Guex and Peitsch, 1997).

et al., 2005), and a change in the  $IC_{50}$  values for EA. The observed similarities in the ANS binding spectra and  $IC_{50}$  values for EA suggest that these minor changes in H-site residue conformations are not significant to the ligand-binding ability of the H-site. The conformations of the G-site amino acids in the mutant protein are similar to those in the wild-type protein. The RMSD value of 0.44 Å is not significant and corroborates the fact that the conformations of the G- and H-site of the mutant do not significantly differ from those of the wild-type protein. This result is expected since the Ile-71 is positioned closer to the G-site (~7 Å from nearest atom of bound GSH) than to the H-site (~12 Å) and is expected to more readily affect the conformation of the G-site residues. The results of the ligandin functional assays are, thus, supported by crystal structures of the proteins. It appears that the cavity formed by the Ile-71 → Val mutation in domain 1 of the mutant protein does not impact the ligandin function of the protein.

### **3.5 Catalytic properties of the I71V and wild-type enzymes**

The confirmation of the conserved secondary and tertiary protein structure and the insignificant change in ligandin function begs the question, ‘What contribution does the conserved Ile-71 residue make to the catalytic function of the hGST A1-1 enzyme?’ Paying consideration to previous studies conducted on the GSTs (please see section 1.4), it appears that the conserved Ile-71 residue could play a role in the overall catalytic activity of the protein and in the stabilization of the  $\sigma$ -complex between the electrophilic substrate and glutathione. In light of this, the standard CDNB-GSH conjugation assay was used to compare the specific activities of the I71V and wild-type hGST A1-1 enzymes and the TNB-GSH conjugation assay to compare the respective formation constants of the  $\sigma$ -complex stabilisation step.

#### **3.5.1 Specific activity**

The measurement of the specific activity of an enzyme is an exquisitely sensitive and rapid test that reveals whether any change in the protein sequence or structure has affected the overall catalytic activity. The specific activity of I71V and wild-type hGST A1-1 was determined at pH 6.5 – the pH at which the non-enzymatic reaction is minimal – using the

standard GSH-CDNB conjugation assay (Habig *et al.*, 1974), as described in section 2.5.2. The formation of the yellow product 1-(S-glutathionyl)-2,4-dinitrobenzene was accompanied by the expected straight-line increase in absorbance at 340 nm. Figure 18 depicts a representative progress curve from which the slope was determined using linear regression. The linear slope indicated that the only limitation on catalytic activity was the performance of the enzyme; the presence of non-linear curves would have otherwise indicated the presence of either substrate depletion, product inhibition or a change in the physical conditions of the reaction. The slope of each progress curve, therefore, provided precise data for the determination of the initial velocity ( $v_0$ ) at each specified concentration of protein.

The individual values of  $v_0$  for the I71V and wild-type hGST A1-1 proteins were plotted against their respective concentrations of protein (Figure 19). A straight-line trend was observed for the plots of initial velocity versus mass of protein for both wild-type (Figure 19 A) and I71V (Figure 19 B) hGST A1-1. A systematic error is observed in the plots in which the intercepts do not pass through the origin of the axes. The specific activity results are not impacted by this error because they are obtained from the slopes of the plots. A plausible reason for this discrepancy in the interception points is that an overcorrection has been made for the non-enzymatic reaction. The specific activity was determined to be  $25.1 \pm 0.8 \mu\text{mol min}^{-1} \text{mg}^{-1}$  for wild-type hGST A1-1 and  $25.2 \pm 1.3 \mu\text{mol min}^{-1} \text{mg}^{-1}$  for I71V hGST A1-1. The wild-type value was in agreement with those reported in the literature:  $34.9 \mu\text{mol min}^{-1} \text{mg}^{-1}$  (Gildenhuis *et al.*, 2010),  $39.42 \pm 0.21 \mu\text{mol min}^{-1} \text{mg}^{-1}$  (Mosebi *et al.*, 2003) and  $44.6 \pm 2.3 \mu\text{mol min}^{-1} \text{mg}^{-1}$  (Nathaniel *et al.*, 2003). The precision and accuracy of the testing conditions were, thus, in agreement with those used in the aforementioned studies.

The similar specific activities of I71V and wild-type hGST A1-1 indicate that the Ile-71  $\rightarrow$  Val in the hydrophobic core of the protein does not significantly change the residues at the active site. Similar studies conducted on the bacterial nuclease barnase have also revealed that the replacement of isoleucine with valine in the hydrophobic core of a protein produces no structural changes that significantly decrease enzymatic activity (Kellis *et al.*, 1989).

The specific activity assays indicate that the extended side chain of Ile-71 does not directly or

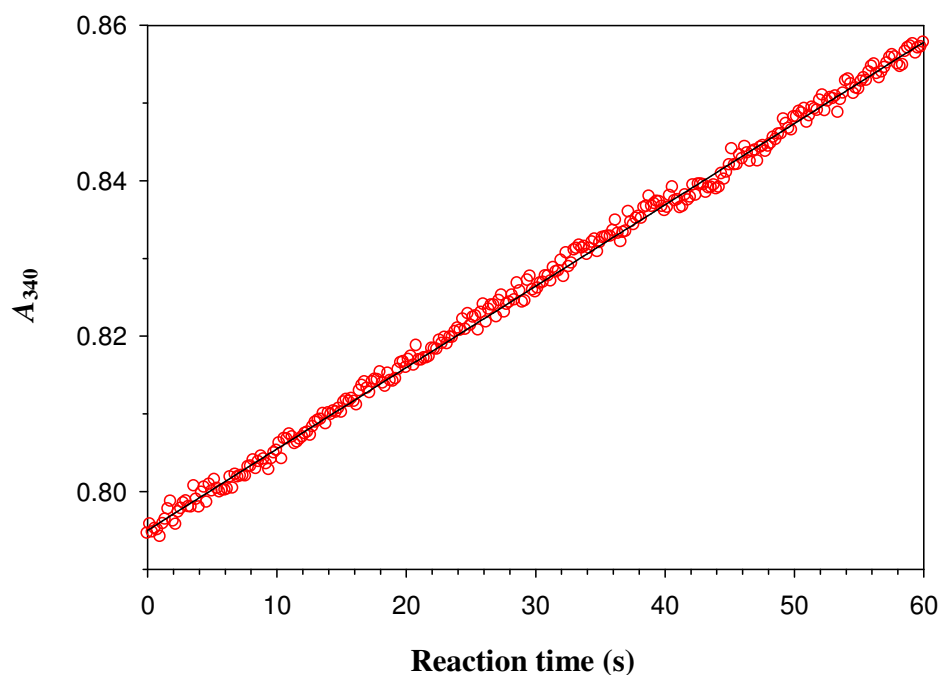


**Figure 18. Progress curve of the conjugation reaction between reduced glutathione and 1-chloro-2,4-dinitrobenzene as catalysed by I71V hGST A1-1.**

The reaction was initiated by the addition of 1 mM CDNB to the buffered protein solution and the reaction monitored at 340 nm by spectrophotometrically measuring the formation of 1-(S-glutathionyl)-2,4-dinitrobenzene ( $\epsilon_{340} = 9600 \text{ M}^{-1} \text{ cm}^{-1}$ ) at 20 °C for one minute. The protein concentration was 6 nM in 0.1 M sodium phosphate buffer, pH 6.5, containing 1 mM EDTA and 0.02% sodium azide in the presence of 1 mM GSH. The final concentration of ethanol was a constant 3% (v/v) in each 3 mL assay solution. The change in absorbance at 340 nm as a function of reaction time was determined by linear regression ( $R^2 = 0.998$ ).

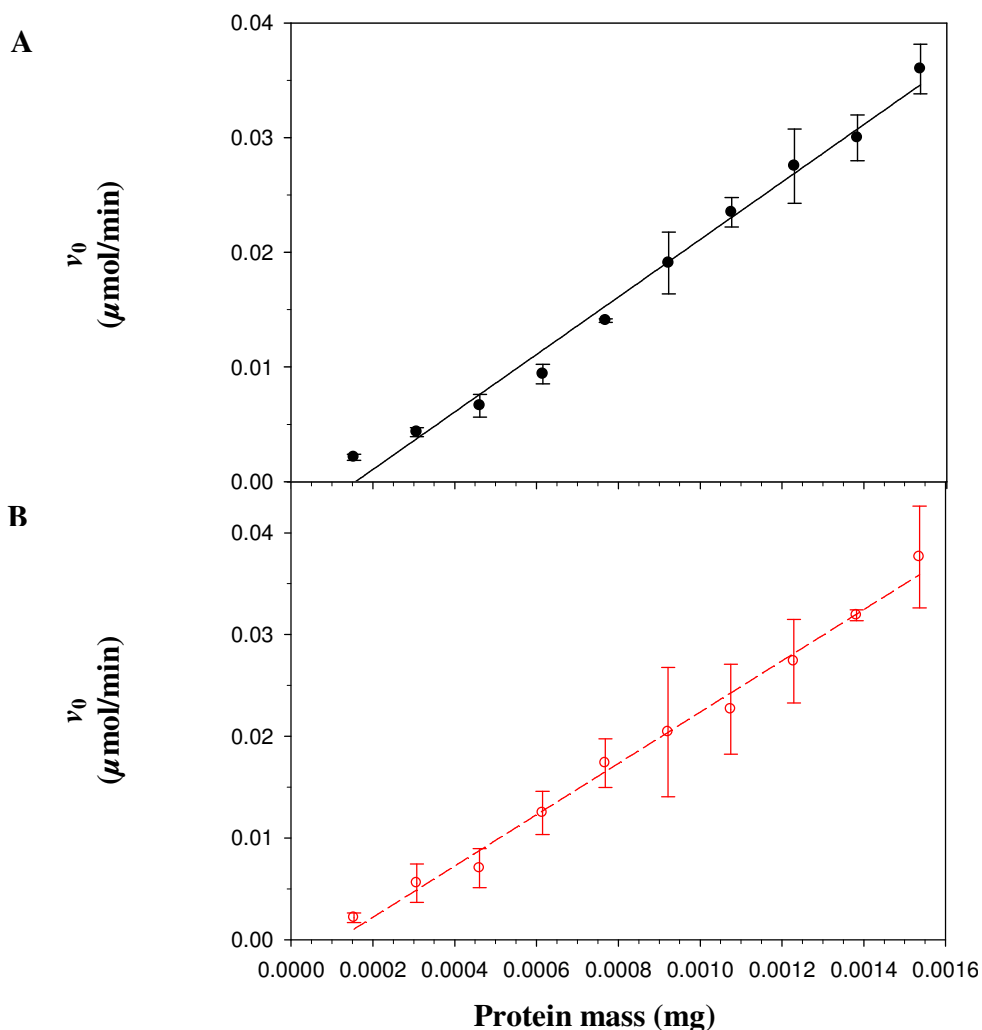


**Figure 19. Specific activity of (A) wild-type and (B) I71V hGST A1-1 using the standard CDNB conjugation assay.**

The conjugation of CDNB by enzyme-bound GSH was monitored by measuring the absorbance at 340 nm of the 1-(*S*-glutathionyl)-2,4-dinitrobenzene complex ( $\epsilon_{340} = 9600 \text{ M}^{-1} \text{ cm}^{-1}$ ) formed in 0.1 M sodium phosphate buffer, pH 6.5, containing 1 mM EDTA and 0.02% sodium azide in the presence of 1 mM GSH and 1 mM CDNB. The final concentration of ethanol was 3% (v/v). The absorbance contribution from the formation of the 1-(*S*-glutathionyl)-2,4-dinitrobenzene product in the absence of enzyme has been subtracted. The specific activity of each enzyme is the slope of the linear regression plots of wild-type hGST A1-1 (—) ( $R^2 = 0.972$ ) and I71V hGST A1-1 (---) ( $R^2 = 0.931$ ). Circles denote the data mean from three replicate samples ( $n = 3$ ) and the error bars represent the standard deviation.

indirectly contribute to the catalytic activity of wild-type hGSTA1-1. This suggests that the Ile-71 residue neither (a) induces tertiary structural changes at the G- or H-site that significantly enhances the lowering of the transition state energy or maintain an efficient orientation of substrates; nor does it (b) increase the enzyme's flexibility that would improve substrate binding or product release.

### 3.5.2 Formation of the $\sigma$ -complex within the active sites

The  $S_NAr$  conjugation reaction between reduced glutathione and 1,3,5-trinitrobenzene results in the reversible formation of a 1-(*S*-glutathionyl)-2,4,6-trinitrocyclohexadienate  $\sigma$ -complex. This  $\sigma$ -complex mimics the transition state formed between reduced glutathione and 1-chloro-2,4-dinitrobenzene in the CDNB conjugation reaction and is therefore used as a probe to investigate the underlying structural features that enable the hGST A1-1 enzyme to catalyse the CDNB reaction.

The titrated solutions of I71V and wild-type hGST A1-1 containing 5 mM reduced glutathione instantaneously changed colour from colourless to a deep, red-orange colour with the colour intensity increasing in proportion to the final concentration of TNB. The visible spectrum of the red-orange  $\sigma$ -complex revealed an absorbance peak at 450 nm and a shoulder at 562 nm (Figure 20). The spectrum recorded at each concentration of TNB for I71V hGST A1-1 was similar to the corresponding spectrum for wild-type hGST A1-1 indicating that the same concentration of  $\sigma$ -complex was formed at equivalent concentrations of substrate and active sites in I71V hGST A1-1 and wild-type hGST A1-1.

The saturation curve was plotted for the titration of GSH bound I71V and wild-type hGST A1-1 with increasing concentrations of TNB (Figure 21). The apparent equilibrium formation constant and extinction coefficient were calculated using non-linear regression analysis of the data in Figure 21 and their values shown in Table 2.

The equilibrium formation constant ( $K_F$ ) and maximum absorbance value ( $A_{max}$ ) determined for the wild-type hGST A1-1 protein are in agreement with those reported in the literature,

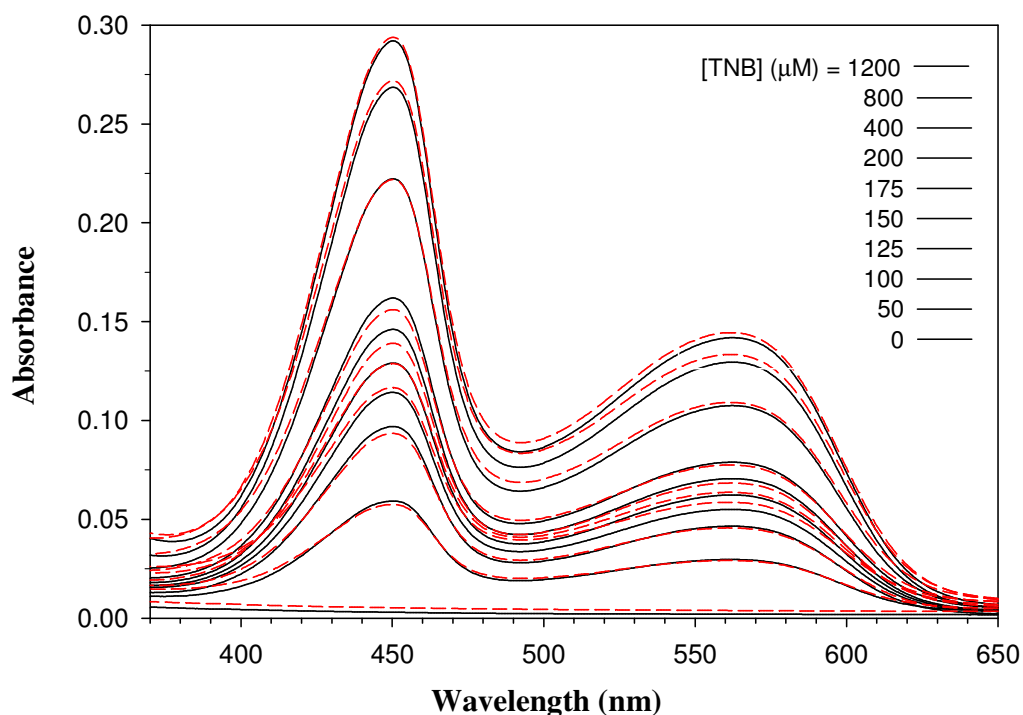


**Figure 20. Absorbance spectra of the  $\sigma$ -complex formed between TNB and GSH in the active sites of I71V (---) and wild-type (—) hGST A1-1.**

The formation of  $\sigma$ -complex between GSH and TNB was initiated by titrating 0–1200  $\mu\text{M}$  TNB into solutions of mutant and wild-type protein and the absorbance spectrum for the  $\sigma$ -complex chromophore recorded. The protein concentration was 20  $\mu\text{M}$  for both mutant and wild-type proteins in 0.1 M sodium phosphate buffer, pH 6.5, containing 1 mM EDTA and 0.02% sodium azide in the presence of 5 mM GSH. The acetonitrile concentration was held constant at 2% (v/v). The formation of  $\sigma$ -complex in the absence of enzyme was subtracted before illustrating the spectra using the SigmaPlot version 10.

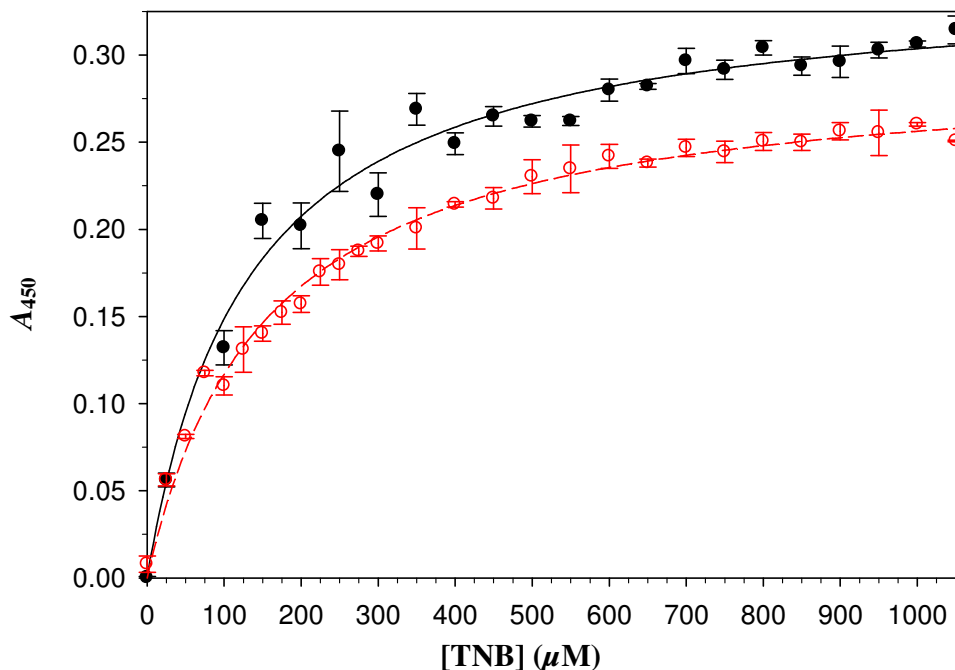


**Figure 21. Saturation curve for the formation of the  $\sigma$ -complex at the active sites of I71V and wild-type hGST A1-1.**

The formation of  $\sigma$ -complex between GSH and TNB was initiated by titrating increasing concentrations of TNB into solutions of mutant and wild-type protein and the reaction monitored at 450 nm. The protein concentration was 17  $\mu\text{M}$  for I71V hGST A1-1 ( $\circ$ ) and 15  $\mu\text{M}$  for wild-type hGST A1-1 ( $\bullet$ ) in 0.1 M sodium phosphate buffer, pH 6.5, containing 1 mM EDTA and 0.02% sodium azide in the presence of 5 mM GSH. The acetonitrile concentration was held constant at 2% (v/v). The absorbance contribution from the formation of the  $\sigma$ -complex in the absence of enzyme was subtracted and the formation constants calculated using non-linear regression analysis on the saturation curves of I71V hGST A1-1 (---) ( $R^2 = 0.983$ ) and wild-type hGST A1-1 (—) ( $R^2 = 0.975$ ) proteins using SigmaPlot version 10. Circles denote the data mean from three replicate samples ( $n = 3$ ) and the error bars represent the standard deviation.

**Table 2. Equilibrium formation parameters for the formation of the 1-(S-glutathionyl)-1,3,5-trinitrocyclohexadienate  $\sigma$ -complex in the active sites of I71V and wild-type hGST A1-1.**

<b>Parameter</b>	<b>I71V hGST A1-1</b>	<b>Wild-type hGST A1-1</b>
$K_F$ ( $M^{-1}$ ) <sup>*</sup>	6500 $\pm$ 200	7600 $\pm$ 500
$A_{max}$ ( $M^{-1} cm^{-1}$ ) <sup>#</sup>	8700 $\pm$ 90	11500 $\pm$ 200

\*  $K_F$  is the constant of formation of the  $\sigma$ -complex derived from the inverse of the constant of dissociation ( $K_d$ ) (i.e.  $K_F = 1/K_d$ ) that is directly determined from the non-linear regression analysis of the curves in Figure 21.

<sup>#</sup>  $A_{max}$  is the absorbance at 450 nm under saturating conditions of GSH and TNB per enzyme active site.

$K_F = 7552 \pm 465 \text{ M}^{-1}$  and  $A_{\text{max}} = 10510 \pm 157 \text{ M}^{-1}\text{cm}^{-1}$  (Lien *et al.*, 2001), and  $K_F = 8900 \pm 1400 \text{ M}^{-1}$  and  $A_{\text{max}} = 12300 \pm 400 \text{ M}^{-1}\text{cm}^{-1}$  (Widersten *et al.*, 1996). These properties provide evidence for the stabilization of the  $\sigma$ -complex. The use of the following equation (Fersht, 1999):

$$\Delta\Delta G = -RT \ln \frac{(k_{\text{cat}}/K_M^{\text{CDNB}})_{\text{mutant}}}{(k_{\text{cat}}/K_M^{\text{CDNB}})_{\text{wild-type}}}$$

where,  $R$  is the gas constant ( $8.314 \text{ J K}^{-1} \text{ mol}^{-1}$ ),  $T$  is the temperature in Kelvin (293 K) and  $k_{\text{cat}}/K_M^{\text{CDNB}}$  the catalytic efficiency for the CDNB substrate, provides the change in free energy for the stabilisation of the transition state which is a measure of the stabilising effect of an enzyme (Nilsson *et al.*, 2002). Since the catalytic efficiency properties ( $k_{\text{cat}}/K_M^{\text{CDNB}}$ ) were not determined in this study, the equation may be adapted to determine the change in free energy from the formation constants of  $\sigma$ -complex formation in the active site of hGST A1-1:

$$\Delta\Delta G = -RT \ln \frac{K_F^{I71V}}{K_F^{\text{wild-type}}}$$

where,  $K_F^{I71V}$  and  $K_F^{\text{wild-type}}$  are the respective apparent equilibrium formation constants for I71V mutant and wild-type hGST A1-1. The  $\Delta\Delta G$  of  $\sigma$ -complex destabilization was  $+ 0.316 \text{ kJ mol}^{-1}$  meaning that the mutant has a reduced ability to stabilise the  $\sigma$ -complex as efficiently as the wild-type. This value is, however, small indicating that this reduced ability of the mutant protein is not significant.

Analysis of the TNB binding spectra reveals that neither a change in intensity nor a shift in wavelength occurs as a result of the I71V mutation. The decreased formation constant and maximum absorbance, for I71V hGST A1-1 in comparison to the wild-type hGST A1-1, are within experimental error and iterate the lack of change in the spectral properties. A change in intensity would have been expected to be corroborated by a change in the apparent formation constant. An increase in intensity would have revealed that a greater concentration

of the  $\sigma$ -complex had formed at a given concentration of TNB; a decrease in intensity would have revealed a decrease in  $\sigma$ -complex formation. A significantly greater formation constant would have revealed that the I71V mutation had caused a significant stabilization of the  $\sigma$ -complex in comparison to wild-type hGST A1-1.

The observed 12% decrease in  $K_F$  for I71V hGST A1-1 equates to a very weak destabilisation energy compared to wild-type hGST A1-1 upon formation of the  $\sigma$ -complex between GSH and TNB. This reveals that the loss of van der Waals contacts of the wild-type hGST A1-1 Ile-71 residue, normally made by the extended alkyl side chain, does not indirectly impact the stabilization of the  $\sigma$ -complex. The similar appearance of the I71V and wild-type hGST A1-1 TNB binding spectra, the comparable magnitudes of  $K_F$  and a value of  $+ 0.3 \text{ kJ mol}^{-1}$  for  $\Delta\Delta G$  for the formation of the  $\sigma$ -complex indicate that the creation of the cavity by the Ile-71  $\rightarrow$  Val mutation results in a minor destabilisation of the transition state. The Ile-71 residue therefore marginally enhances the stabilisation of the transition state via an unknown means. The  $\sigma$ -complex formed between TNB and GSH is proposed to mimic the transition state of the reaction between CDNB and GSH (Graminski *et al.*, 1989). The insignificant change in the formation constant for I71V hGST A1-1 reveals that the Ile-71  $\rightarrow$  Val mutation does not greatly impact the active site residues involved in the stabilization of the  $\sigma$ -complex. A structural study conducted on the topologically equivalent Ile-68 in human class Pi GST revealed that the non-conservative substitution of the Ile-68 residue for tyrosine led to a >95% decrease in specific activity and an almost complete loss in ability to bind glutathione compared to the wild-type protein (Manoharan *et al.*, 1992). It is expected that the introduction of the non-isosteric, bulkier tyrosine residue in hGST Pi disrupted the conformation of the catalytically active residue in the adjacent G-site which led to the observed decreases in catalytic and ligandin function. This study on hGST Pi provides a brief insight into the possible outcome that was not met in the conservative substitution of Ile-71 for valine in hGST A1-1. Despite the proximity of the Val-71 residue to the G-site in the mutant hGST A1-1 protein, the conformation of the catalytically active residues were not impacted by the presence of the cavity in the hydrophobic core in domain 1 of the mutant protein.

There is no crystal structure, at present, for the 1-(*S*-glutathionyl)-2,4,6-trinitrocyclohexadienate  $\sigma$ -complex bound to the active sites of the hGST A1-1 protein. The impact of the cavity, created by the Ile-71  $\rightarrow$  Val, on the ability of hGST A1-1 to stabilise the  $\sigma$ -complex may, however, still be assessed using the conclusions drawn from a recent molecular docking study performed by Gildenhuis *et al.* (2010) on the  $\sigma$ -complex and hGST A1-1. The molecular docking study revealed that the GSH moiety of the  $\sigma$ -complex binds the G-site in a similar fashion to that observed for the binding of GSH (Gildenhuis *et al.*, 2010), i.e., the involvement of Tyr-9, Arg-15, Arg-45, Val-55, Gln-67, Thr-68, Asp-101 (from the opposite monomer), Glu-104 and Arg-131 (from the opposite monomer) (Sinning *et al.*, 1993). The trinitrocyclohexadienate moiety of the  $\sigma$ -complex was found to bind the same hydrophobic pocket in the H-site as that of the hexyl chain of *S*-hexylglutathione making interactions with the side chains of Tyr-9, Phe-10, Gly-14, Arg-15, Leu-107, Leu-108, Val-111, Phe-220 and Phe-222 (Gildenhuis *et al.*, 2010). The H-site catalytic residues in the hGST A1-1 enzyme is believed to assist the resonance stabilisation of the anionic charge of the  $\sigma$ -complex trinitrocyclohexadienate moiety (Figure 22) through the formation of hydrogen bonds between the hydroxyl group of Tyr-9 and the *pro-R* *o*-nitro group of the trinitrocyclohexadienate moiety (Gildenhuis *et al.*, 2010). Figure 22 depicts a ball-and-stick representation of the structural-alignment of the catalytic residues and bound ligand, *S*-hexylglutathione, in the subunit B active site of the crystal structures of I71V hGST A1-1 (2R6K; Dirr *et al.*, to be published) and wild-type hGST A1-1 (1K3L; Le Trong *et al.*, 2002). An assessment of the catalytically active residues involved in both the G- and H-site reveal that the majority of these residues have similar conformations in the mutant and wild-type proteins. The respective catalytically active G-site residues have similar conformations and have been shown in dull colours for clarity (Figure 22). The majority of the catalytically active H-site residues have similar conformations between the mutant and wild-type proteins with the conformation of Tyr-9 exhibiting no difference in its properties. The catalytically most significant residue in the stabilisation of the  $\sigma$ -complex appears, thus, to be unaffected by the presence of the cavity in domain 1 of the mutant protein. Small differences are detected between the respective conformations of Val-111, Leu-107, and Leu-108, as noted in section 3.4.2, in the mutant and wild-type proteins that appear to have contributed to the observed shift in the hexyl moiety of the *S*-hexylglutathione ligand. It is, however, noted that

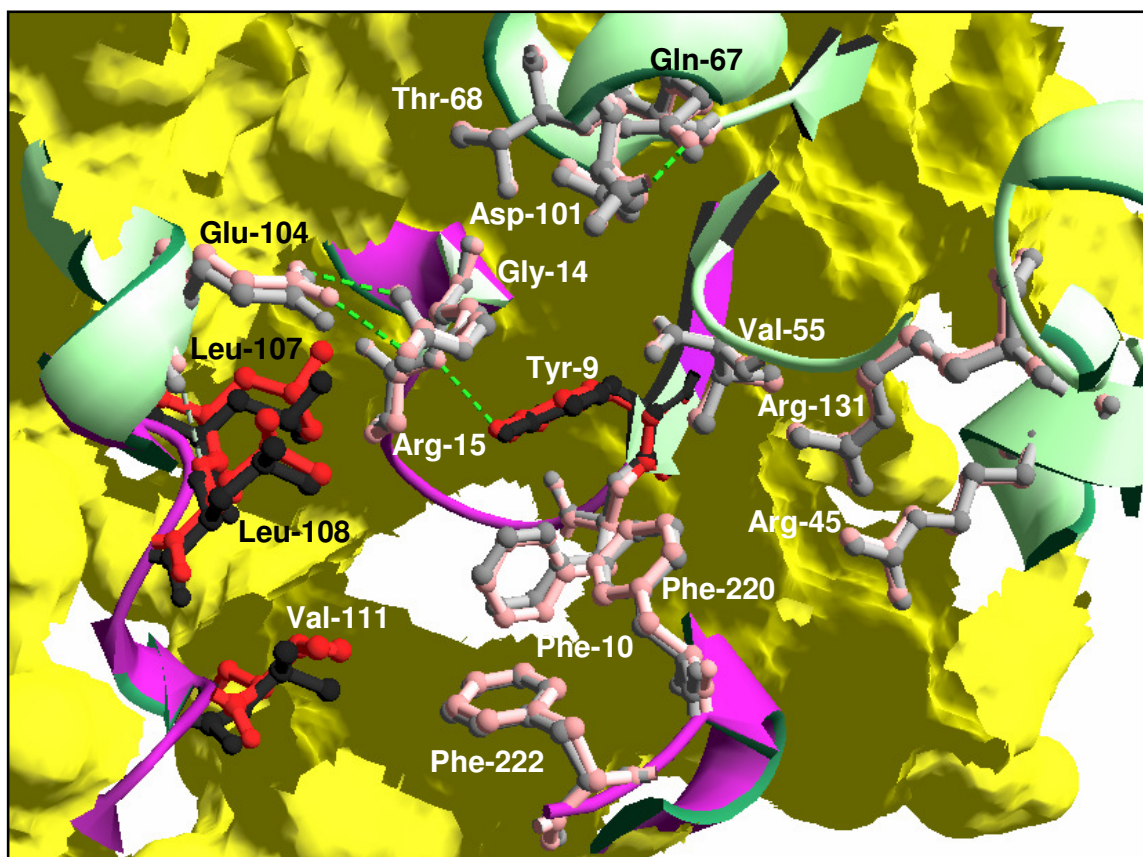


**Figure 22. Ball-and-stick representation of the active-site residues involved in van der Waals interactions with the  $\sigma$ -complex bound to hGST A1-1.**

The superimposed crystal structures of the active site in subunit B of the mutant and wild-type proteins. This structural representation is used to model the conformation of the residues in the G- and H-site that form van der Waals interactions with the  $\sigma$ -complex. Residues attached to the purple secondary structural elements form van der Waals contacts with the trinitrocyclohexadienate moiety of the  $\sigma$ -complex. Residues attached to the green secondary structural elements form van der Waals contacts with the glutathione moiety of the  $\sigma$ -complex. The residues of similar conformation in the I71V and wild-type proteins are coloured pink and grey, respectively. The residues of interest, as discussed in the text, which include the residues of different conformations between the mutant and wild-type proteins, are coloured red (mutant) and black (wild-type). The hydrogen bonds between interacting residues are indicated by green dashed lines. (RMSD = 0.42 Å) This figure was generated from pdb files 2R6K (Dirr *et al.*, to be published) and 1K3L (Le Trong *et al.*, 2002) using Swiss-PdbViewer version 4.0.1 (Guex and Peitsch, 1997).

the variation in conformation of the *S*-hexyl chain within the H-site of the wild-type protein has been attributed to the large volume of the H-site (Le Trong *et al.*, 2002). It is, thus, unlikely that the changes to the conformations of the hydrophobic, nonpolar Val-111, Leu-107, and Leu-108 residues have an impact on the enzyme's ability to stabilise the  $\sigma$ -complex because of their lack of involvement with the stabilisation of the anionic charge.

The similarity of the conformations of the active site residues in the crystal structures support the similarities in catalytic function detected by the specific activity and the  $\sigma$ -complex stabilisation assays. The cavity in domain 1 of the mutant protein does not appear to influence the catalytic function of the hGST A1-1 protein and suggests that Ile-71 does not make a significant contribution to the catalytic function of the protein.

### **3.6 Thermal stability of the I71V and wild-type proteins**

The thermal stability of the I71V and wild-type hGST A1-1 proteins was investigated by monitoring the change in ellipticity at 222 nm in response to a uniform change in temperature over the range 4–80 °C (Figure 23). The thermal-unfolding curve of the native I71V mutant did not overlay with the unfolding curve of wild-type hGST A1-1 but both curves were characterised by a sigmoidal shape (Figure 23 A). The mean residue ellipticity  $[\Theta]$  value at 222 nm of native I71V mutant began to increase in magnitude at ~42 °C whereas that of native wild-type hGST A1-1 began to increase ~48 °C. The slope of the transition region for mutant protein was qualitatively assessed to be smaller than that of the wild-type protein. The final  $[\Theta]$  value for each protein was  $-2000 \text{ deg cm}^2 \text{ dmol}^{-1}$  indicating the presence of residual secondary structural features in the protein at 80 °C. This result is consistent with the formation of an aggregate of partially unfolded protein during the thermal inactivation process that maintains a small proportion of secondary structural content but is unable to refold to the native protein conformation. The thermal refolding diagram of the unfolded I71V and wild-type proteins depicted a straight line at a  $[\Theta]$  value of  $-2000 \text{ deg cm}^2 \text{ dmol}^{-1}$  (Figure 23 B). The constant  $[\Theta]$  value at  $-2000 \text{ deg cm}^2 \text{ dmol}^{-1}$  indicates that the secondary structural content of I71V mutant and wild-type hGST A1-1 remains constant upon return to more stable thermal conditions.

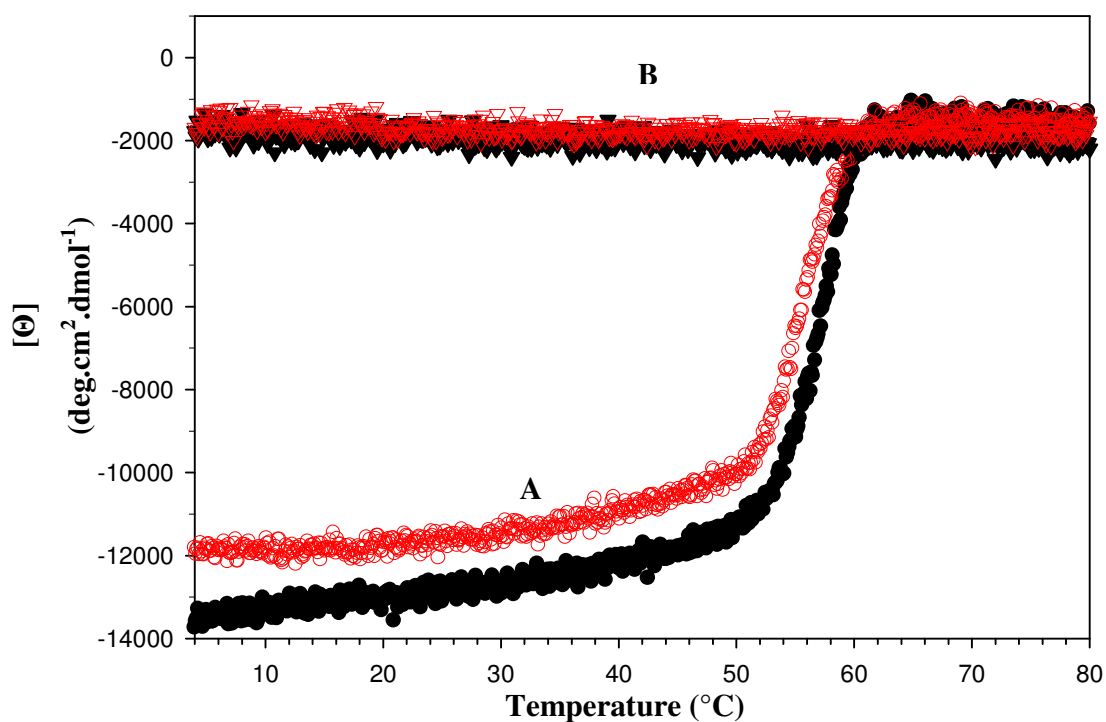


**Figure 23. Thermal-induced transitions of I71V mutant and wild-type hGST A1-1.**

(A) Thermal unfolding transitions of I71V mutant ( $\circ$ ) and wild-type ( $\bullet$ ) hGST A1-1, and (B) lack of refolding of aggregated I71V ( $\nabla$ ) and wild-type ( $\blacktriangledown$ ) hGST A1-1. Progression of the transitions, as a function of  $\alpha$ -helical protein content, was followed at 222 nm using a 5 nm bandwidth and a linear temperature gradient of 1 °C/min. The concentration of I71V and wild-type hGST A1-1 protein was 2  $\mu$ M in 20 mM sodium phosphate buffer, pH 6.5, containing 1 mM EDTA and 0.02% sodium azide.

The thermal unfolding transitions were irreversible and prevented the accurate fitting of mathematical models to the data. The unfolding transitions were, therefore, plotted without normalisation of the data. Values of the transition temperature indicating a 50% change in ellipticity ( $T_m$ ) were, however, determined for comparative purposes by normalising the data and using non-linear regression on the unfolding transitions of I71V mutant ( $R^2 = 0.987$ ) and wild-type ( $R^2 = 0.988$ ) hGST A1-1. The  $T_m$  value for the mutant protein ( $T_m = 54.71 \pm 0.06$  °C) was found to be lower than that for the wild-type protein ( $T_m = 56.45 \pm 0.02$  °C). The values reported above are similar to the values reported in a thermal inactivation study of an initial increase in ellipticity at about 50 °C and a  $T_m$  (the temperature at which 50% activity remained) of about 58 °C for wild-type hGST A1-1 (Wallace *et al.*, 1998b).

The lower transition temperature ( $T_m$ ) for I71V hGST A1-1 indicates that the global protein conformation is destabilised upon introduction of the Ile-71 → Val mutation. This result is consistent with the expectation that the hydrophobic core becomes destabilized because of the loss in hydrophobic interactions between the truncated valine side chain and the surrounding hydrophobic residues.

Mutational studies at the interface between an  $\alpha$ -helix and  $\beta$ -sheet in barnase have revealed that the replacement of a valine residue for the naturally-occurring isoleucine residue destabilises a protein structure by 1.1 kcal mol<sup>-1</sup> due to the loss of the methylene group (Kellis, 1988). The results of the Ile-71 → Val mutation in the current study reveal that they draw strong parallels with the Wallace *et al.* (1998b) study where the diminished protein stability is in response to the truncation of the topologically conserved bulky aliphatic isoleucine residue, on  $\alpha$ -helix 3, in the hydrophobic core of domain 1.

An analysis of the aligned crystal structures of the I71V (2R6K, Dirr *et al.*, to be published) and wild-type (1K3L, Le Trong *et al.*, 2002) proteins reveals that the cavity created upon the replacement of Ile-71 with valine results in a decrease in the van de Waals contacts between the side chain of the amino acid at position 71 and the surrounding residues (Figure 12 B). Both mutant enzyme Val-71 residue side chain and the wild-type Ile-71 residues side chain form hydrophobic contacts with the  $\alpha$ -helix residues Thr-19 ( $\alpha$ -helix 1) and Ile-75 ( $\alpha$ -helix

3), and the  $\beta$ -strand residues Val-58 ( $\beta$ -strand 3) and Leu-65 ( $\beta$ -strand 4). The contact distances between the side chain of residue 71 in the mutant and wild-type proteins and these hydrophobic residues are similar in both the mutant and wild-type proteins, therefore, indicating a similar binding-interaction strength between the respective residues in the mutant and wild-type proteins. The terminal methyl group on the truncated side chain of Val-71 is, however, further from the pyrrolidine side-chain of Pro-56 in the mutant protein (5.4 Å) as compared to the Ile-71 residue in the wild-type protein (3.9 Å) (Figure 12 B). The larger inter-residue distance and formation of the cavity prevents the formation of a van der Waals contact between Val-71 and Pro-56 in the mutant protein which decreases the stability of the protein. The absence of any structural shifts in the environment of the cavity to reform this van der Waals contact and minimise the cavity volume leaves the hydrophobic core within domain 1 of the mutant protein destabilised compared to the corresponding hydrophobic core in the wild-type protein. Computational studies conducted on globular proteins have revealed that isoleucine residues have the greatest propensity to form the greatest number of long range contacts (an average of 5.58 contacts per isoleucine residue) (Gromiha and Selvaraj, 1997; Gromiha and Selvaraj, 2004). It is thus expected that Ile-71 is topologically conserved in order to maximise the number of long-range van der Waals contacts (including the contact with Pro-56) formed between its extended hydrophobic side chain and surrounding residues, as well as to optimise the packing in the hydrophobic core of domain 1 in hGST A1-1 as a means to stabilise domain 1.

## CHAPTER 4

### CONCLUSIONS

The conservative substitution of Ile-71 → Val introduces a truncated valine side chain in the hydrophobic core of domain 1 in the mutant hGST A1-1 protein that lacks the methyl group of the extended side chain of Ile-71 in the wild-type protein. The terminal  $\delta$ -methyl group on the side chain of Ile-71 in the wild-type hGST A1-1 protein protrudes into the hydrophobic core created between Thr-19, Pro-56 and Val-58 residues. The inter-digitation of side chains between these residues culminates in efficient, cavity-free packing in the hydrophobic core in domain 1. The equivalent  $\gamma$ -methyl group on Val-71 in I71V hGST A1-1 is too short to efficiently inter-digitate between Thr-19, Pro-56 and Val-58 residues. This shortcoming introduces a  $27 \text{ \AA}^3$  cavity between  $\alpha$ -helices 1 and 3 and  $\beta$ -sheets 3 and 4 in the hydrophobic core in domain 1 of the I71V hGST A1-1 protein. The secondary structure and tertiary conformation of the protein remain unaffected by the truncated Val-71 side chain and associated cavity and the retained conformations of the active site residue side chains leave the catalytic and non-substrate ligandin functions of the mutant protein similar to that of the wild-type protein. The loss of optimised packing in the hydrophobic core in domain 1 of the mutant protein results in the reduction of van der Waals contacts between the hydrophobic core residue side chains. The mutant is therefore destabilised in comparison to the wild-type protein. This study suggests that the topologically conserved Ile-71 residue does not play a significant role in the structure and function of hGST A1-1 but makes a significant contribution to the stability of the protein by optimising the packing of the side chains in the hydrophobic core of domain 1.

## CHAPTER 5

### REFERENCES

Advanced Chemistry Development, Inc. (2009) ACD/Chemsketch (freeware) version 12.01. Available at <http://www.acdlabs.com>.

Altschul, S.F., Gish, W., Miller, W., Myers, E.W. and Lipman, D.J. (1990) Basic local alignment search tool. *J. Mol. Biol.* **215**, 403–410.

Anfinsen, C.B. (1973) Principles that govern the folding of protein chains. *Science* **181**, 223–230.

Anfinsen, C.B., Haber, E., Sela, M. and White Jr., F.H. (1961) The kinetics of formation of native ribonuclease during oxidation of the reduced polypeptide chain. *Proc. Natl. Acad. Sci. USA* **47**, 1309–1314.

Armstrong, R.N. (1991) Glutathione *S*-transferases: Reaction mechanism, structure, and function. *Chem. Res. Toxicol.* **4**, 131–140.

Armstrong, R.N. (1997) Structure, catalytic mechanism, and evolution of the glutathione transferases. *Chem. Res. Toxicol.* **10**, 2–18.

Atkins, W.M., Dietze, E.C. and Ibarra, C. (1997) Pressure-dependent ionization of Tyr 9 in glutathione *S*-transferase A1-1: Contribution of the C-terminal helix to a “soft” active site. *Protein Sci.* **6**, 873–881.

Axe, D.D., Foster, N.W. and Fersht, A.R. (1996) Active barnase variants with completely random hydrophobic cores. *Proc. Natl. Acad. Sci. USA* **93**, 5590–5594.

Baker, E.N. and Hubbard, R.E. (1984) Hydrogen bonding in globular proteins. *Prog. Biophys. Mol. Biol.* **44**, 97–179.

Berman, H.M., Westbrook, J., Feng, Z., Gilliland, G., Bhat, T.N., Weissig, H., Shindyalov, I.N. and Bourne, P.E. (2000) The protein data bank. *Nucleic Acids Res.* **28**, 235–242.

Bernasconi, C.F. (1980) Mechanism of nucleophilic aromatic and hetero-aromatic substitution. Recent developments. *Chimica* **34**, 1–11.

Birdsall, B., King, R.W., Wheeler, M.R., Lewis, Jr., C.A., Goode, S.R., Dunlap, R.B. and Roberts, G.C.K. (1983) Correction for light absorption in fluorescence studies of protein-ligand interactions. *Anal. Biochem.* **132**, 353–361.

Birnboim, H.C. and Doly, J. (1979) A rapid alkaline extraction procedure for screening recombinant plasmid DNA. *Nucl. Acid Res.* **7**, 1513–1523.

Björnstedt, R., Stenberg, G., Widersten, M., Board, P.G., Sinning, I., Jones, T.A. and Mannervik, B. (1995) Functional significance of Arginine 15 in the active site of human class Alpha glutathione transferase A1-1. *J. Mol. Biol.* **247**, 765–773.

Chen, W.J., Graminski, G.F. and Armstrong, R.N. (1988) Dissection of the catalytic mechanism of isoenzyme 4-4 of glutathione *S*-transferase with alternative substrates. *Biochemistry* **27**, 647–654.

Chothia, C. (1976) The nature of the accessible and buried surfaces in proteins. *J. Mol. Biol.* **105**, 1–14.

Clark, A.G. and Sinclair, M. (1988) The Meisenheimer complex of glutathione and trinitrobenzene. A potent inhibitor of the glutathione *S*-transferase from *Galleria Mellonella*. *Biochem. Pharm.* **37**, 259–263.

Dill, K.A. (1990) Dominant forces in protein folding. *Biochemistry* **29**, 7133–7155.

Dill, K.A. and Chan, H.S. (1997) From Levinthal to pathways to funnels. *Nat. Struct. Biol.* **4**, 10–19.

Di Nardo, A.A., Larson, S.M. and Davidson, A.R. (2003) The relationship between conservation, thermodynamic stability, and function in the SH3 domain hydrophobic core. *J. Mol. Biol.* **333**, 641–655.

Dirr, H., Reinemer, P. and Huber, R. (1994) X-ray crystal structures of cytosolic glutathione *S*-transferases. Implications for protein architecture, substrate recognition and catalytic function. *Eur. J. Biochem.* **220**, 645–661.

Dirr, H.W. and Wallace, L.A. (1999) Role of the C-terminal helix 9 in the stability and ligandin function of class  $\alpha$  glutathione transferase A1-1. *Biochemistry* **38**, 15631–15640.

Dirr, H.W., Fisher, L., Burke, J.P.W.G., Sayed, M. and Sewell, T. Crystal structure of an I71V hGSTA1-1 mutant in complex with S-hexylglutathione. (PDB accession code: 2R6K). (To be published).

Dirr, H.W., Little, T., Kuhnert, D.C. and Sayed, Y. (2005) A conserved N-capping motif contributes significantly to the stabilisation and dynamics of the C-terminal region of class Alpha glutathione *S*-transferases. *J. Biol. Chem.* **280**, 19480–19487.

Eklund, H., Ingelman, M., Söderberg, B.-O., Nordlund, T.U.P., Nikkola, M., Sonnerstam, U., Joelson, T. and Petratos, K. (1992) Structure of oxidized bacteriophage T4 glutaredoxin (thioredoxin). Refinement of native and mutant proteins. *J. Mol. Biol.* **228**, 596–618.

Epp., O., Ladenstein, R. and Wendel, A. (1983) The refined structure of the selenoenzyme glutathione peroxidase at 0.2-nm resolution. *Eur. J. Biochem.* **133**, 51–69.

Fersht, A.R. (1999) Structure and mechanisms in protein science: a guide to enzyme catalysis and protein folding. *W. H. Freeman and Co., New York.*

Finucane, M.D. and Woolfson, D.N. (1999) Core-directed protein design. II. Rescue of a multiply mutated and destabilized variant of ubiquitin. *Biochemistry* **38**, 11613–11623.

Gan, L.-H. (1977) Kinetic studies of the reactions of glutathione and aromatic compounds. *Aust. J. Chem.* **30**, 1475–1479.

Gasteiger, E., Hoogland, C., Gattiker, A., Duvaud, S., Wilkins, M.R., Appel, R.D. and Bairoch, A. (2005) Protein identification and analysis tools on the ExPASy server. In *The proteomics protocols handbook* (Walker, J.M., ed.) pp. 571–607. Humana Press, NJ.

Gildenhuis, S., Dobрева, M., Kinsley, N., Sayed, Y., Burke, J., Pelly, S., Gordon, G.P., Sayed, M., Sewell, T. and Dirr, H.W. (2010) Arginine 15 stabilizes an S<sub>N</sub>Ar reaction transition state and the binding of anionic ligands at the active site of human glutathione transferase A1-1. *Biophys. Chem.* **146**, 118–125.

Graminski, G.F., Zhang, P., Sesay, M.A., Ammon, H.L. and Armstrong, R. N. (1989) Formation of the 1-(S-glutathionyl)-2,4,6-trinitrocyclohexadienate anion at the active site of glutathione S-transferase: Evidence for enzymatic stabilization of  $\sigma$ -complex intermediates in nucleophilic aromatic substitution reactions. *Biochemistry* **28**, 6252–6258.

Gromiha, M.M. and Selvaraj, S. (1997) Influence of medium and long range interactions in different structural classes of globular proteins. *J. Biol. Phys.* **23**, 151–162.

Gromiha, M.M. and Selvaraj, S. (2004) Inter-residue interactions in protein folding and stability. *Prog. Biophys. Mol. Biol.* **86**, 235–277.

Guex, N. and Peitsch, M.C. (1997) SWISS-MODEL and the Swiss-PdbViewer: An environment for comparative protein modeling. *Electrophoresis* **18**, 2714–2723.

Habig, W.H., Pabst, M.J. and Jakoby, W.B. (1974) Glutathione S-transferases. The first enzymatic step in mercapturic acid formation. *J. Biol. Chem.* **249**, 7130–7139.

Hayes, J.D. and McLellan, L.I. (1999) Glutathione and glutathione-dependent enzymes represent a co-ordinately regulated defence against oxidative stress. *Free Radical Res.* **31**, 273–300.

Hayes, J.D. and Pulford, D.J. (1995) The glutathione S-transferase supergene family: Regulation of GST and the contributions of the isoenzymes to cancer chemoprotection and drug resistance. *CRC Crit. Rev. Biochem. Mol. Biol.* **30**, 445–600.

Hayes, J.D., Flanagan, J.U. and Jowsey, I.R. (2005) Glutathione transferases. *Annu. Rev. Pharmacol. Toxicol.* **45**, 51–88.

Holmgren, A., Söderberg, B.-O., Eklund, H. and Brändén, C.-I. (1975) Three-dimensional structure of *Escherichia coli* thioredoxin-S<sub>2</sub> to 2.8 Å resolution. *Proc. Natl. Acad. Sci. USA* **72**, 2305–2309.

Ish-Horowicz, D. and Burke, J.F. (1981) Rapid and efficient cosmid cloning. *Nucl. Acid Res.* **9**, 2989–2998.

IUPAC-IUB Commission on Biochemical Nomenclature. (1974) Abbreviations and symbols for nucleic acids, polynucleotides and their constituents. Rules approved 1974.

IUPAC-IUB Joint Commission on Biochemical Nomenclature (JCBN). (1984) Nomenclature and symbolism for amino acids and peptides. Recommendations 1983. *Eur. J. Biochem.* **138**, 9–37.

Ji, X., Armstrong, R.N. and Gilliland, G.L. (1993) Snapshots along the reaction coordinate of an S<sub>N</sub>Ar reaction catalyzed by glutathione transferase. *Biochemistry* **32**, 12949–12954.

Kellis Jr., J.T., Nyberg, K. and Fersht, A.R. (1989) Energetics of complementary side chain packing in a protein hydrophobic core. *Biochemistry* **28**, 4914–4922.

Kellis Jr., J.T., Nyberg, K., Sali, D. and Fersht, A.R. (1988) Contribution of hydrophobic interactions to protein stability. *Nature* **333**, 784–786.

Kelly, S.M., Jess, T.J. and Price, N.C. (2005) How to study proteins by circular dichroism. *Biochim. Biophys. Acta* **1751**, 119–139.

Ketley, J.N., Habig, W.H. and Jakoby, W.B. (1975) Binding of nonsubstrate ligands to the glutathione S-transferases. *J. Biol. Chem.* **250**, 8670–8673.

Koonin, E.V., Mushegian, A.R., Tatusov, R.L., Altschul, S.F., Bryant, S.H., Bork, P. and Valencia, A. (1994) Eukaryotic translation elongation factor 1 $\gamma$  contains a glutathione transferase domain—Study of a diverse, ancient protein superfamily using motif search and structural modeling. *Protein Sci.* **3**, 2045–2054.

Lakowicz, J.R. (1983) Principles of fluorescence spectroscopy. pp. 76–78. Plenum Press, New York

Larkin, M.A., Blackshields, G., Brown, N.P., Chenna, R., McGettigan, P.A., McWilliam, H., Valentin, F., Wallace, I.M., Wilm, A., Lopez, R., Thompson, J.D., Gibson, T.J. and Higgins, D.G. (2007) Clustal W and Clustal X version 2.0. *Bioinformatics* **23**, 2947–2948.

Le Trong, I., Stenkamp, R.E., Ibarra, C., Atkins, W.M. and Adman, E.T. (2002) 1.3-Å resolution structure of human glutathione S-transferase with S-hexyl glutathione bound reveals possible extended ligandin binding site. *Proteins: Struct. Funct. Genet.* **48**, 618–627.

Levinthal, C. (1968) Are there pathways for protein folding? *J. Chim. Phys.* **65**, 44–45.

Lien, S., Gustafsson, A., Andersson, A.-K. and Mannervik, B. (2001) Human glutathione transferase A1-1 demonstrates both half-of-the-sites and all-of-the-sites reactivity. *J. Biol. Chem.* **276**, 35599–35605.

Lim, W.A. and Sauer, R.T. (1989) Alternative packing arrangements in the hydrophobic core of lamda repressor. *Nature* **339**, 31–36.

Maniatis, T., Fritsch, E. F., and Sambrook, J. (1982) In *Molecular Cloning: A Laboratory Manual*, p. 468, Cold Spring Harbor Laboratory, Cold Spring Harbor, New York.

Mannervik, B., Guthenberg, C., Jakobson, I. and Warholm, M. (1978) Glutathione conjugation: reaction mechanism of glutathione S-transferase A. In *Conjugation Reactions in Drug Biotransformations* (Aitio, A., ed.), pp. 101–110, Elsevier/North-Holland Biomedical Press, Amsterdam.

Manoharan, T.H., Gulick, A.M., Puchalski, R.B., Servais, A.L. and Fahl, W.E. (1992) Structural studies on human glutathione transferase  $\pi$ . Substitution mutations to determine amino acids necessary for binding glutathione. *J. Biol. Chem.* **267**, 18940–18945.

Miller, J. (1968) In *Reaction mechanisms in organic chemistry* (Eaborn, C. and Chapman, N.B. eds.), 8, pp. 137–179. Elsevier Science Publishing Co., Inc., New York.

Miller, S.L., Schopf, J.W. and Lazcano, A. (1997) Oparin's "Origin of life": Sixty years later. *J. Mol. Evol.* **44**, 351–353.

Mosebi, S., Sayed, Y., Burke, J. and Dirr, H.W. (2003) Residue 219 impacts on the dynamics of the C-terminal region in glutathione transferase A1-1: Implications for stability and catalytic and ligandin functions. *Biochemistry* **42**, 15326–15332.

Murzin, A.G., Brenner, S.E., Hubbard, T. and Chothia, C. (1995) SCOP: A structural classification of proteins database for the investigation of sequences and structures. *J. Mol. Biol.* **247**, 536–540.

Nathaniel, C., Wallace, L.A., Burke, J. and Dirr, H.W. (2003) The role of an evolutionary conserved *cis*-proline in the thioredoxin-like domain of human class Alpha glutathione transferase A1-1. *Biochem. J.* **372**, 241–246.

Nilsson, L.O., Edalat, M., Pettersson, P.L. and Mannervik, B. (2002) Aromatic residues in the C-terminal region of glutathione transferase A1-1 influence rate-determining steps in the catalytic mechanism. *Biochem. Biophys. Acta.* **1597**, 157–163.

Pace, C.N. (1986) Determination and analysis of urea and guanidine hydrochloride denaturation curves. *Methods Enzymol.* **131**, 266–280.

Perkins, S.J. (1986) Protein volumes and hydration effects. The calculations of partial specific volumes, neutron scattering matchpoints and 280-nm absorption coefficients for proteins and glycoproteins from amino acid sequences. *Eur. J. Biochem.* **157**, 169–180.

Ratnaparkhi, G.S. and Varadarajan, R. (2000) Thermodynamic and structural studies of cavity formation in proteins suggest that the loss of packing interactions rather than the hydrophobic effect dominates the observed energetics. *Biochemistry* **39**, 12365–12374.

Richards, F.M. (1977) Areas, volumes, packing and protein structure. *Annu. Rev. Biophys. Bioeng.* **6**, 151–176.

Rushmore, T.H. and Pickett, C.B. (1993) Glutathione *S*-transferases, structure, regulation, and therapeutic implications. *J. Biol. Chem.* **268**, 11475–11478.

Sanger, F., Nicklen, S. and Coulson, A.R. (1977) DNA sequencing with chain-terminating inhibitors. DNA polymerase/nucleotide sequences/bacteriophage  $\phi$ X174. *Proc. Natl. Acad. Sci. USA* **74**, 5463–5467.

Sheehan, D., Meade, G., Foley, V.M. and Dowd, C.A. (2001) Structure, function and evolution of glutathione transferases: implications for classification of non-mammalian members of an ancient enzyme superfamily. *Biochem. J.* **360**, 1–16.

Shortle, D., Stites, W.E. and Meeker, A.K. (1990) Contributions of the large hydrophobic amino acids to the stability of staphylococcal nuclease. *Biochemistry* **29**, 8033–8041.

Sinning, I., Kleywegt, G.J., Cowan, S.W., Reinemer, P., Dirr, H.W., Huber, R., Gilliland, G.L., Armstrong, R.N., Ji, X., Board, P.G., Olin, B., Mannervik, B. and Jones, T.A. (1993) Structure determination and refinement of human Alpha class glutathione Transferase A1-1, and a comparison with the Mu and Pi class enzymes. *J. Mol. Biol.* **232**, 192–212.

Slavik, J. (1982) Anilinonaphthalene sulfonate as a probe of membrane composition and function. *Biochim. Biophys. Acta.* **694**, 1–25.

Sluis-Cremer, N., Naidoo, N.N., Kaplan, W.H., Manoharan, T.H., Fahl, W.E. and Dirr, H.W. (1996) Determination of a binding site for a non-substrate ligand in mammalian cytosolic glutathione S-transferases by means of fluorescence-resonance energy transfer. *Eur. J. Biochem.* **241**, 484–488.

Stenberg, G., Björnstedt, R. and Mannervik, B. (1992) Heterologous expression of recombinant glutathione transferase A1-1 from a hepatoma cell line. *Protein Expr. Pur.* **3**, 80–84.

Stenberg, G., Board, P.G. and Mannervik, B. (1991) Mutation of an evolutionarily conserved tyrosine residue in the active site of a human class Alpha glutathione transferase. *FEBS Lett.* **293**, 153–155.

Van Ommen, B., Bogaards, J.J.P., Peters, W.H.M., Blaauboer, B. and van Bladeren, P.J. Quantification of human hepatic glutathione *S*-transferases. *Biochem. J.* **269**, 609–613.

Vlassi, M., Cesareni, G. and Kokkinidis, M. (1999) A correlation between the loss of hydrophobic core packing interactions and protein stability. *J. Mol. Biol.* **285**, 817–827.

Wallace, L.A., and Dirr, H.W. (1999) Folding and assembly of dimeric human glutathione transferase A1-1. *Biochemistry* **38**, 16686–16694.

Wallace, L.A., Blatch, G.L. and Dirr, H.W. (1998b) A topologically conserved aliphatic residue in  $\alpha$ -helix 6 stabilizes the hydrophobic core in domain II of glutathione transferases and is a structural determinant for the unfolding pathway. *Biochem. J.* **336**, 413–418.

Wallace, L.A., Sluis-Cremer, N. and Dirr, H.W. (1998a) Equilibrium and kinetic unfolding properties of dimeric human glutathione transferase A1-1. *Biochemistry* **37**, 5320–5328.

Weber, G. and Young, L.B. (1964) Fragmentation of bovine serum albumin by pepsin. I. The origin of the acid expansion of the albumin molecule. *J. Biol. Chem.* **239**, 1415–1423.

Widersten, M., Björnstedt, R. and Mannervik, B. (1996) Involvement of the carboxyl groups of glutathione in the catalytic mechanism of human glutathione transferase A1-1. *Biochemistry* **35**, 7731–7742.

Wilce, M.C.J., and Parker, M.W. (1994) Structure and function of glutathione *S*-transferases. *Biochim. Biophys. Acta* **1205**, 1–18.

Winder, A.F., and Gent, W.L.G. (1971) Correction of light-scattering errors in spectrophotometric protein determinations. *Biopolymers* **10**, 1243–1251.

Woody, R.W. (1995) Circular dichroism. *Methods Enzymol.* **246**, 34–71.

Woody, R.W. (1996) Theory of circular dichroism of proteins, In *Circular dichroism and the conformational analysis of biomolecules*, (Fasman, G.D., ed.) pp. 25–67, Plenum, New York.

Xu, J., Baase, W.A., Baldwin, E. and Matthews, B.W. (1998) The response of T4 lysozyme to large-to-small substitutions within the core and its relation to the hydrophobic effect. *Protein Sci.* **7**, 158–177.